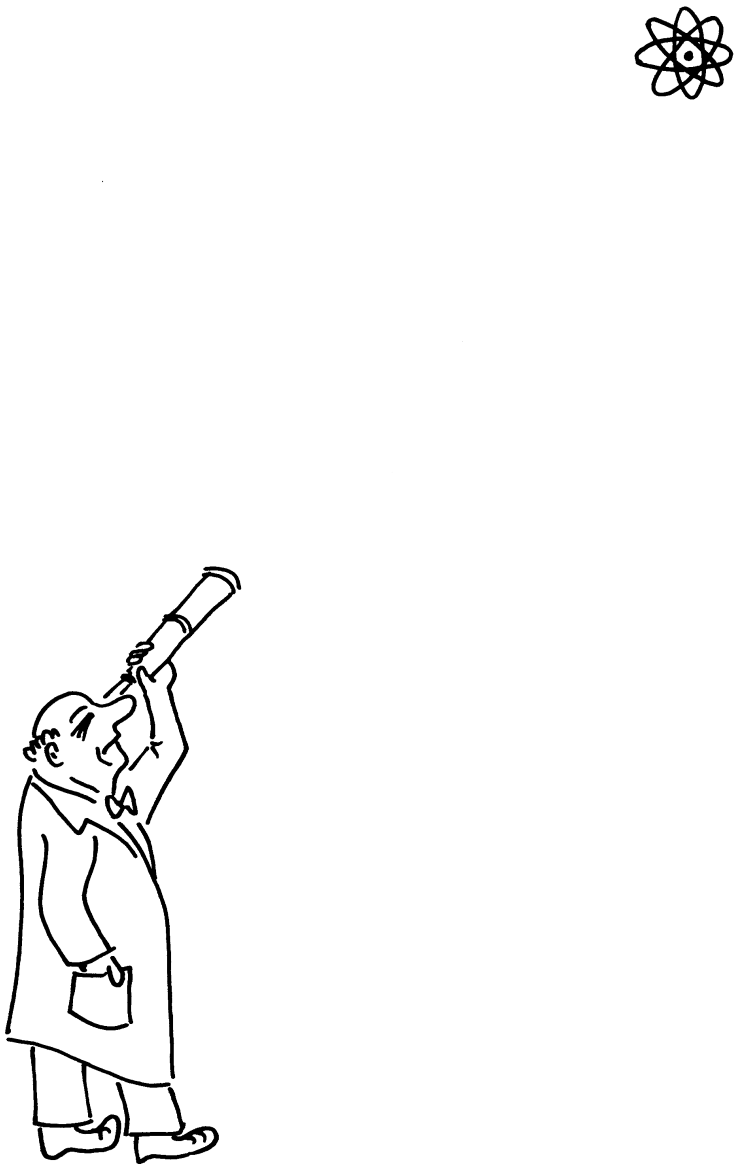

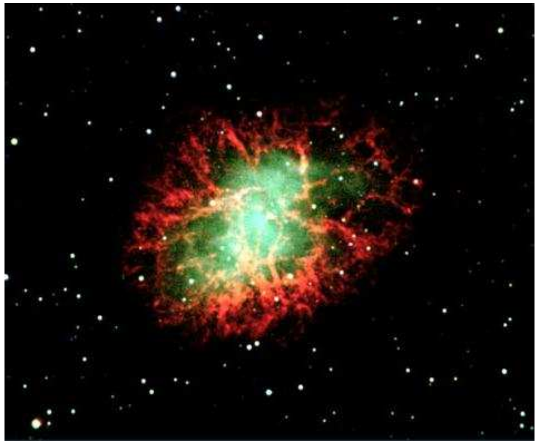

Figure 1.1: Crab Nebula {1}

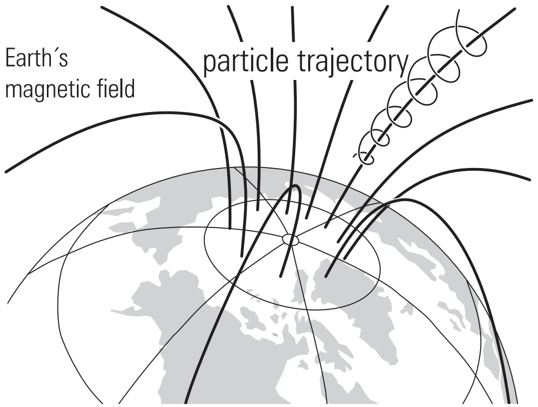

Figure 1.2: Helical trajectory of an electron in the Earth's magnetic field

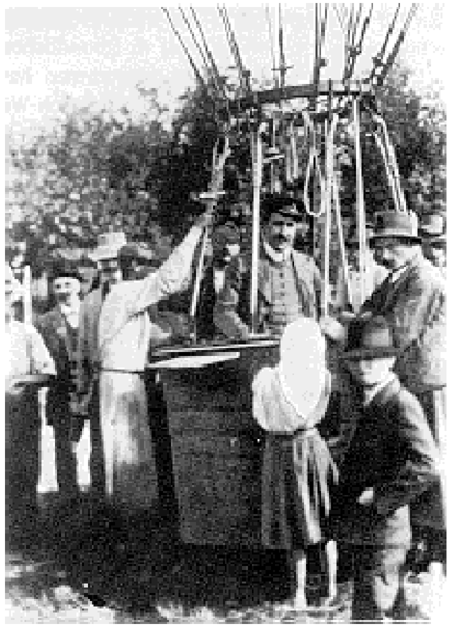

Figure 1.3: Victor Hess at a balloon ascent for measuring cosmic radiation {2}

Figure 1.4: Robert Millikan at a take-off of balloon experiments in Bismarck, North Dakota (1938) {3}

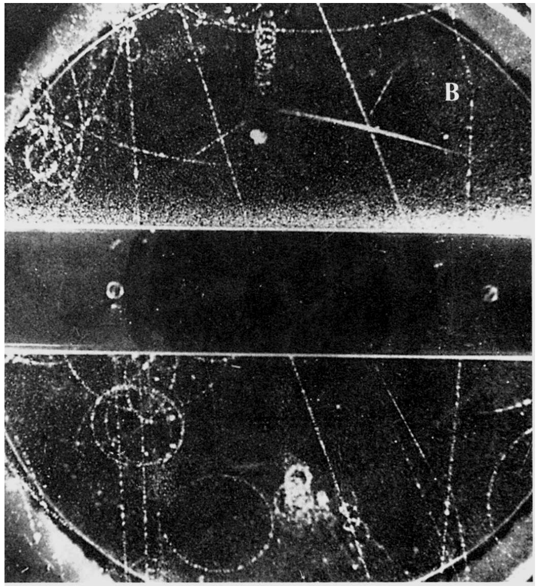

Figure 1.5: Tracks of cosmic particles in a cloud chamber {4}

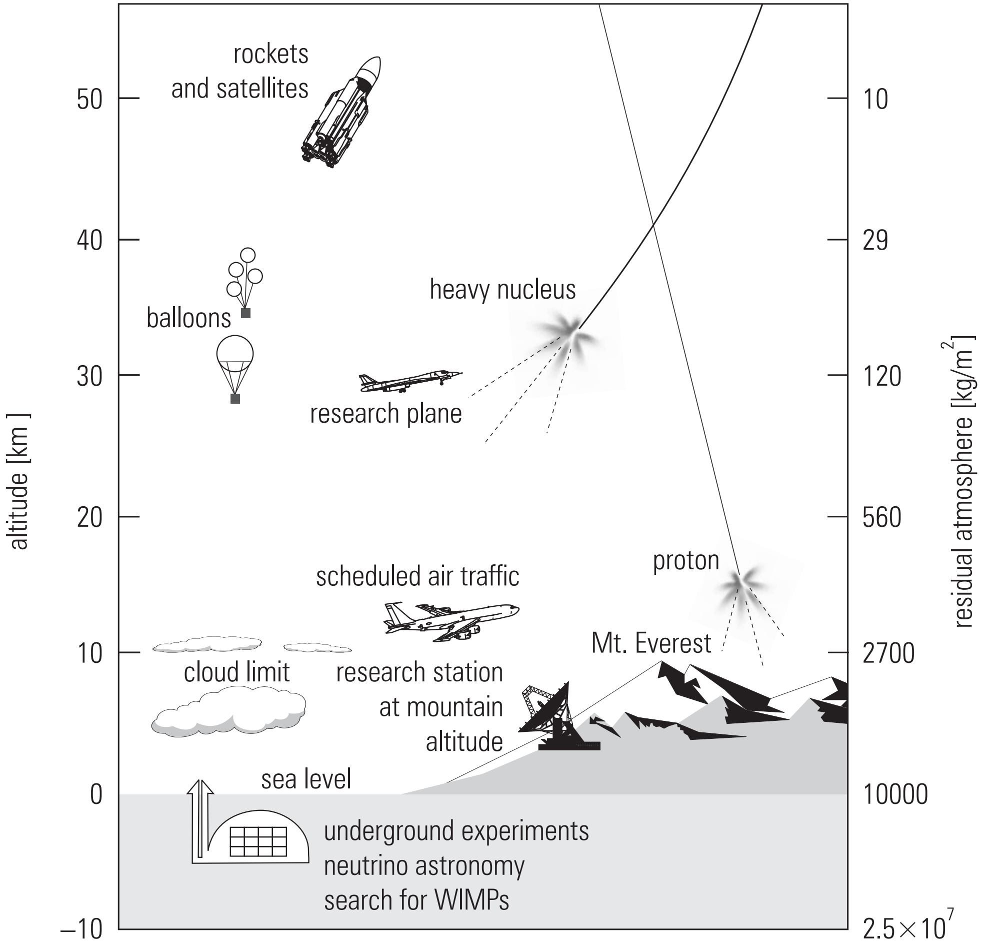

Figure 1.6: Possibilities for experiments in the field of cosmic rays

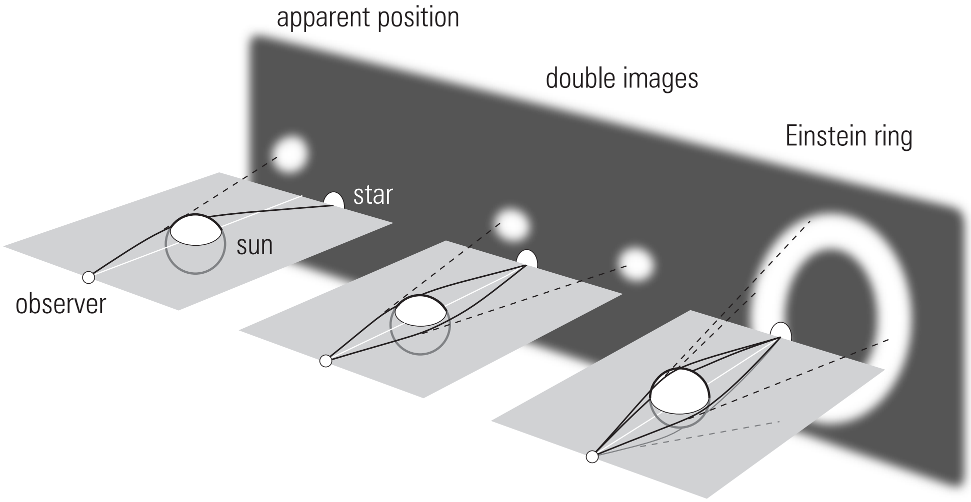

Figure 1.7: Gravitational lensing by a massive object:
a) deflection of light,
b) double images,
c) Einstein ring

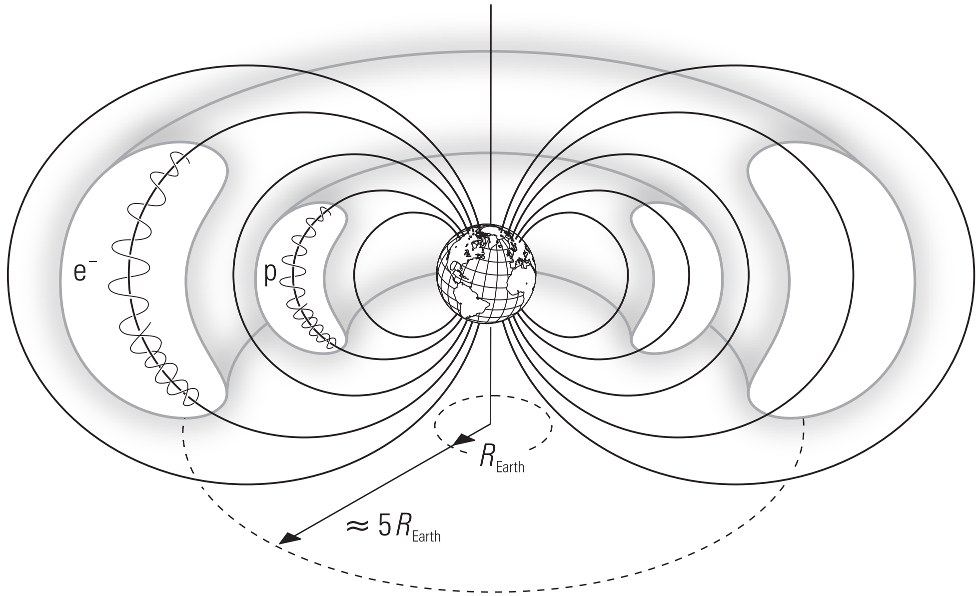

Figure 1.9: Van Allen belts

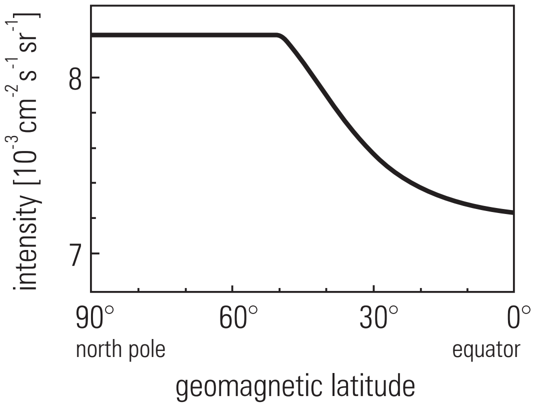

Figure 1.8: Latitude effect: geomagnetic and atmospheric cutoff

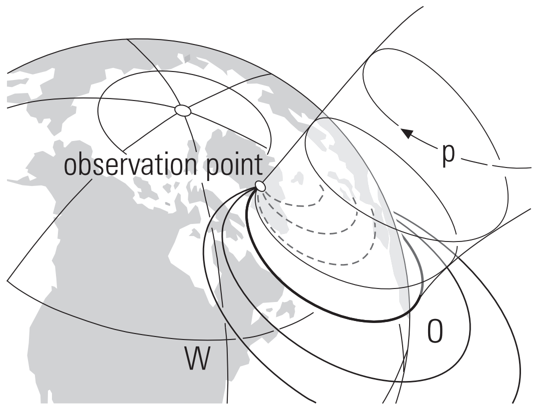

Figure 1.10: East–west effect

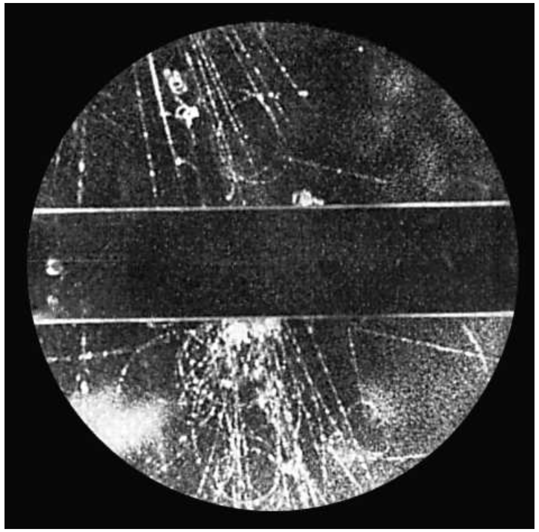

Figure 1.11: Decays of neutral kaons in a cloud chamber {4}

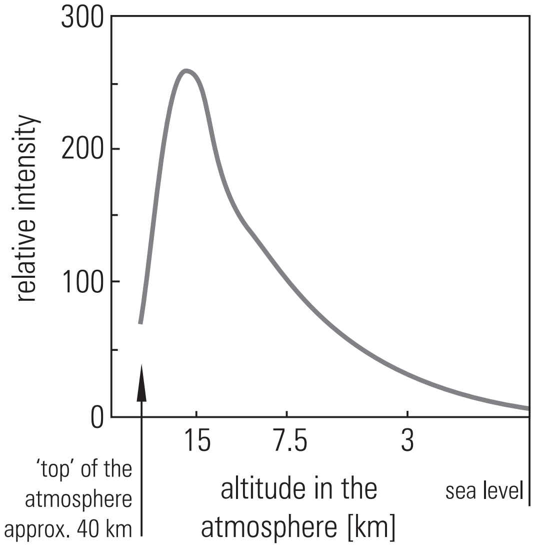

Figure 1.12: Intensity profile of cosmic particles in the atmosphere

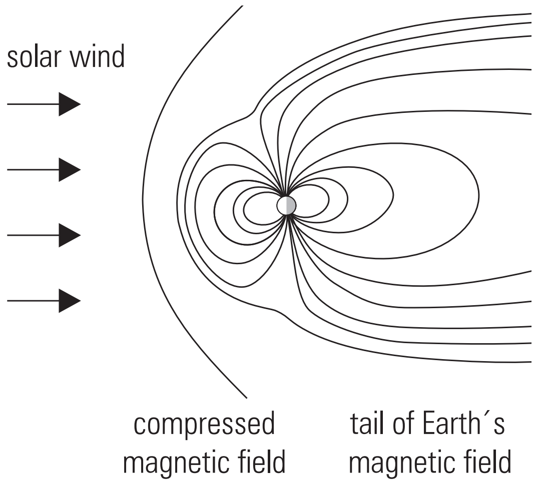

Figure 1.13: Influence of the solar wind on the Earth's magnetic field

Figure 1.14: Penzias and Wilson in front of their horn antenna used for measuring of the blackbody radiation {5}

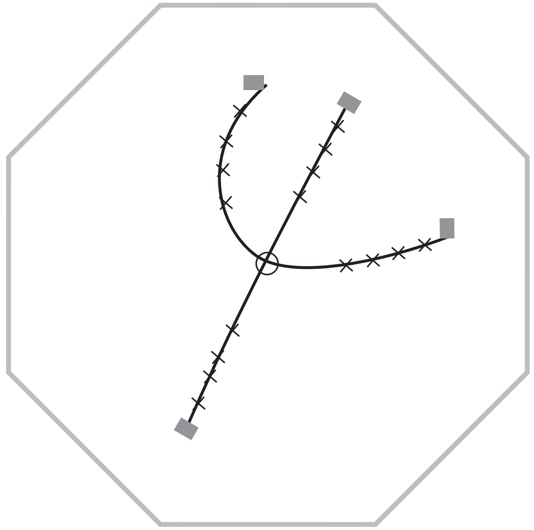

Figure 1.15: Decay of an excited charm particle ($\psi' \to \psi + \pi^+ + \pi^-$, with the subsequent decay $\psi \to \mu^+ + \mu^-$)

Figure 1.16: Supernova explosion SN 1987A in the Tarantula Nebula {6}

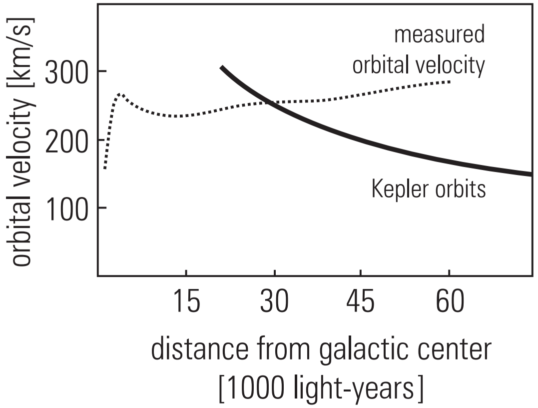

Figure 1.17: Orbital velocities of stars in the Milky Way in comparison with Keplerian trajectories

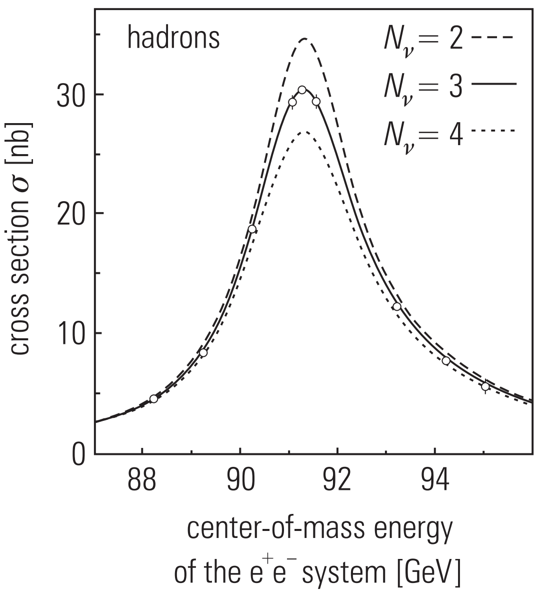

Figure 2.1: Determination of the number of neutrino generations from Z decay

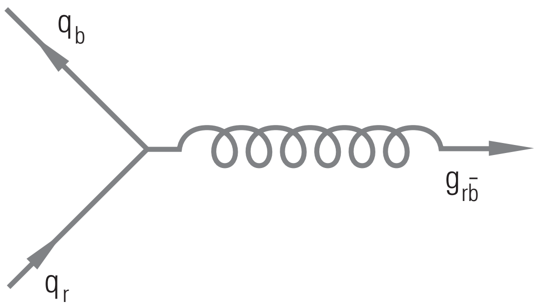

Figure 2.2: Creation of coloured gluons by quarks

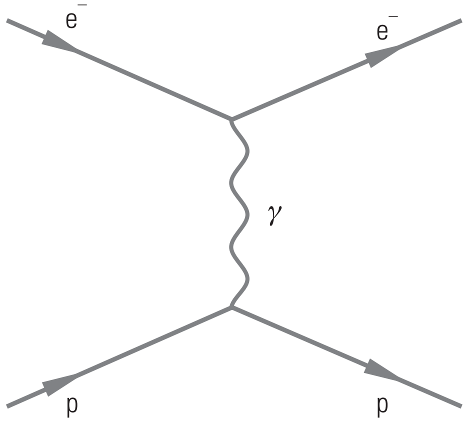

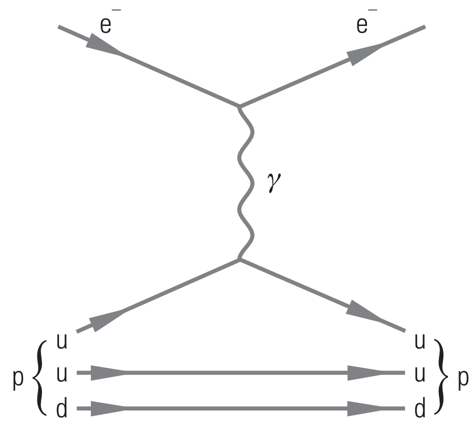

Figure 2.3: Rutherford scattering of electrons on protons

Figure 2.4: Rutherford scattering as photon–quark subprocess

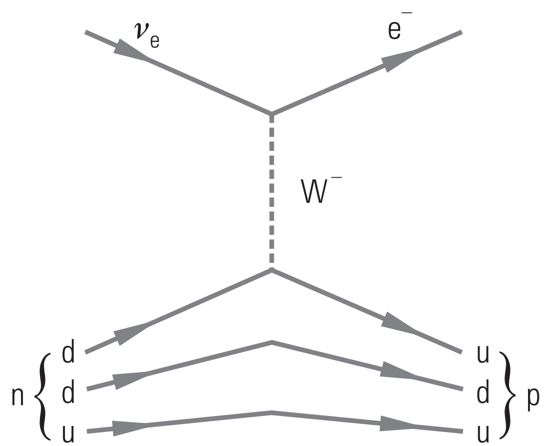

Figure 2.5: Neutrino–neutron scattering by charged currents

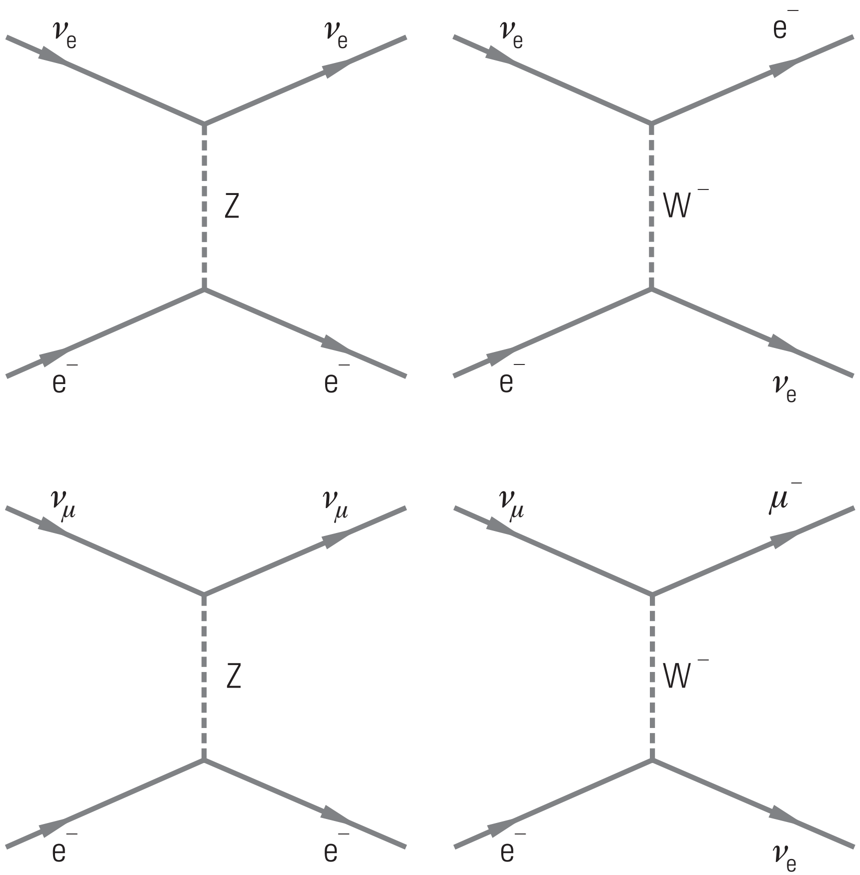

Figure 2.6: Different Feynman diagrams contributing to the scattering of neutrinos on electrons

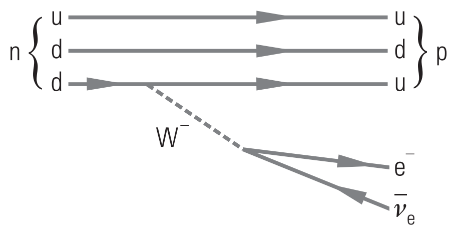

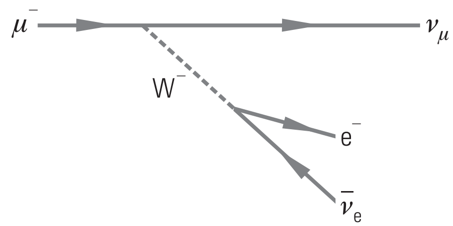

Figure 2.7: Neutron decay

Figure 2.8: Muon decay

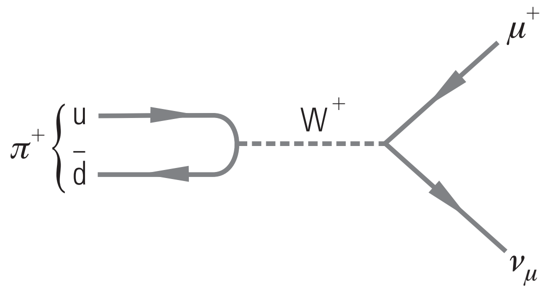

Figure 2.9: Pion decay

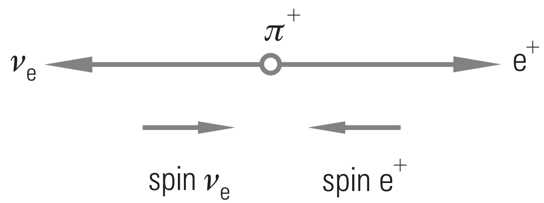

Figure 2.10: Helicity conservation in π^+ decay

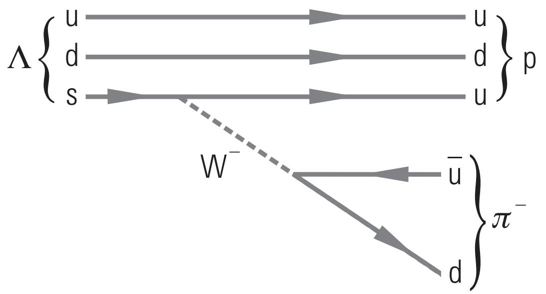

Figure 2.11: Lambda decay: $\Lambda \rightarrow p + \pi^{-}$

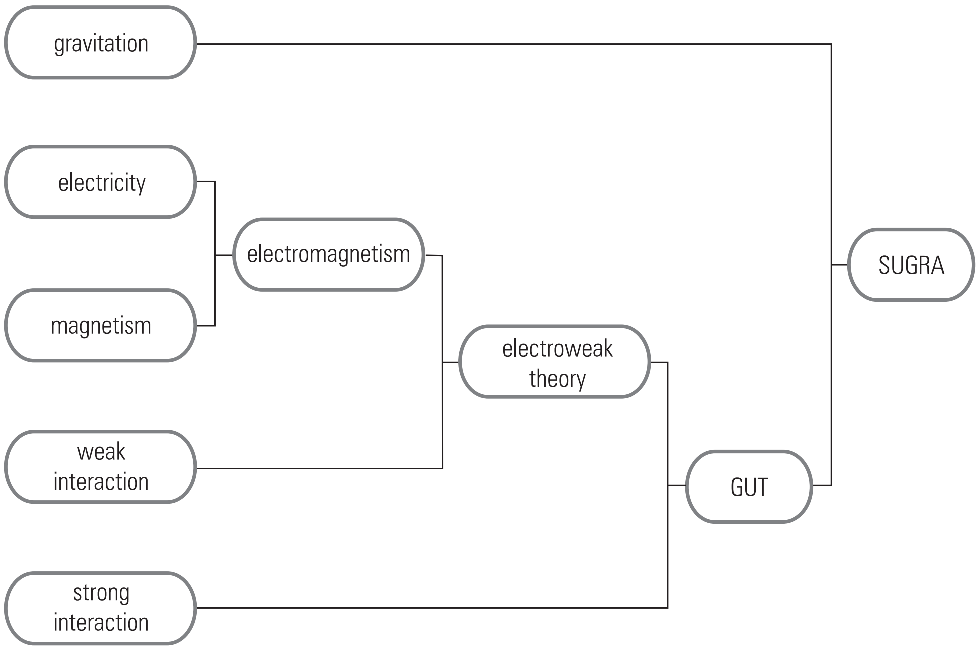

Figure 2.12: Unification of all different interactions into a Theory of Everything (GUT – Grand Unified Theory, SUGRA – Super Gravitation)

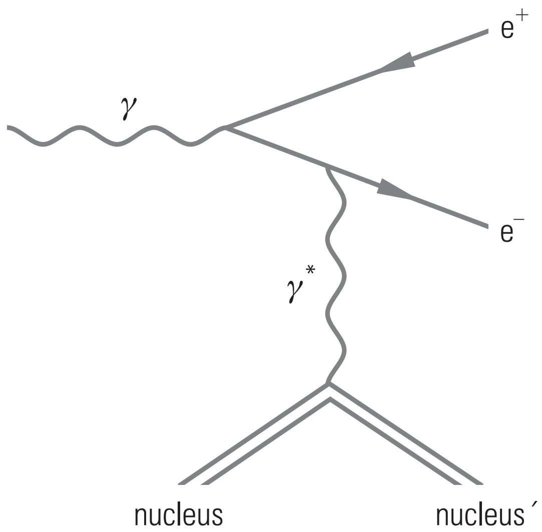

Figure 3.1: The processγ + nucleus $\rightarrow e^+ + e^- +$ nucleus$'$

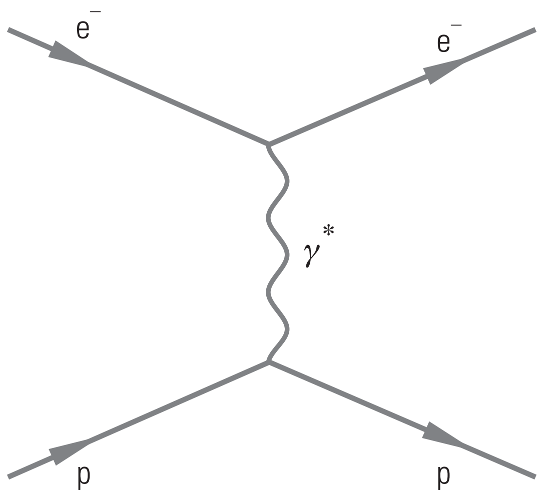

Figure 3.2: The process $e^- + p \rightarrow e^- + p$

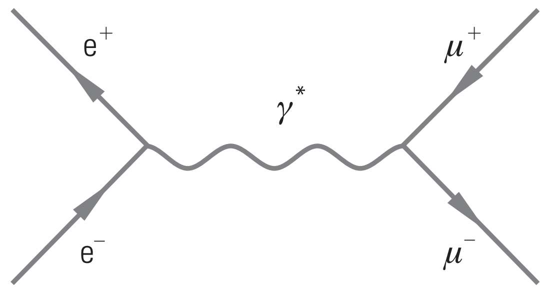

Figure 3.3: The process $e^+e^- \rightarrow \mu^+\mu^-$

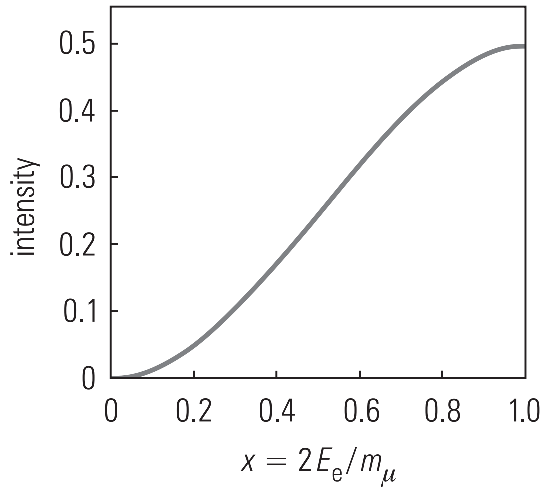

Figure 3.4: Energy spectrum of electrons from muon decay

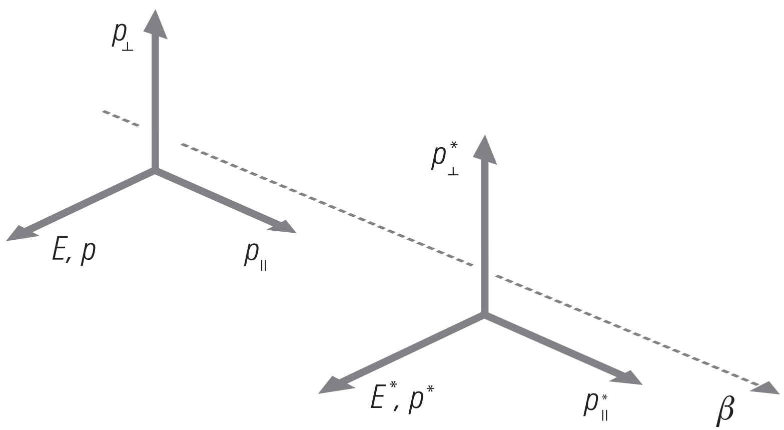

Figure 3.5: Illustration of a Lorentz transformation

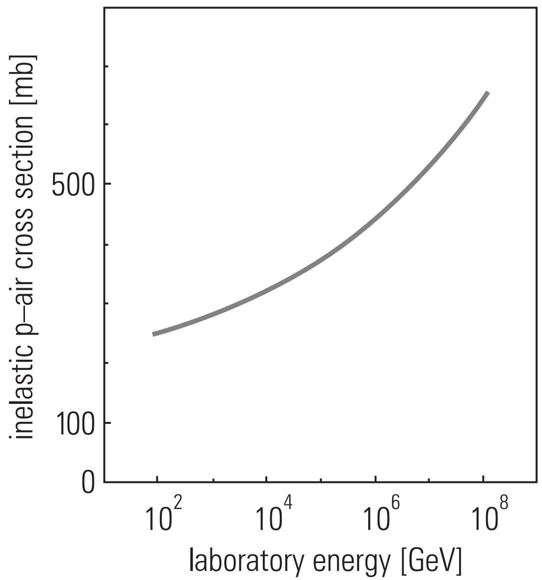

Figure 4.1: Cross section for proton–air interactions

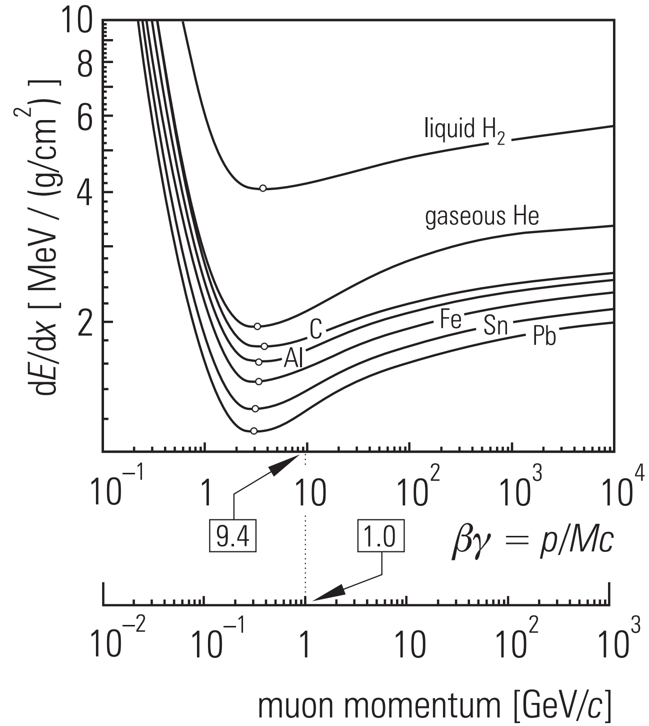

Figure 4.2: Energy loss of charged particles in various targets [2]

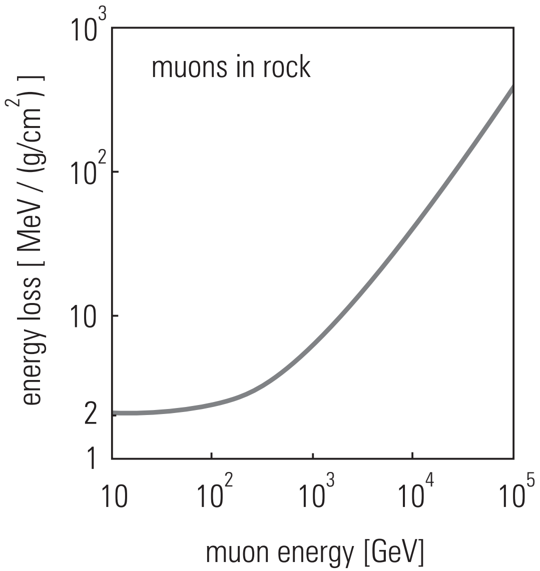

Figure 4.3: Energy loss of muons in standard rock

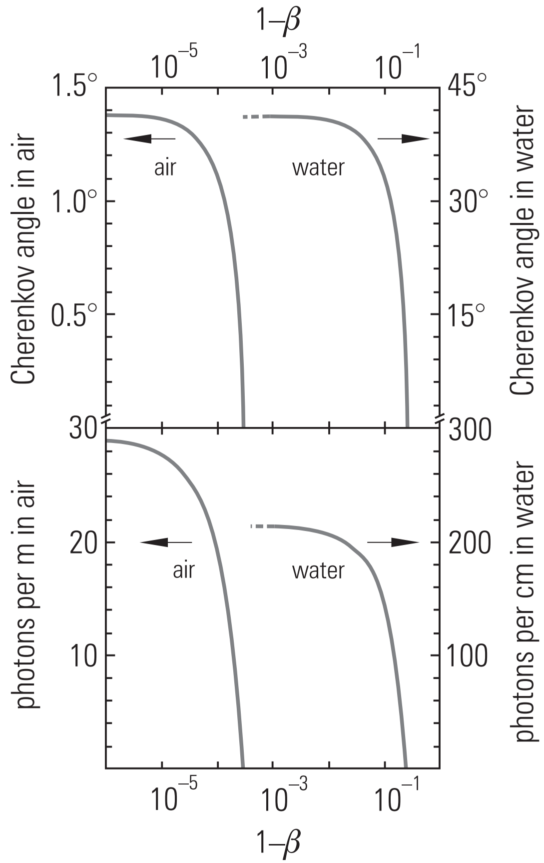

Figure 4.4: Variation of the Cherenkov angle and photon yield of singly charged particles in water and air

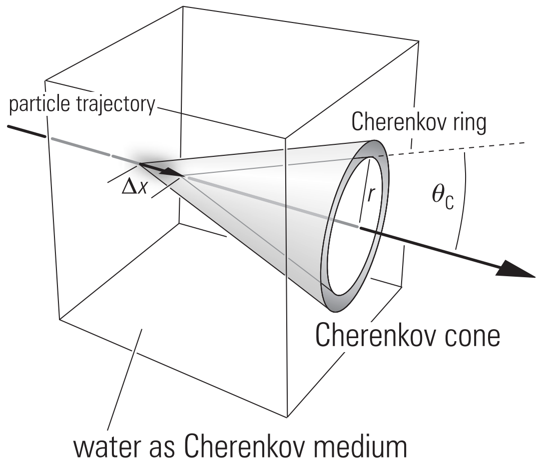

Figure 4.5: Production of a Cherenkov ring in a water Cherenkov counter

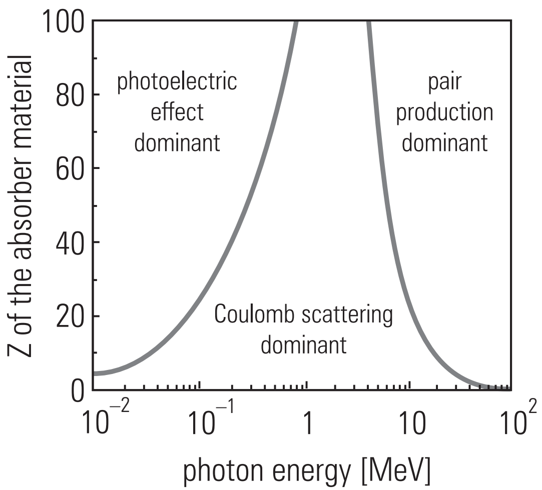

Figure 4.6: Domains, in which various photon interactions dominate, shown in their dependence on the photon energy and the nuclear charge of the absorber

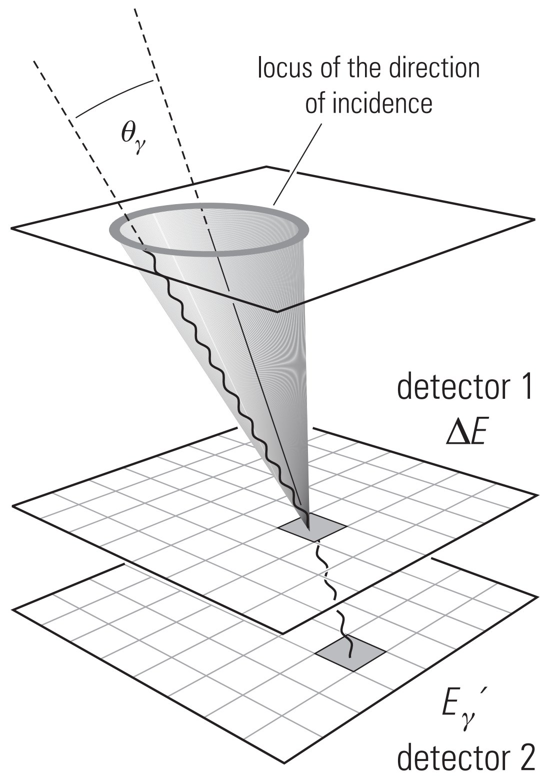

Figure 4.7: Schematic of a Compton telescope

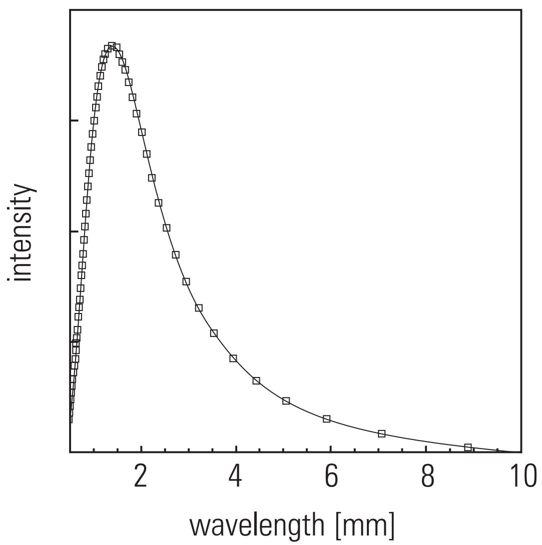

Figure 4.8: Blackbody spectrum of cosmic microwave background photons

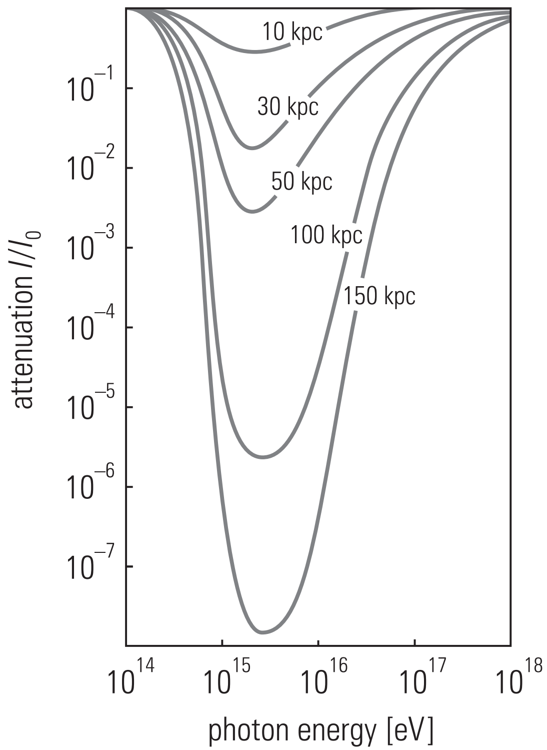

Figure 4.9: Attenuation of the intensity of energetic primary cosmic photons by interactions with blackbody radiation

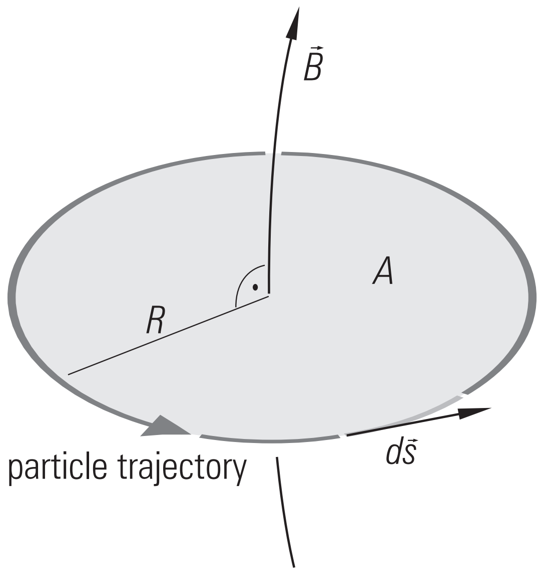

Figure 5.1: Principle of particle acceleration by variable sunspots

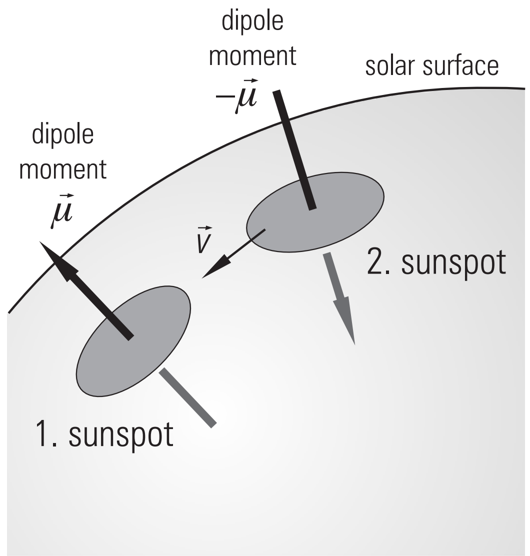

Figure 5.2: Sketch of a sunspot pair

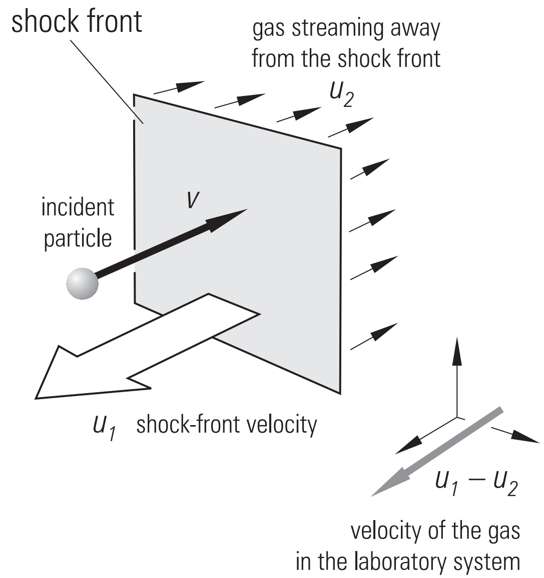

Figure 5.3: Schematics of shock-wave acceleration

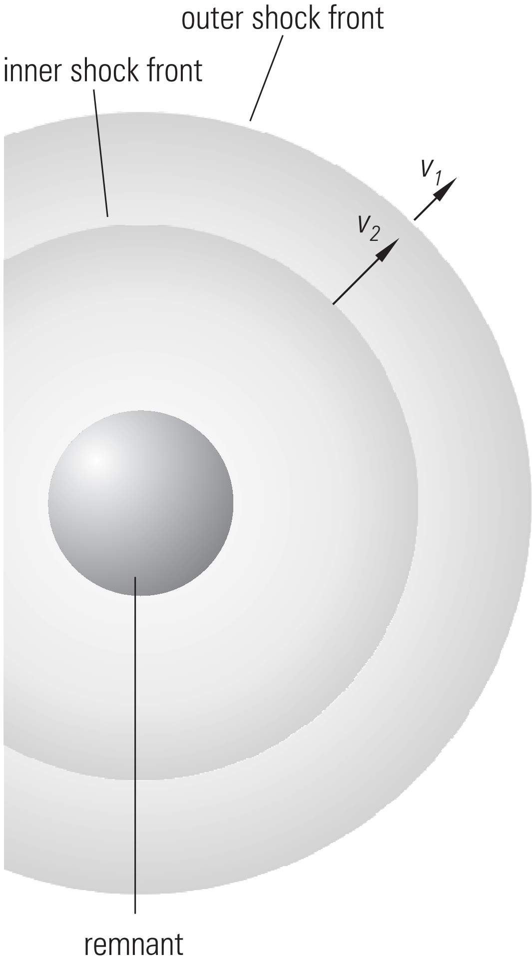

Figure 5.4: Particle acceleration by multiple reflection between two shock fronts

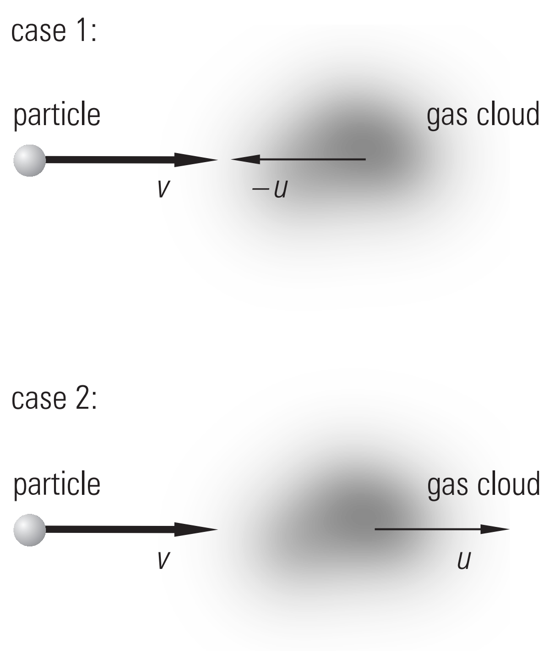

Figure 5.5: Energy gain of a particle by a reflection from a magnetic cloud

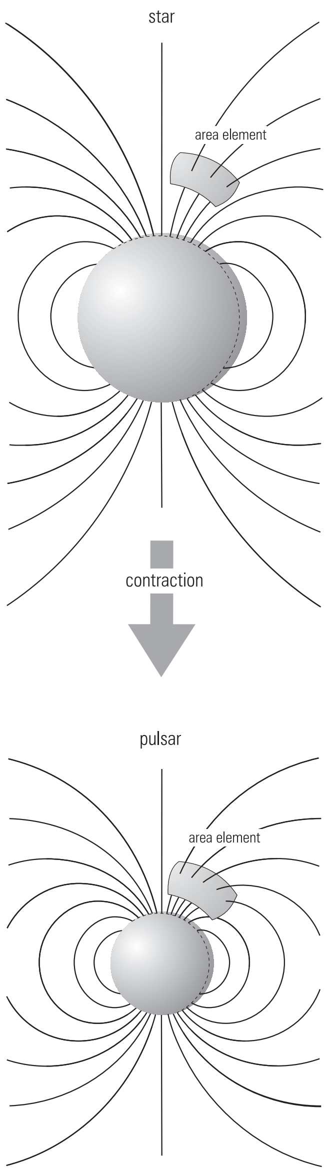

Figure 5.6: Increase of the magnetic field during the gravitational collapse of a star

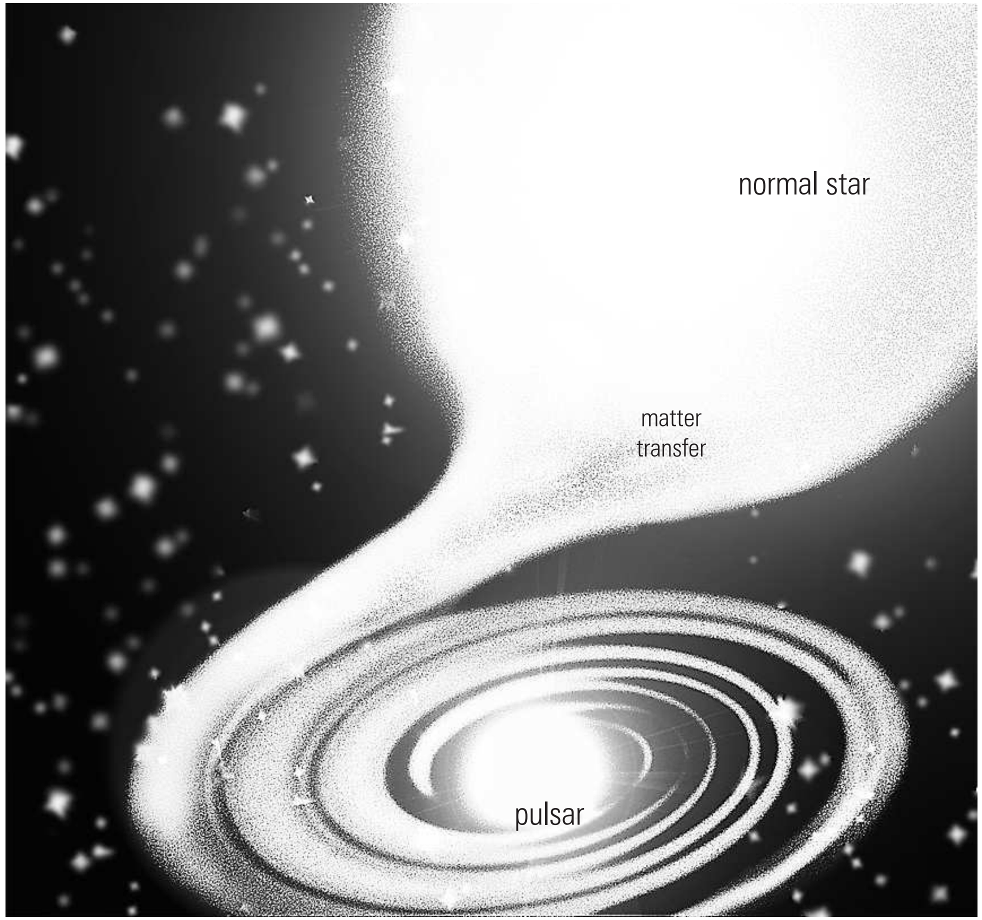

Figure 5.7: Formation of accretion disks in binaries

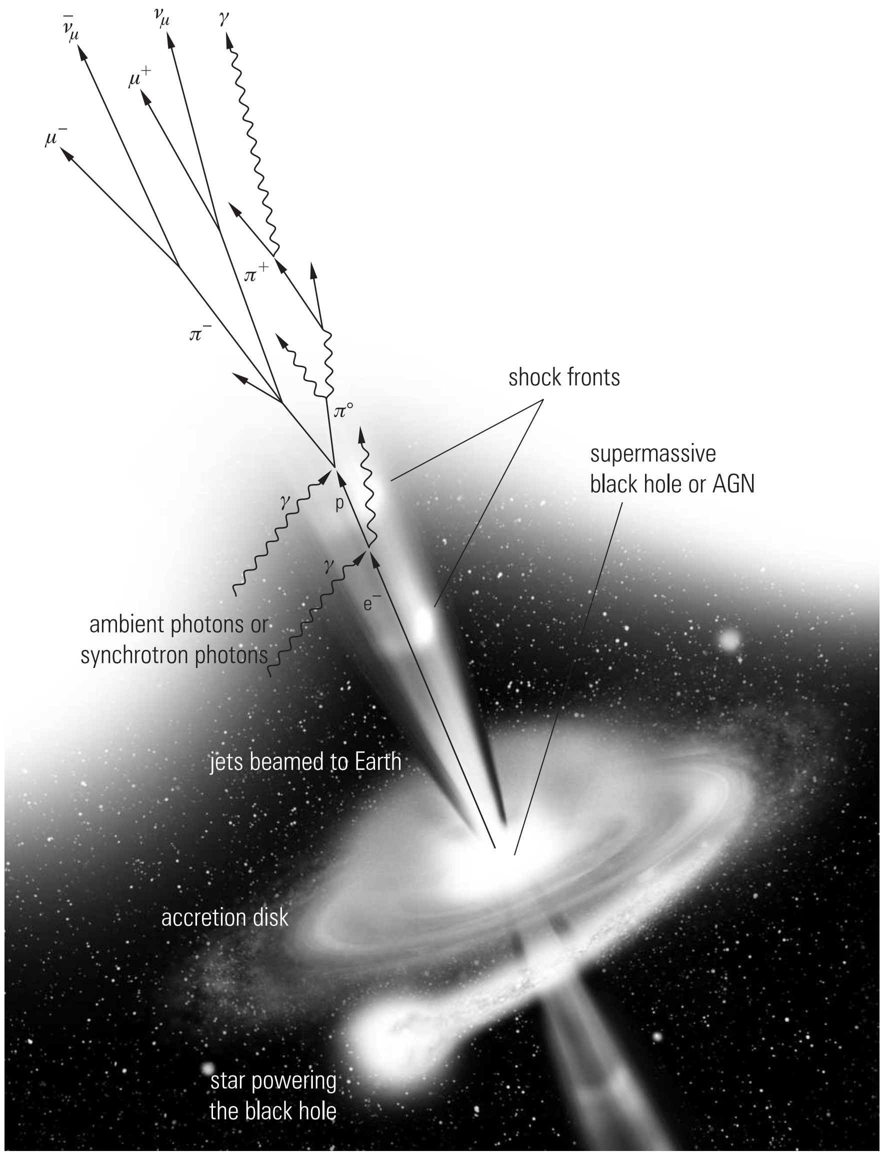

Figure 5.8: Acceleration model for relativistic jets powered by a black hole or an active galactic nucleus (the reactions are only sketched)

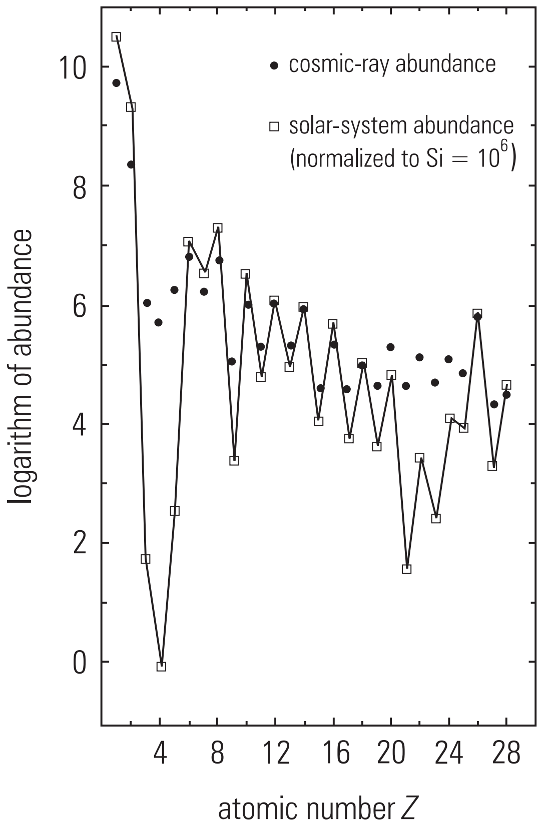

Figure 6.1: Elemental abundance of primary cosmic rays for $1 \leq Z \leq 28$

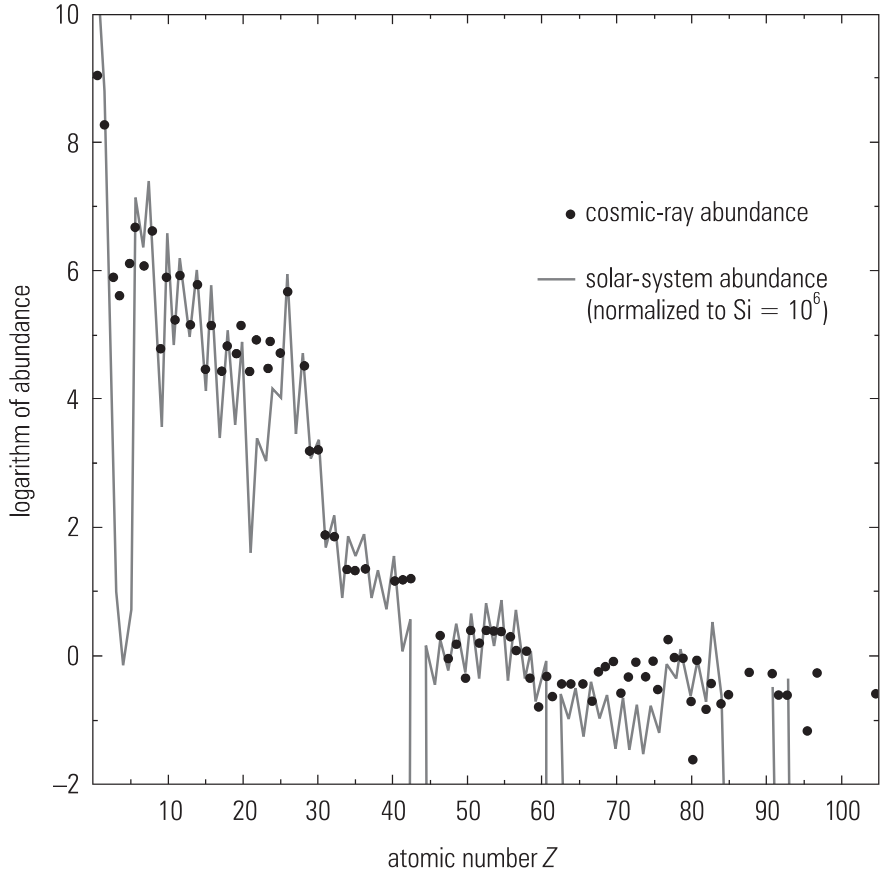

Figure 6.2: Elemental abundance of primary cosmic rays for $1 \leq Z \leq 100$

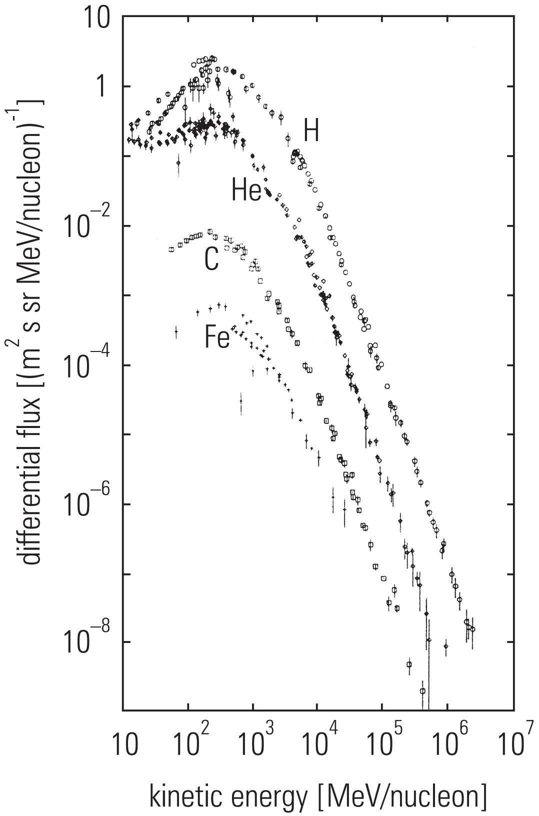

Figure 6.3: Energy spectra of the main components of charged primary cosmic rays

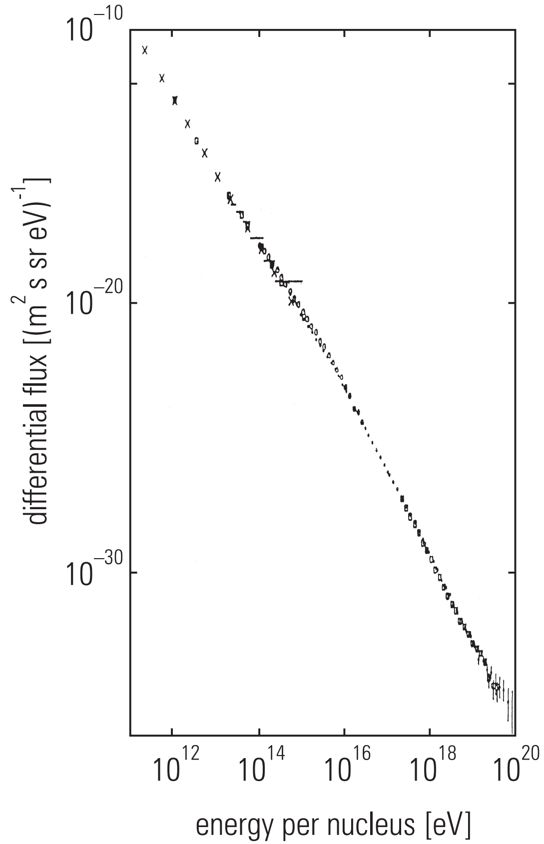

Figure 6.4: Energy spectrum of all particles of primary cosmic rays

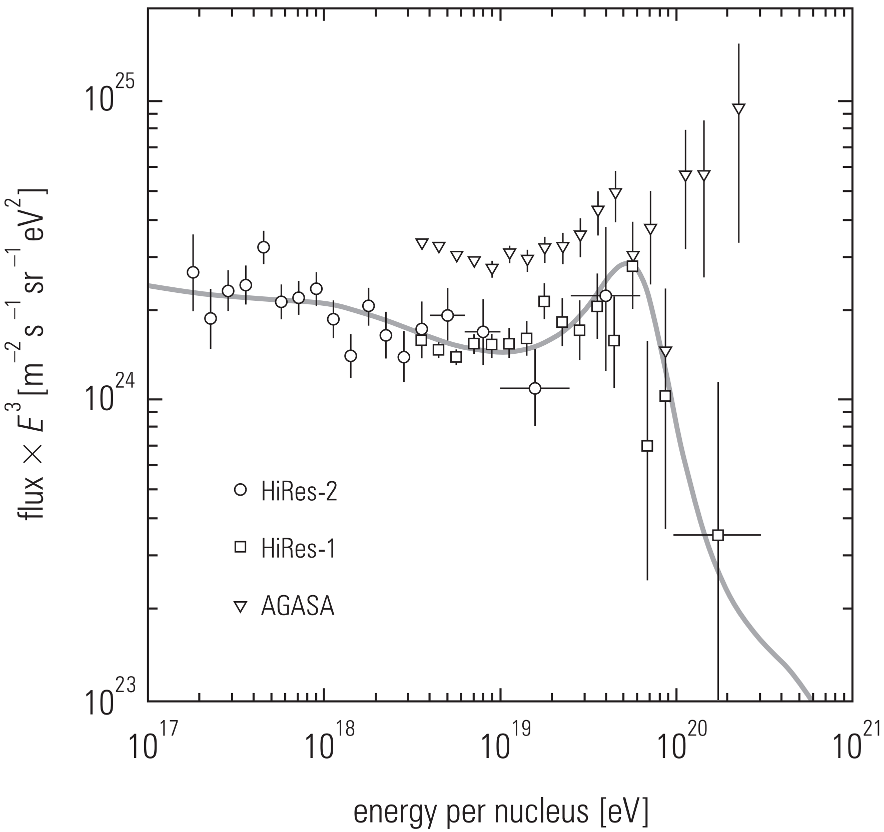

Figure 6.5: Energy spectrum of primary cosmic rays scaled by a factor E^3. The data from the Japanese air-shower experiment AGASA agree well – except at very high energies – with the air-scintillation results of the Utah High Resolution experiment as far as the spectral shape is concerned, but they disagree in absolute intensity (AGASA – Akeno Giant Air Shower Array, HiRes – High Resolution Fly's Eye)

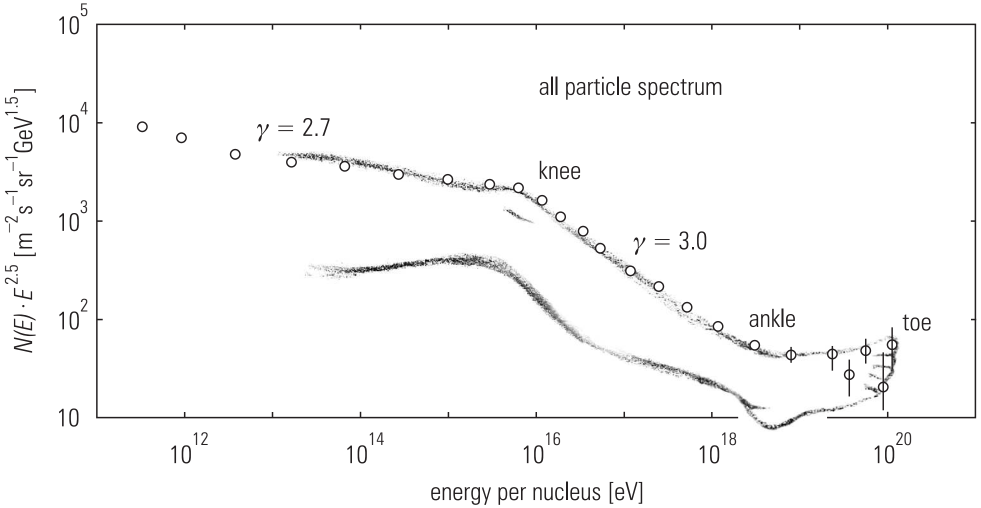

Figure 6.6: Artist's impression of the different structures in the primary cosmic-ray spectrum

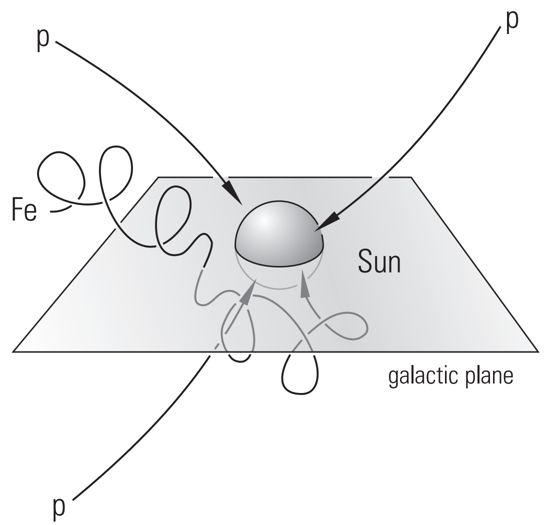

Figure 6.7: Sketch of proton and iron-nucleus trajectories in our Milky Way at 10^{18} eV

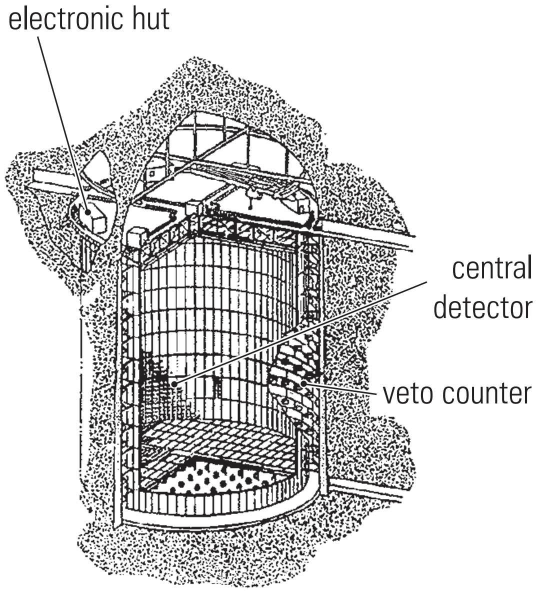

Figure 6.8: The Super-Kamiokande detector in the Kamioka mine in Japan {8}

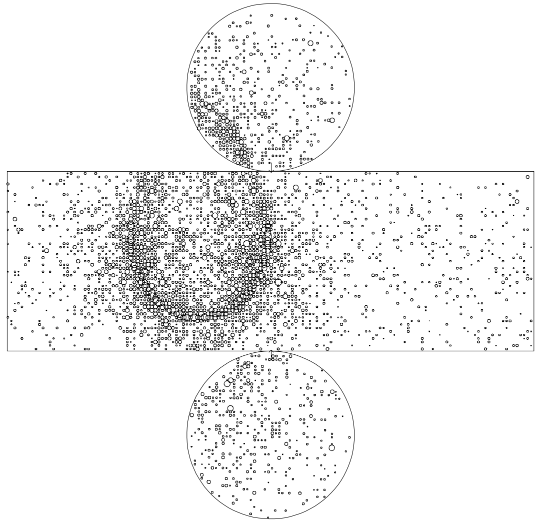

Figure 6.9: Cherenkov pattern of an energetic electron in the Super-Kamiokande Detector {9}

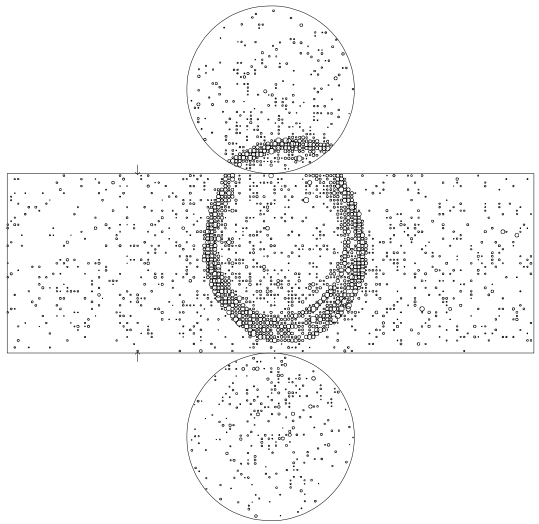

Figure 6.10: Cherenkov pattern for an energetic muon in the Super-Kamiokande detector {9}

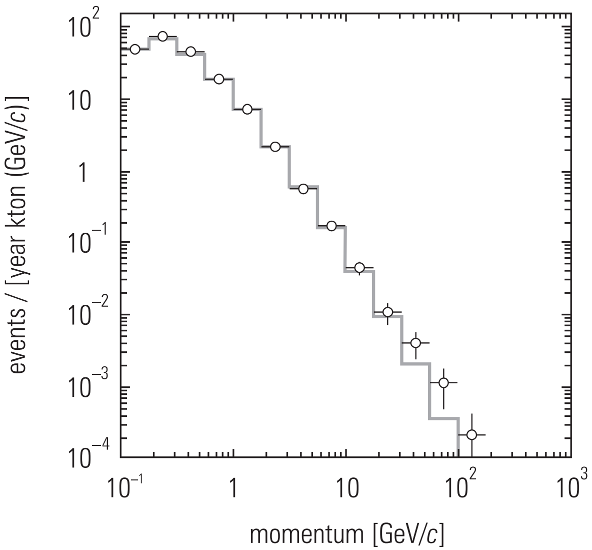

Figure 6.11: Momentum spectrum of single-ring electron-like events in Super-Kamiokande. The *solid line* represents the Monte Carlo expectation {9}

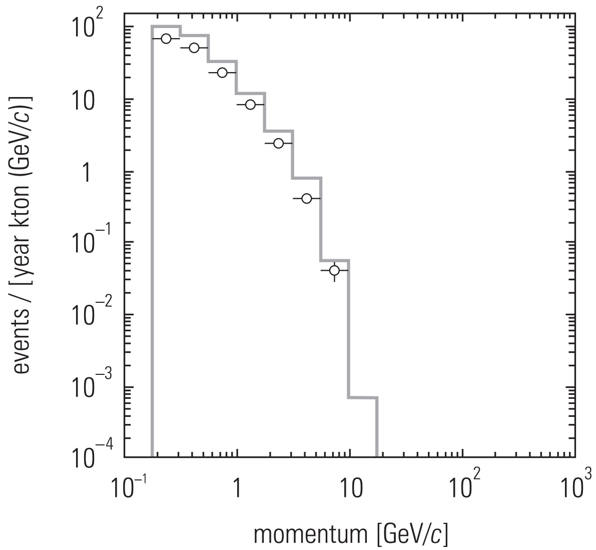

Figure 6.12: Momentum spectrum of single-ring muon-like events in Super-Kamiokande. The *solid line* represents the Monte Carlo expectation. The cutoff arround 10 GeV originates from the condition that the muon tracks must be contained in the detector {9}

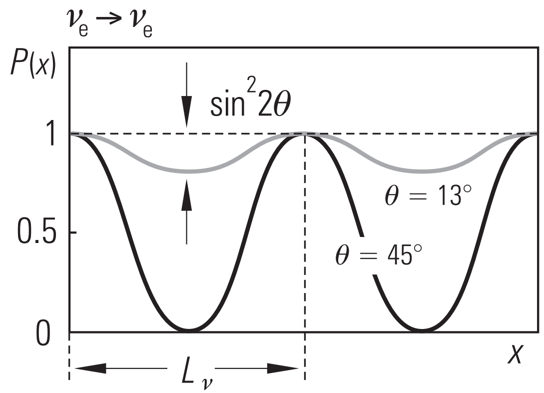

Figure 6.13: Oscillation model for ν_e–ν_μ mixing for different mixing angles

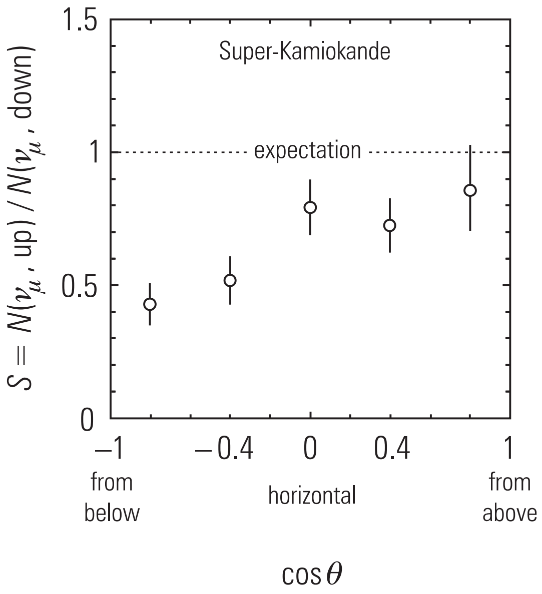

Figure 6.14: Ratio of ν_μ fluxes as a function of zenith angle as measured in the Super-Kamiokande experiment

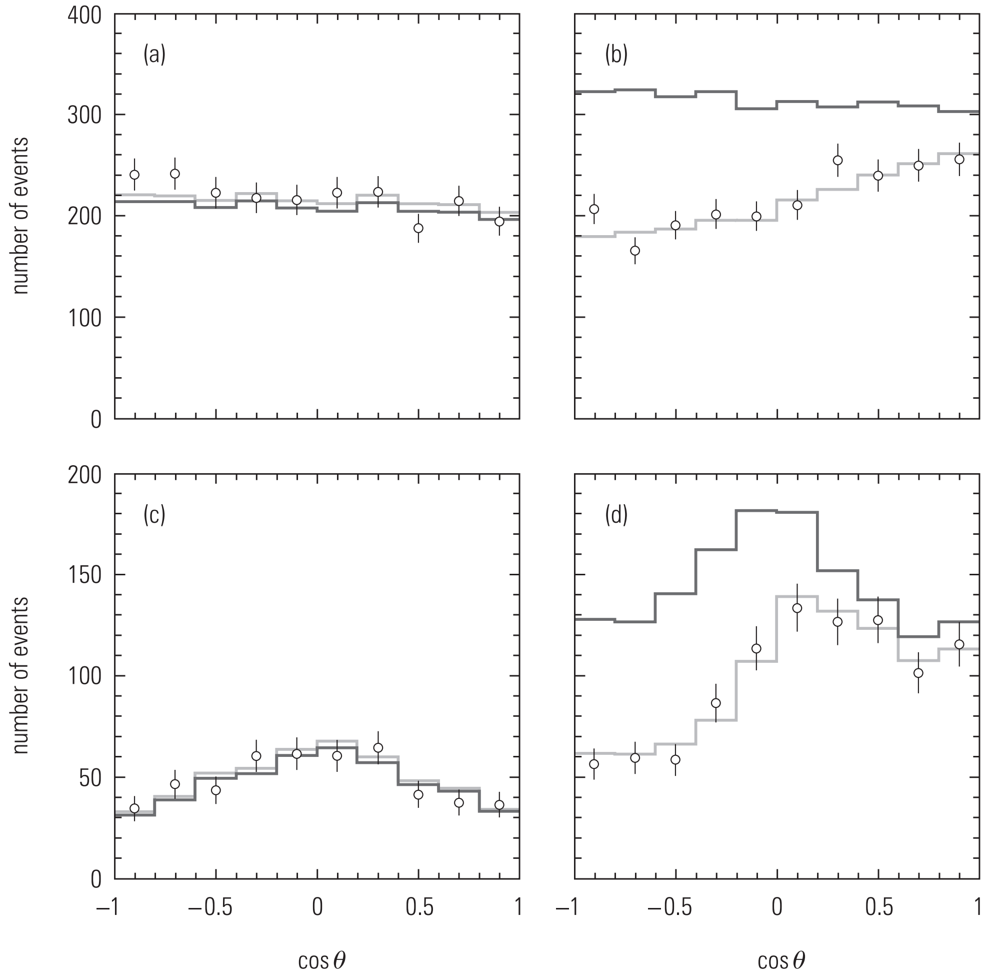

Figure 6.15: Zenith-angle distribution of electron-like and muon-like events for the sub-GeV range (**a:** electrons, **b:** muons) and the multi-GeV range (**c:** electrons, **d:** muons) in Super-Kamiokande. The *dark grey line* is the expectation for the null hypothesis (no oscillations) while the *light grey histogram* represents the expectation for oscillations with maximal mixing ($\sin^2 2\theta = 1$) and $\delta m^2 = 3 \times 10^{-3}\,\mathrm{eV}^2$ {9}

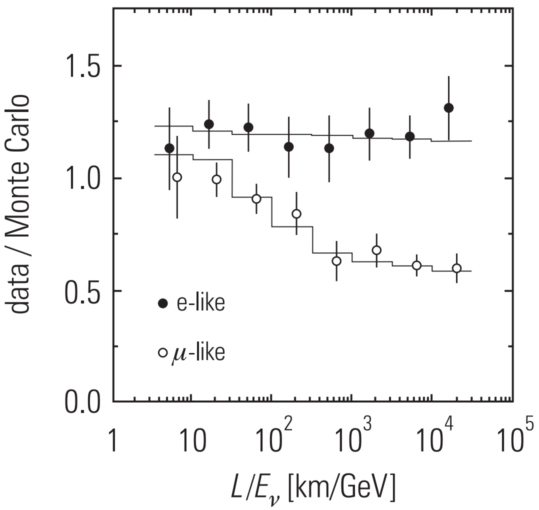

Figure 6.16: Ratio of fully contained events measured in the Super-Kamiokande detector as a function of the reconstructed value of distance over energy (L/E_ν). The *lower histogram* for μ-like events corresponds to the expectation for $\nu_\mu \leftrightarrow \nu_\tau$ oscillations with $\delta m^2 = 2.2 \times 10^{-3}\,\mathrm{eV}$ and $\sin 2\theta = 1$ {10}

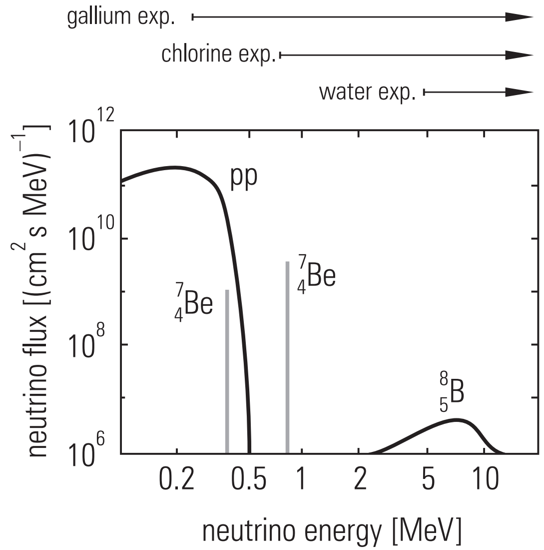

Figure 6.17: Neutrino spectra from solar fusion processes. The reaction thresholds of the gallium, chlorine, and water Cherenkov experiments are indicated. The line fluxes of beryllium isotopes are given in units of $\mathrm{cm}^{-2}\,\mathrm{s}^{-1}$

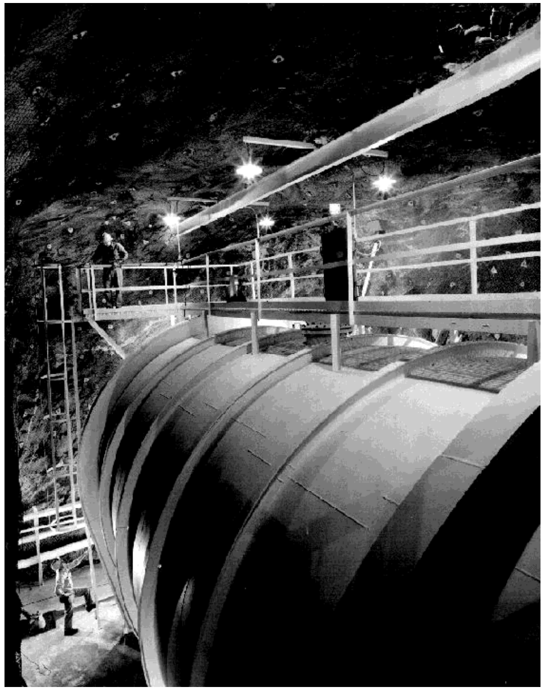

Figure 6.18: The detector of the chlorine experiment of R. Davis for the measurement of solar neutrinos. The detector is installed at a depth of 1400 m in the Homestake Mine in South Dakota. It is filled with 380 000 liters of perchlorethylene {11}

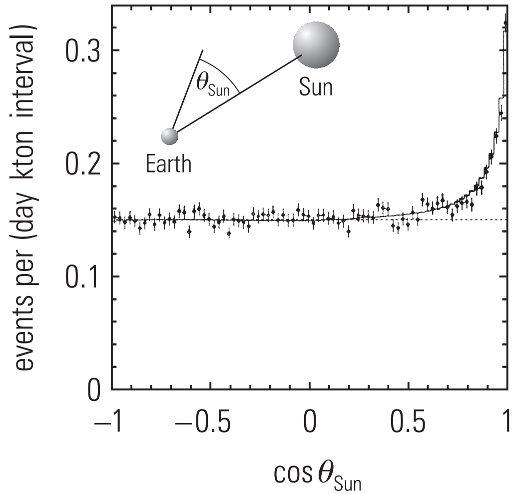

Figure 6.19: Arrival directions of neutrinos measured in the Super-Kamiokande experiment

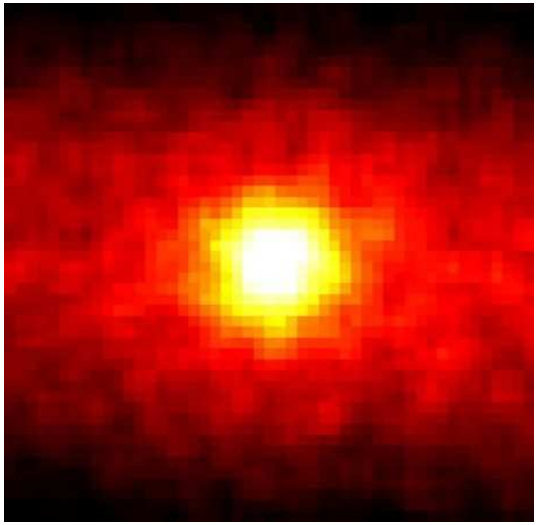

Figure 6.20: Reconstructed image of the Sun in the light of solar neutrinos. Due to the limited spatial and angular resolution of Super-Kamiokande, the image of the Sun appears larger than it really is {12}

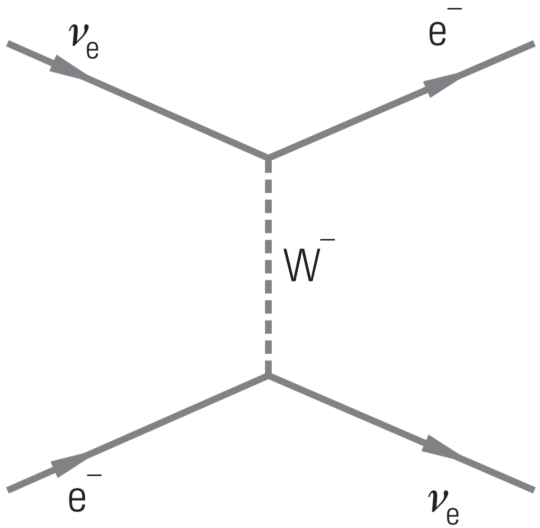

Figure 6.21: Feynman diagram responsible for matter oscillation (MSW effect). Given the energy of solar neutrinos and the fact that there are only target electrons in the Sun, this process can only occur for ν_e, but not for ν_μ or ν_τ

Figure 6.22: Supernova 1987A in the Tarantula Nebula {6}

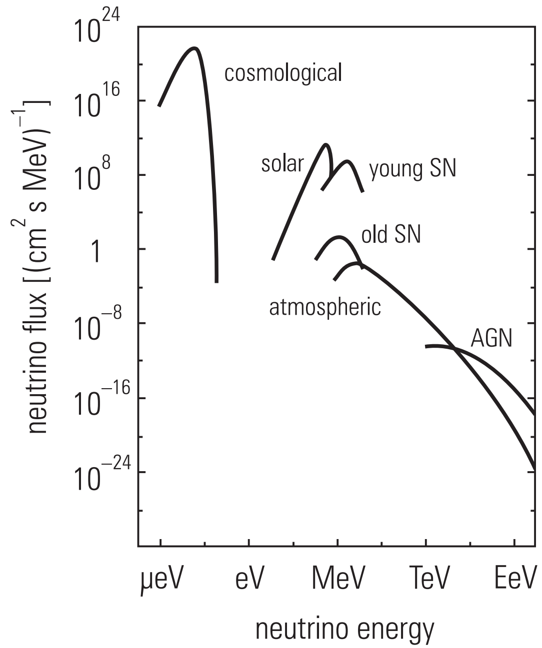

Figure 6.23: Comparison of cosmic neutrino fluxes in different energy domains

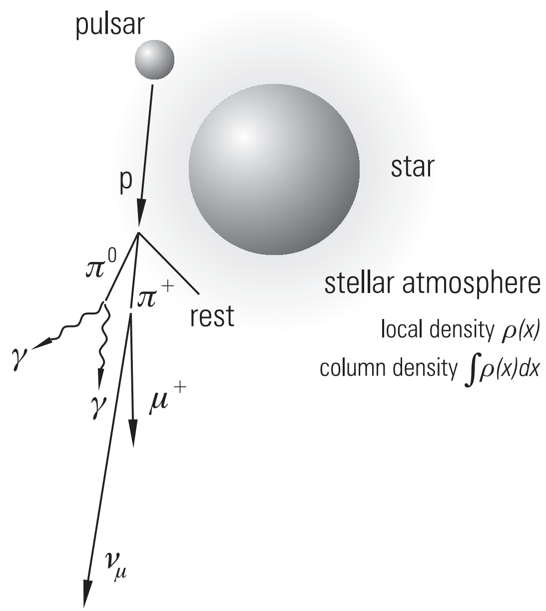

Figure 6.24: Production mechanism of high-energy neutrinos in a binary system

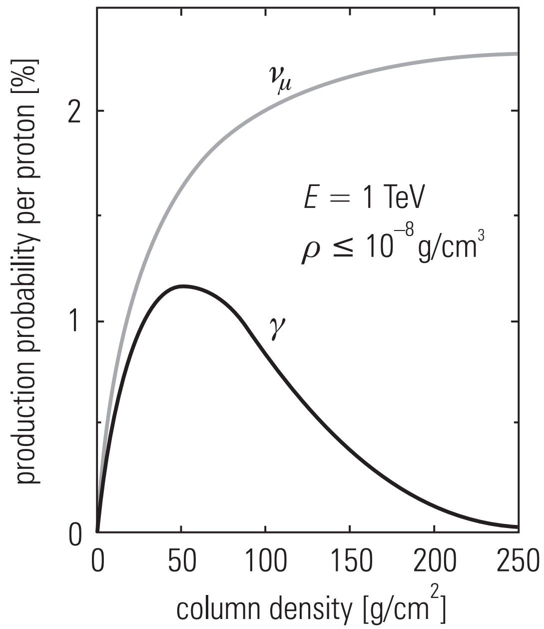

Figure 6.25: Competition between production and absorption of photons and neutrinos in a binary system

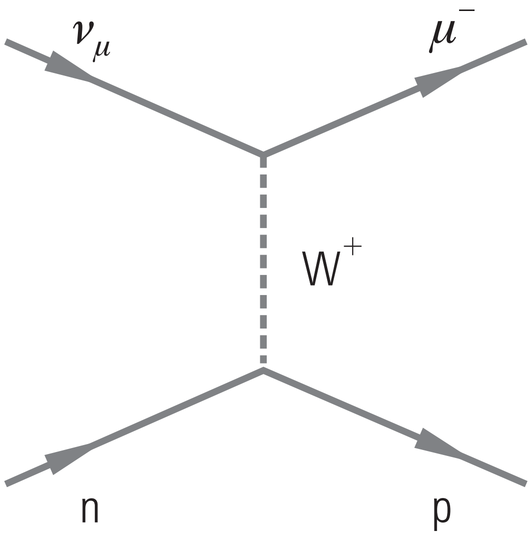

Figure 6.26: Reaction for muon neutrino detection

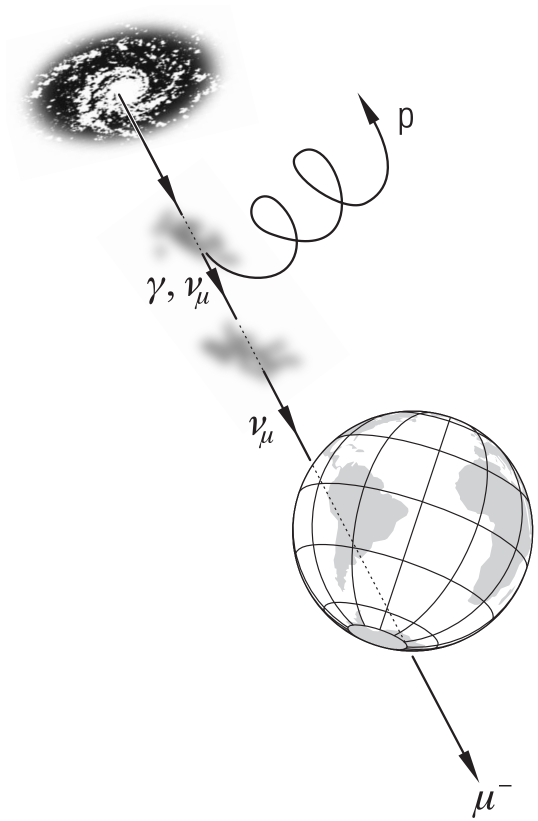

Figure 6.27: Neutrino production, propagation in intergalactic space, and detection at Earth

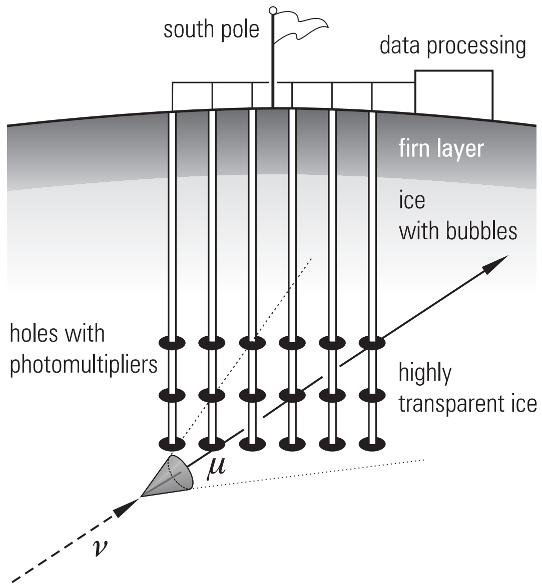

Figure 6.28: Sketch of a neutrino detector for high-energy extragalactic neutrinos

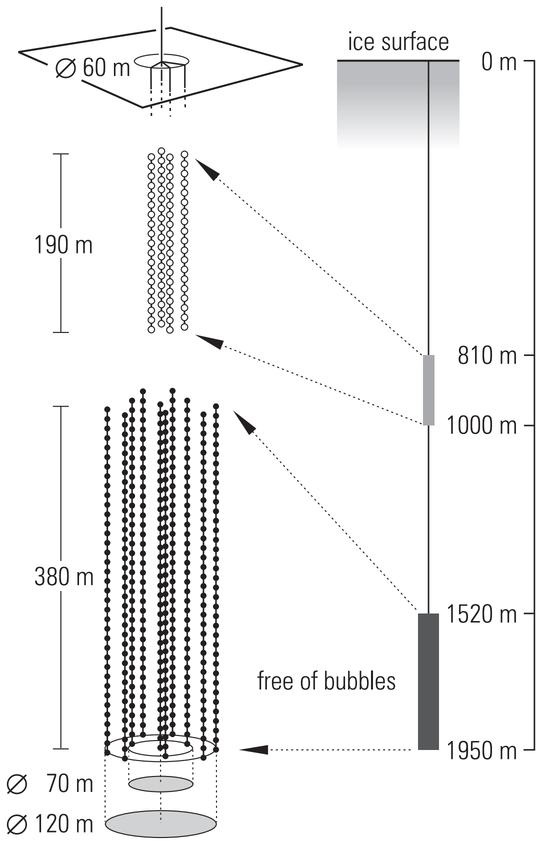

Figure 6.29: Setup of the AMANDA detector at the Sourth Pole (AMANDA – Antarctic Muon And Neutrino Detector Array)

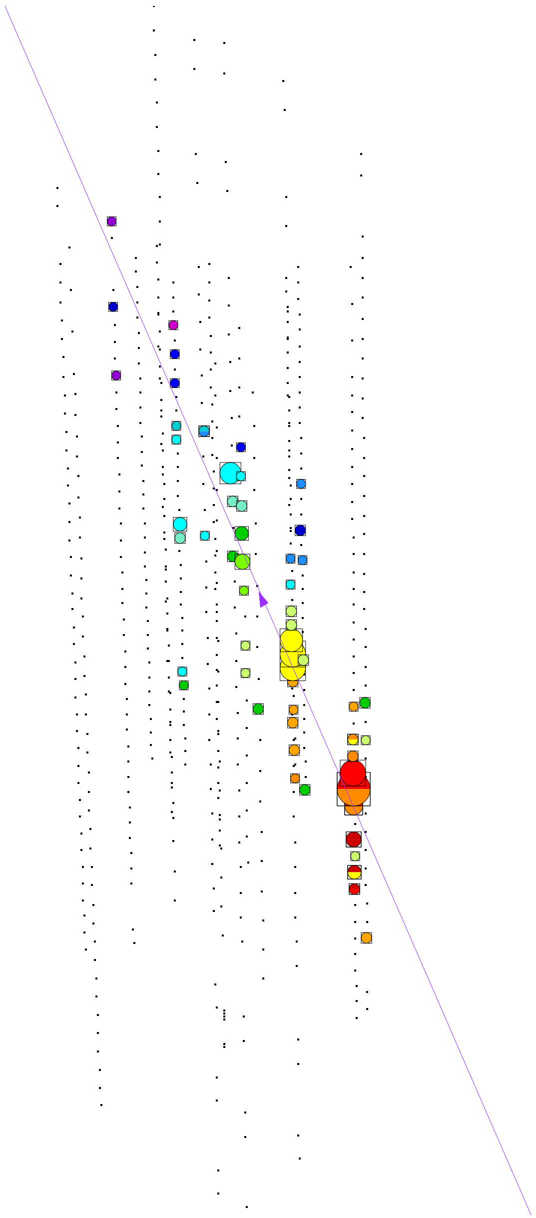

Figure 6.30: A neutrino-induced upward-going muon recorded in AMANDA. The size of the symbols is proportional to the measured Cherenkov light {13}

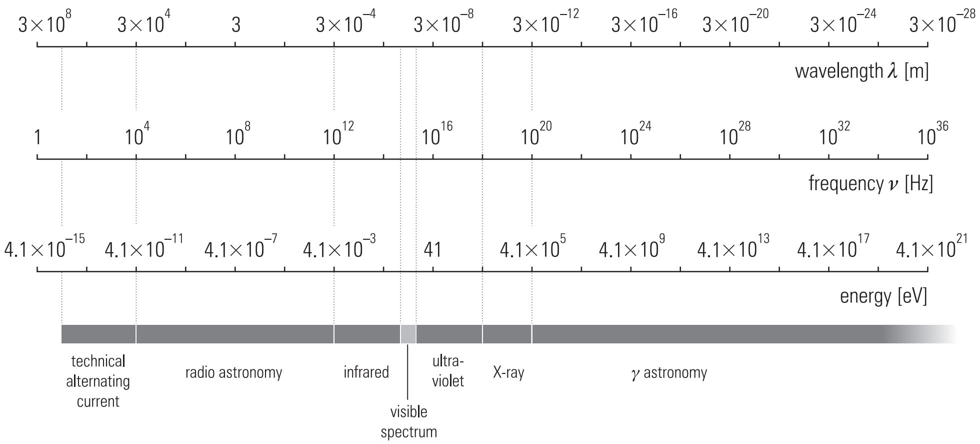

Figure 6.31: Spectral range of electromagnetic radiation

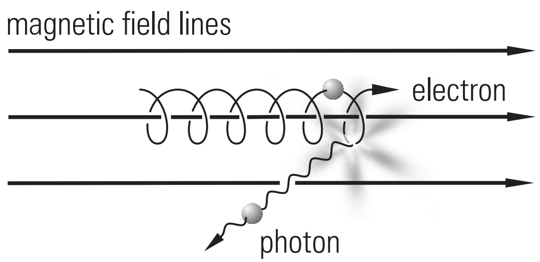

Figure 6.32: Production of synchrotron radiation by deflection of charged particles in a magnetic field

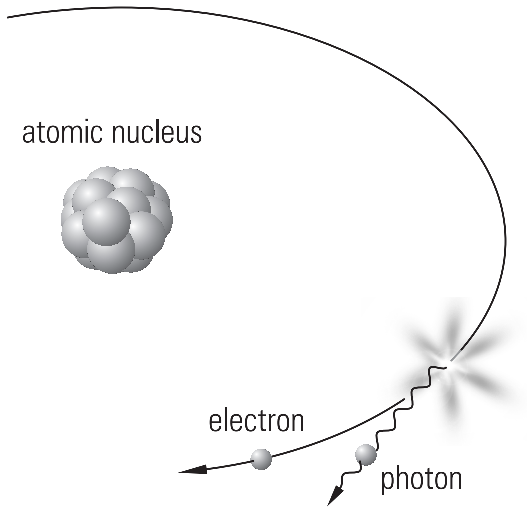

Figure 6.33: Production of bremsstrahlung by deflection of charged particles in the Coulomb field of a nucleus

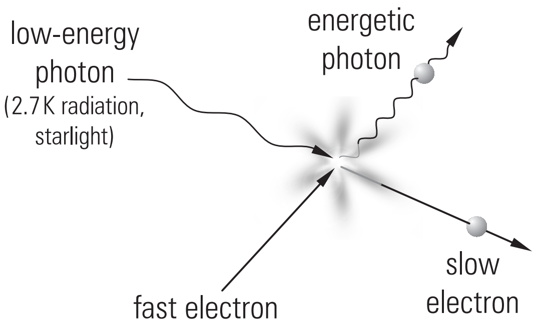

Figure 6.34: Collision of an energetic electron with a low-energy photon. The electron transfers part of its energy to the photon and is consequently slowed down

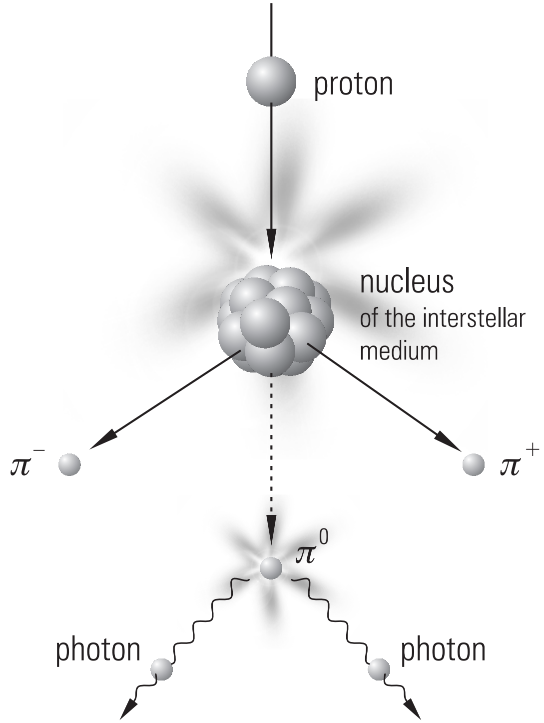

Figure 6.35: π^0 production in proton interactions and π^0 decay into two photons

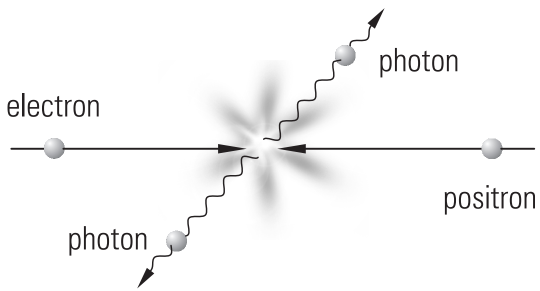

Figure 6.36: e^+e^- pair annihilation into two photons

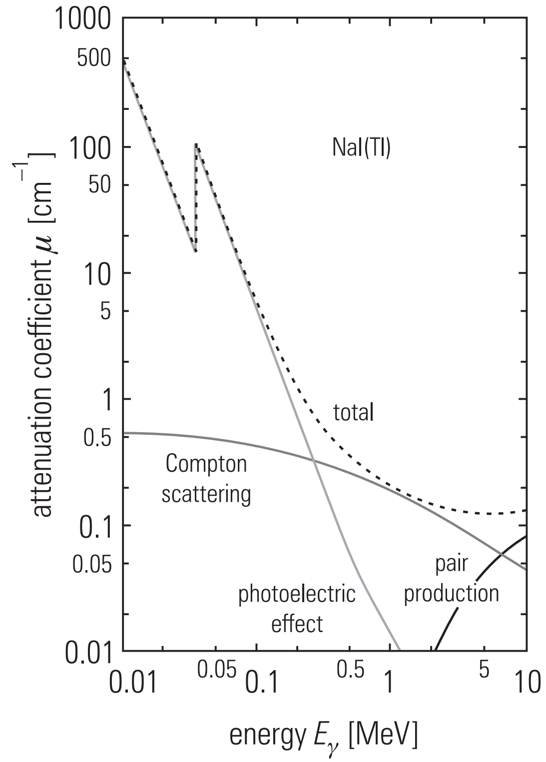

Figure 6.37: Mass attenuation coefficient for photons in a sodium-iodide scintillation counter

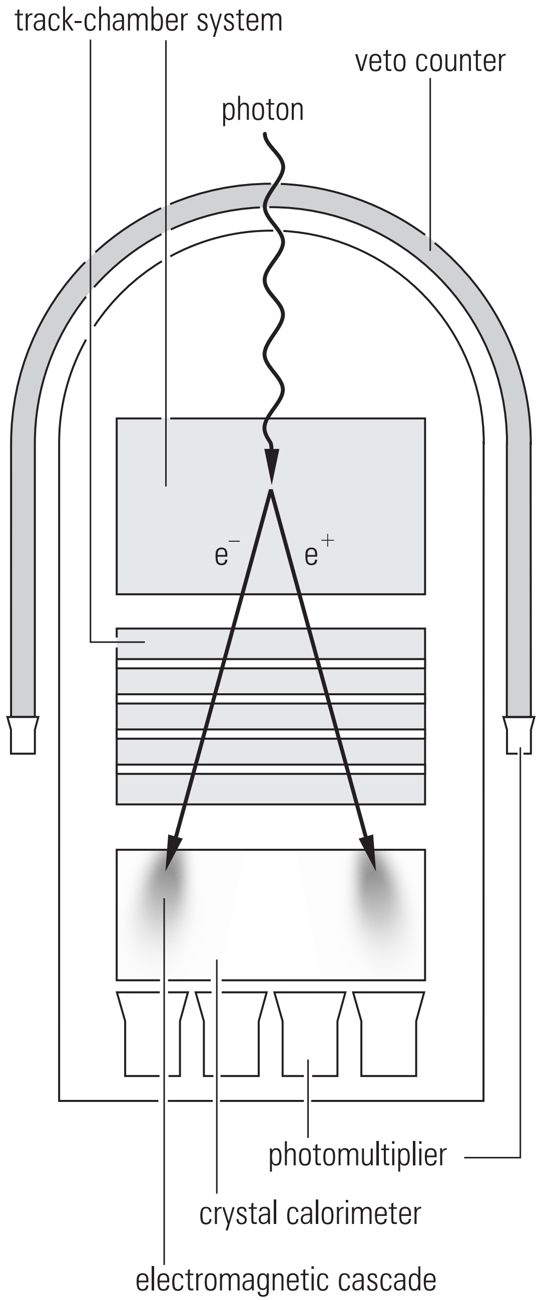

Figure 6.38: Sketch of a satellite experiment for the measurement of γ rays in the GeV range

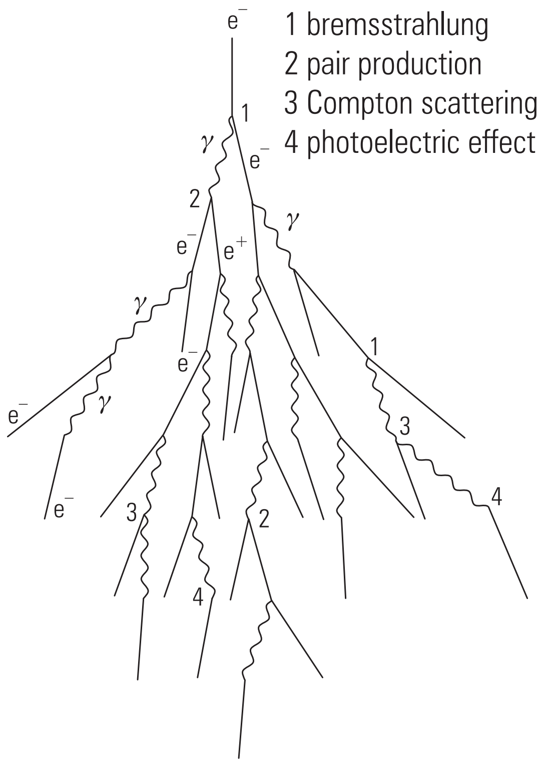

Figure 6.39: Schematic representation of an electron cascade

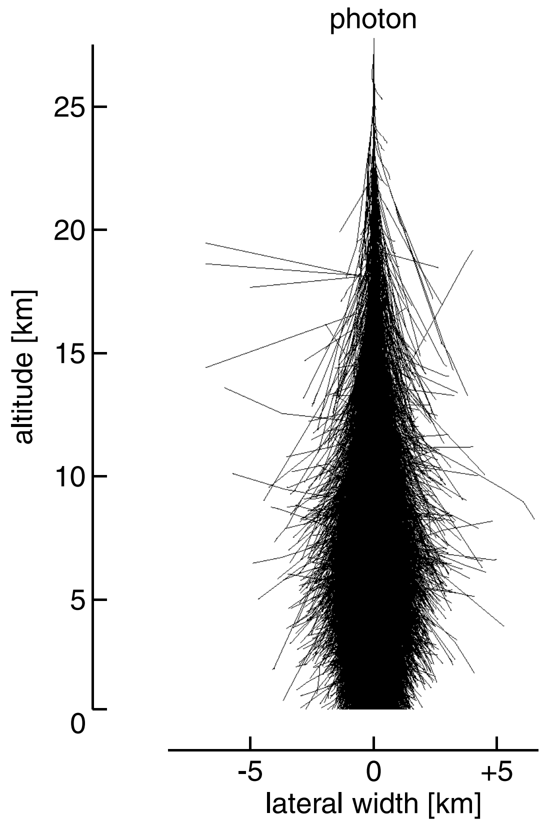

Figure 6.40: Monte Carlo simulation of an electromagnetic shower in the atmosphere initiated by a photon of energy 10^{14} eV. All secondaries with energies $E \geq 3\,\mathrm{MeV}$ are shown {14}

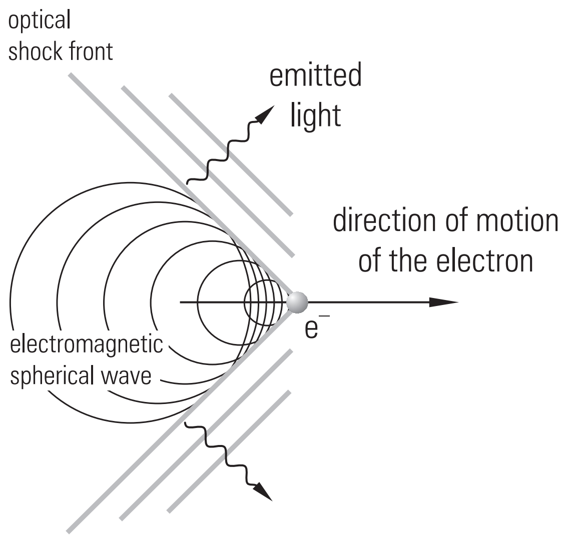

Figure 6.41: Emission of Cherenkov radiation in an optical shock wave by particles traversing a medium of refractive index n with a velocity exceeding the velocity of light in that medium ($v > c/n$)

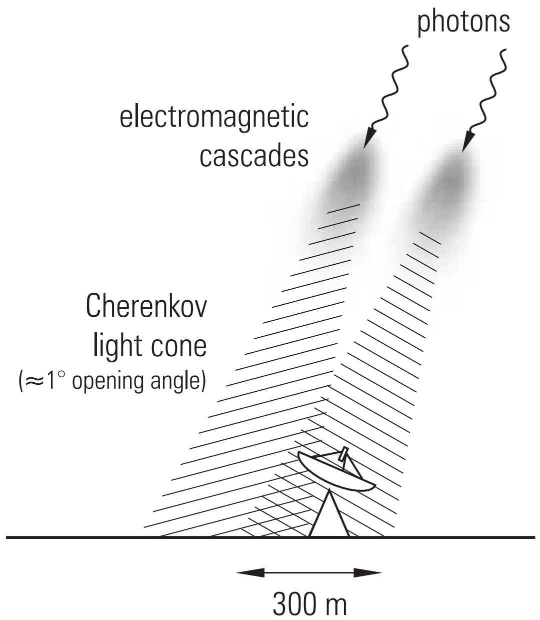

Figure 6.42: Measurement of Cherenkov light of photon-induced electromagnetic cascades in the atmosphere

Figure 6.43: Photograph of the air Cherenkov telescope CANGAROO (CANGAROO – Collaboration of Australia and Nippon (Japan) for a GAmma-Ray Observatory in the Outback) {15}

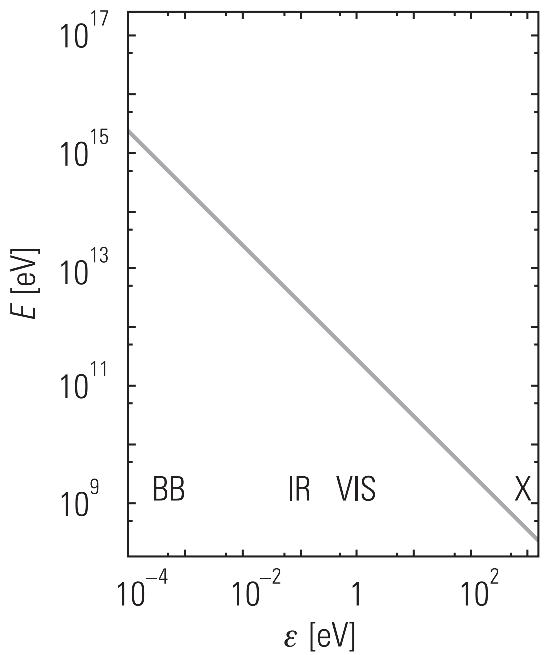

Figure 6.44: Dependence of the threshold energy E for $\gamma\gamma$ absorption on the energy of the target photons (BB – blackbody radiation, IR – infrared, VIS – visible spectral range, X – X rays

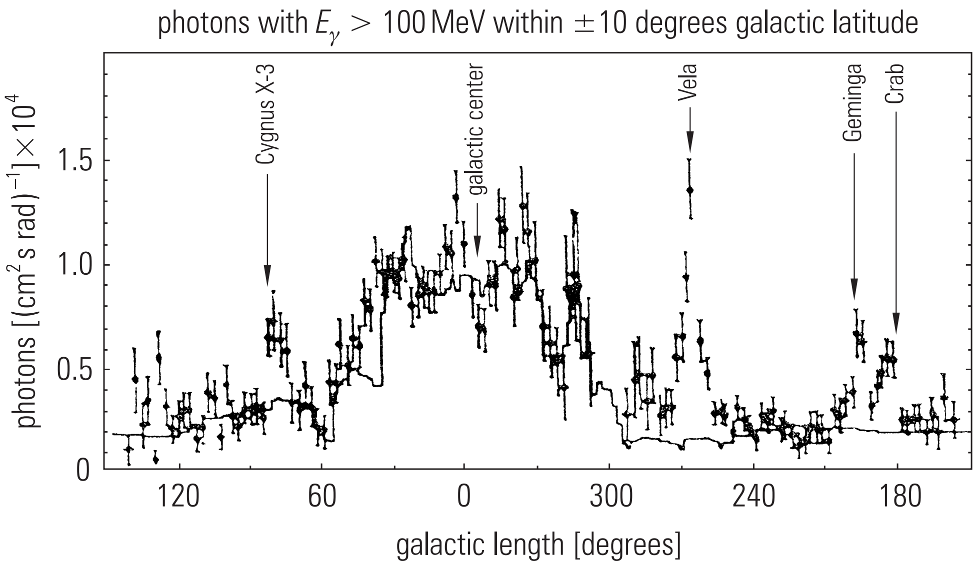

Figure 6.45: Measurement of the intensity of galactic γ radiation for photon energies $> 100\,\text{MeV}$. The *solid line* represents the expected γ-ray intensity on the basis of the column density of interstellar gas in that direction

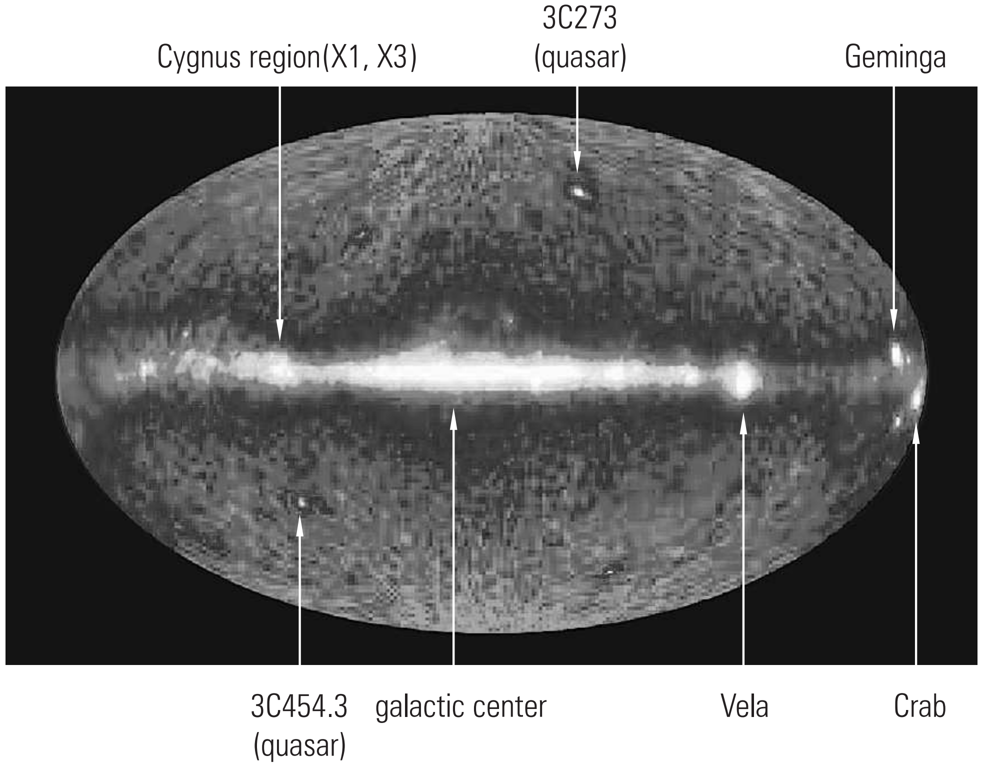

Figure 6.46: All-sky survey in the light of γ rays {16}

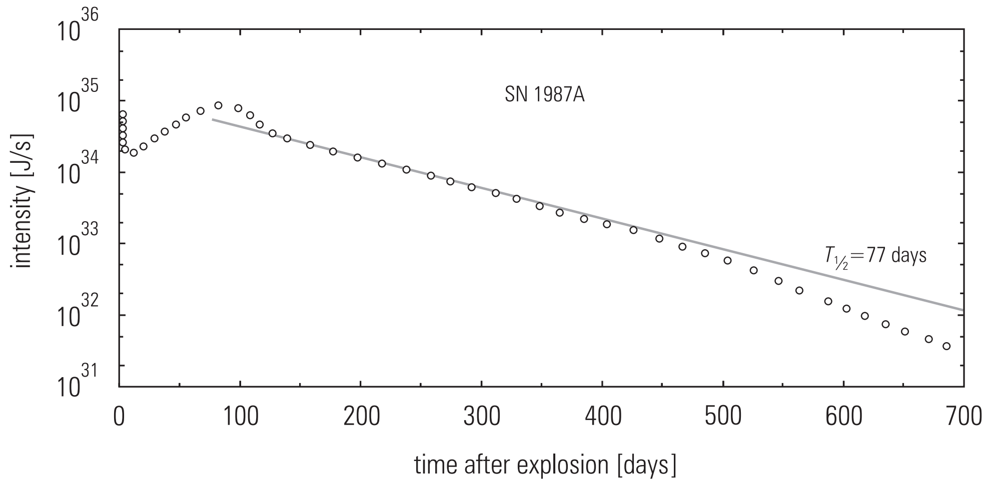

Figure 6.47: Light curve of SN 1987A. The *solid line* corresponds to complete conversion of ^{56}Co γ rays into the infrared, optical, and ultraviolet spectral range

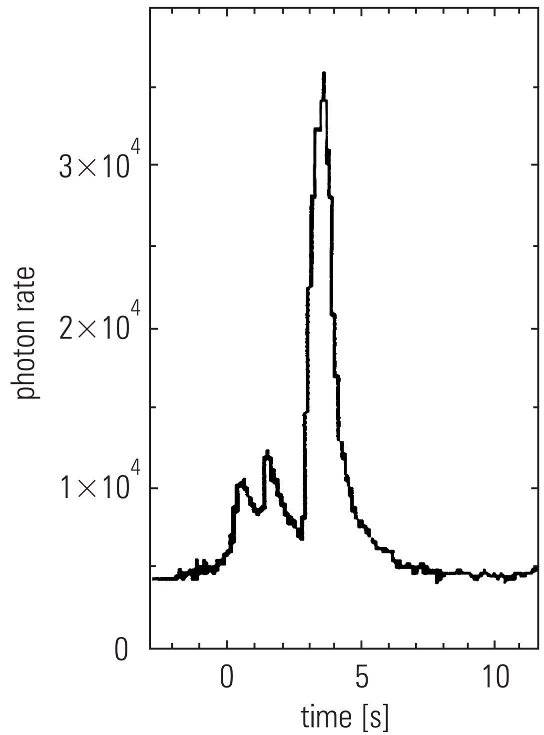

Figure 6.48: Light curve of a typcial γ-ray burst

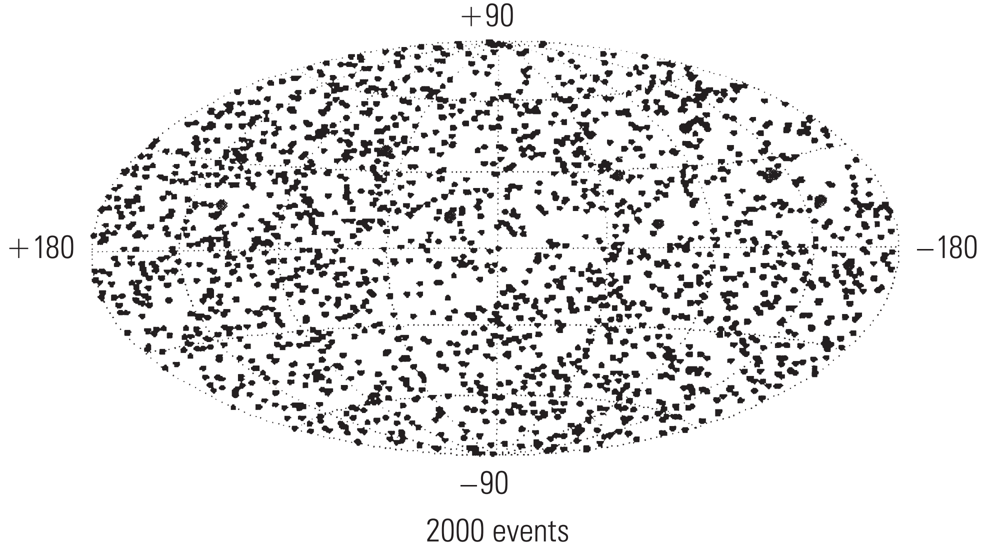

Figure 6.49: Angular distribution of 2000 γ-ray bursts in galactic coordinates recorded with the BATSE detector (Burst And Transient Source Experiment) on board the CGRO satellite (Compton Gamma Ray Observatory) {17}

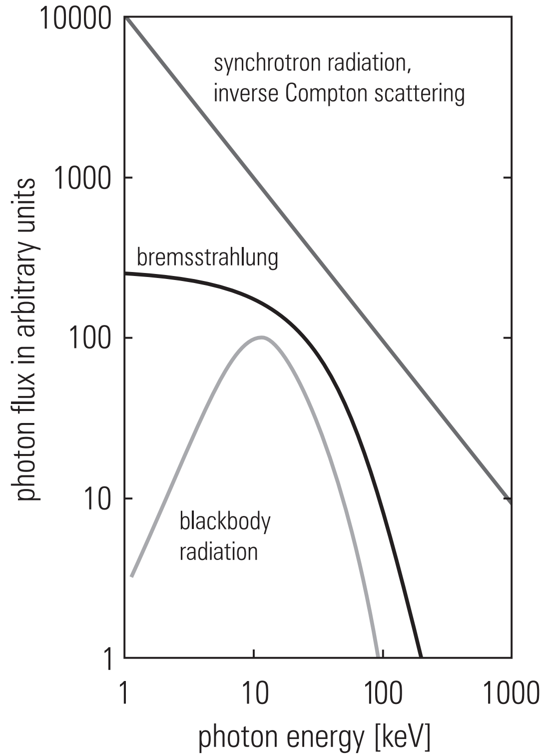

Figure 6.50: Standard X-ray spectra originating from various production processes

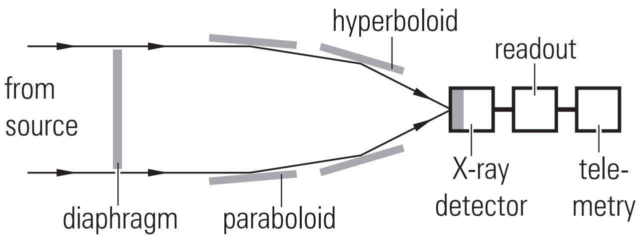

Figure 6.51: Cross section through an X-ray telescope with parabolic and hyperbolic mirrors

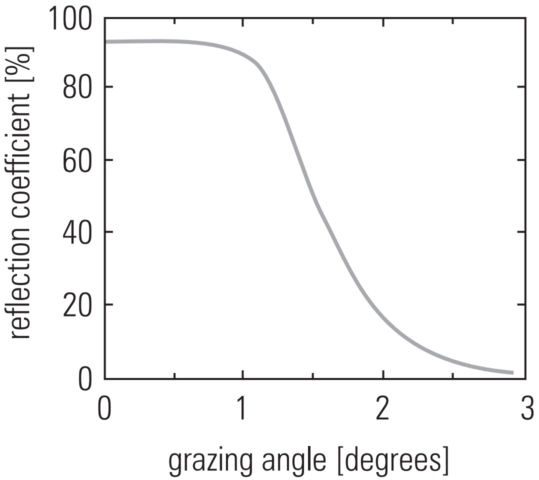

Figure 6.52: Angular-dependent reflection power of metal mirrors

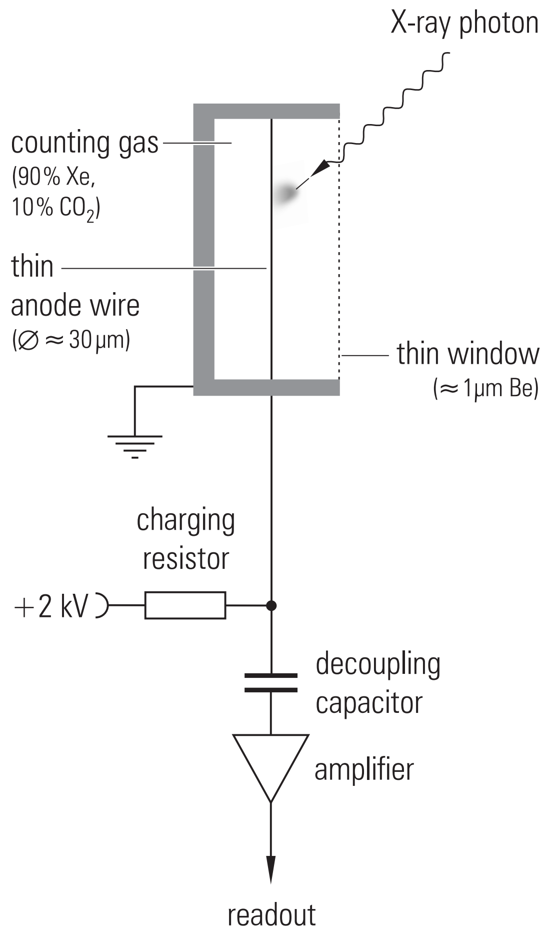

Figure 6.53: Principle of operation of a proportional counter

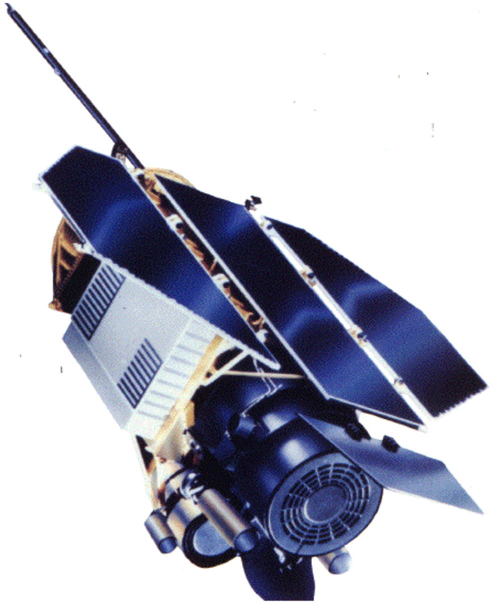

Figure 6.54: Photograph of the X-ray satellite ROSAT {18}

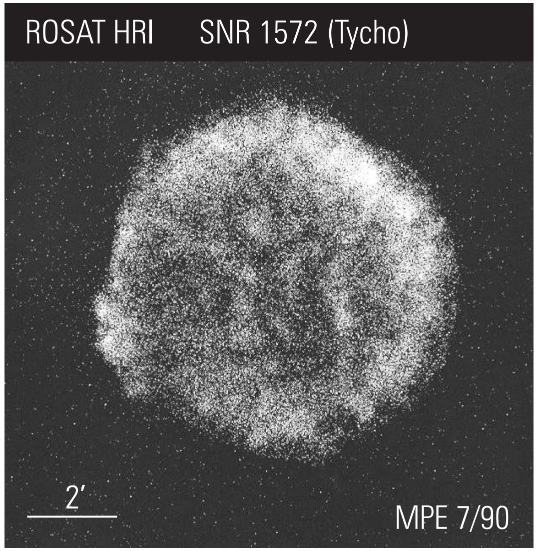

Figure 6.55: Supernova remnant SNR 1572 recorded with the HRI detector (High Resolution Instrument) on board the ROSAT satellite {18}

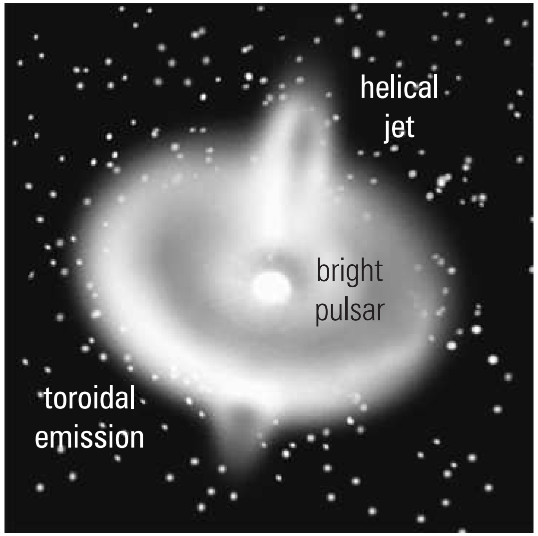

Figure 6.56: Sketch of X-ray emission from the Crab pulsar

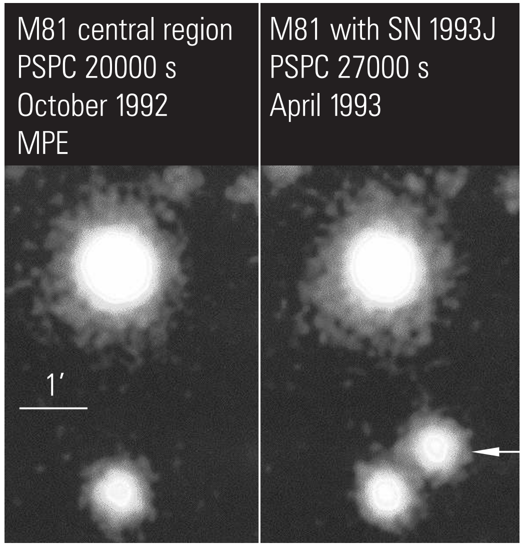

Figure 6.57: Sprial galaxy M81 with the supernova SN 1993J. The image was recorded with the PSPC detector (Position Sensitive Proportional Counter) of the ROSAT satellite {18}

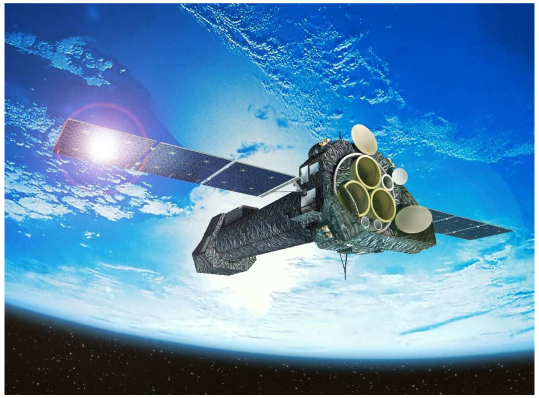

Figure 6.58: Photo of the XMM X-ray satellite {19}

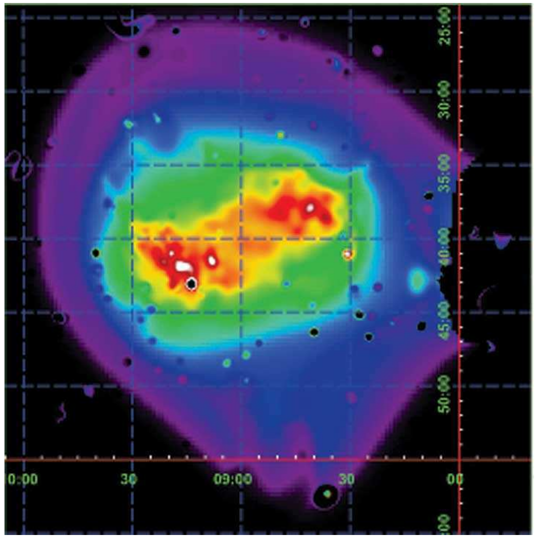

Figure 6.59: Collision of two merging galactic clusters, each containing hundreds of galaxies. The site of this catastophic event is Abell 754 at a distance of about 9 million light-years. The photo shows a coded pressure map of this region, where the galaxies themselves are confined around the white spots which correspond to regions of high pressure, followed by decreasing pressure as one goes away from the centers {20}

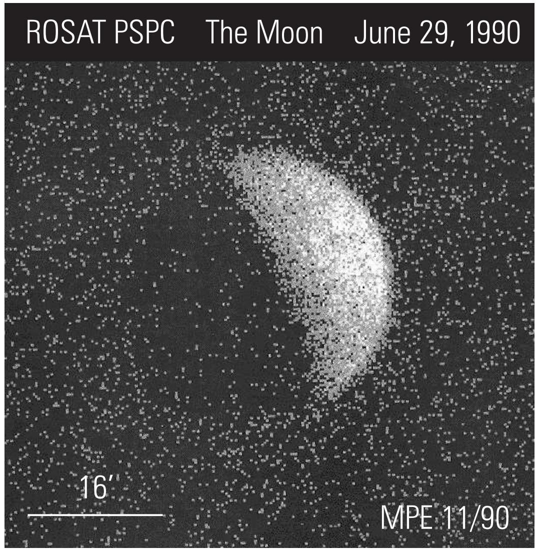

Figure 6.60: X-ray emission from the Moon recorded with the PSPC detector on board of ROSAT. The dark side of the Moon shields the cosmic X-ray background {18}

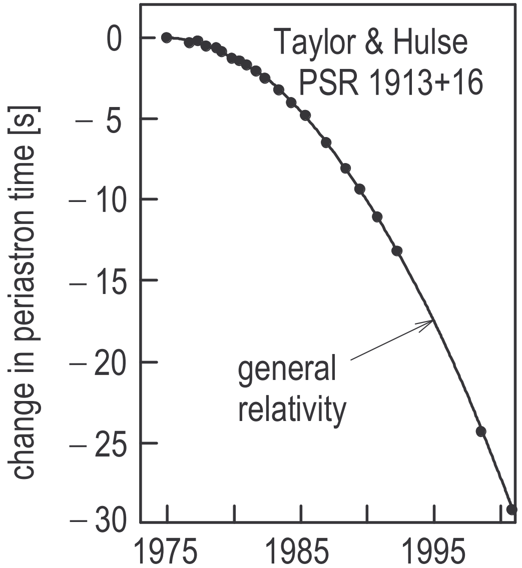

Figure 6.61: Observed changes in periastron time of the binary system PSR 1913+16 over more than 20 years in comparison to the expectation based on Einstein's theory of general relativity. The agreement between theory and observation is better than 0.1%

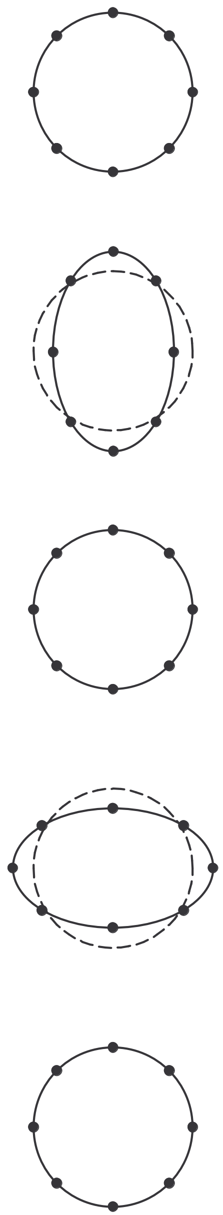

Figure 6.62: Oscillation modes of a spherical antenna upon the impact of a gravitational wave causing it to undergo quadrupole oscillations

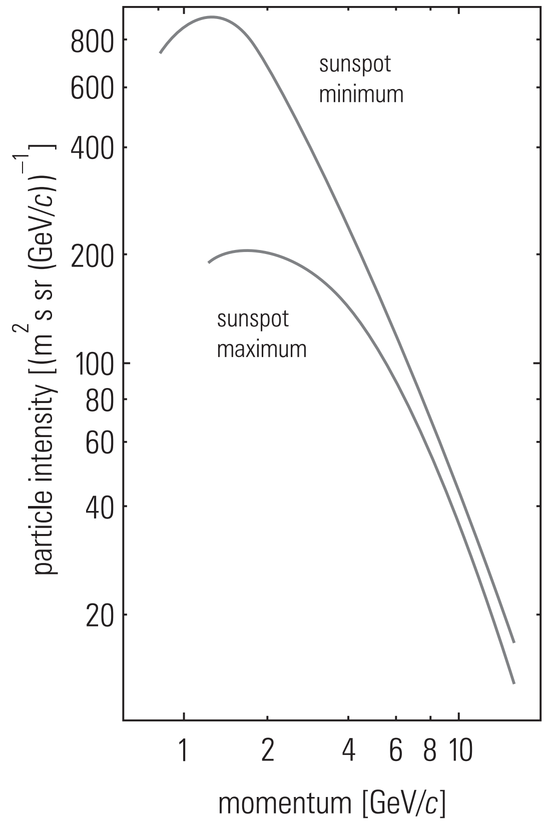

Figure 7.1: Modulation of the primary spectrum by the 11-year cycle of the Sun

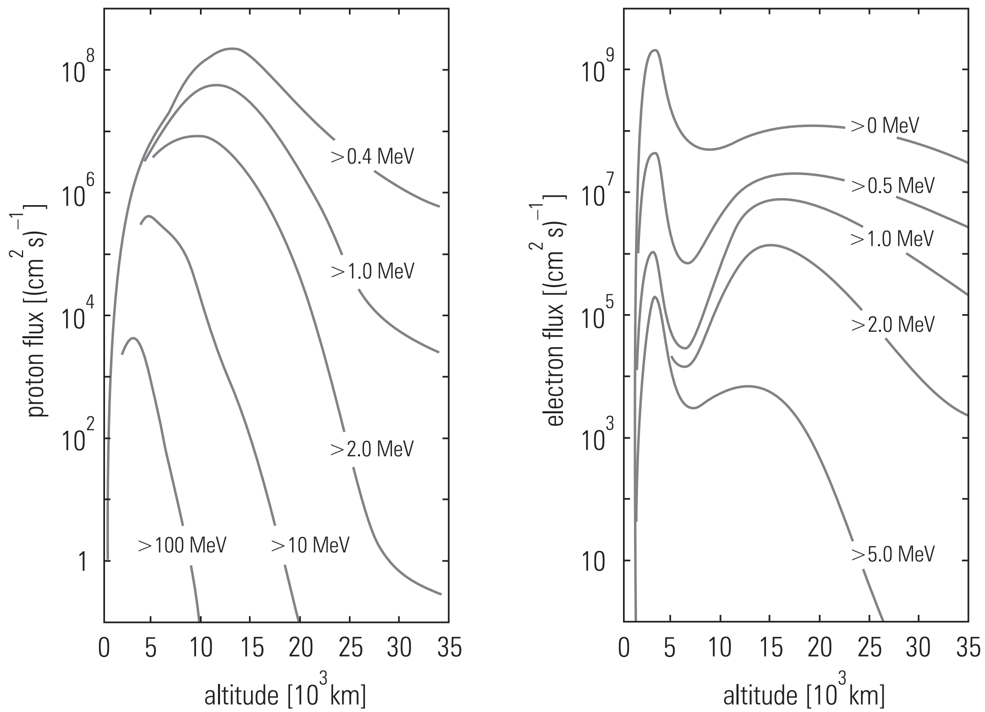

Figure 7.2: Flux densities of protons and electrons in the radiation belts of the Earth

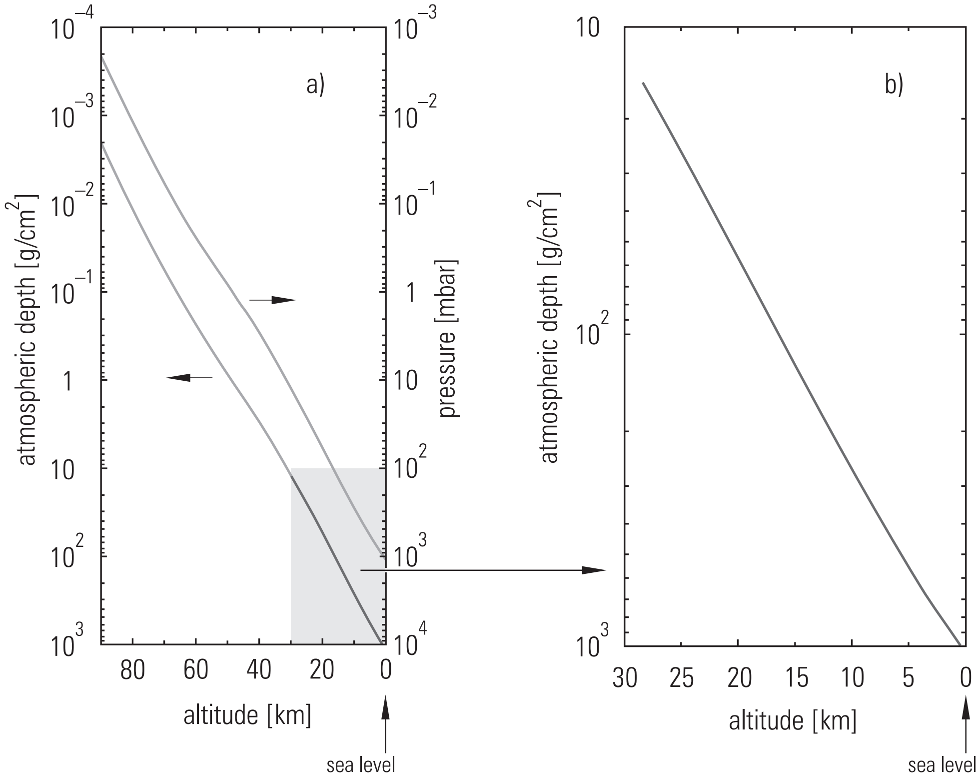

Figure 7.3: **(a)** Relation between atmospheric depth (column density) and pressure
(b) column density of the atmosphere as a function of altitude up to 28 km

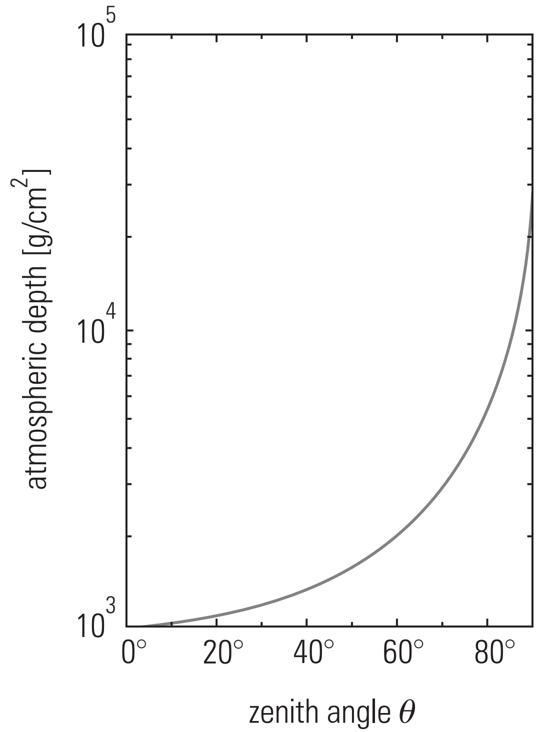

Figure 7.4: Relation between zenith angle and atmospheric depth at sea level

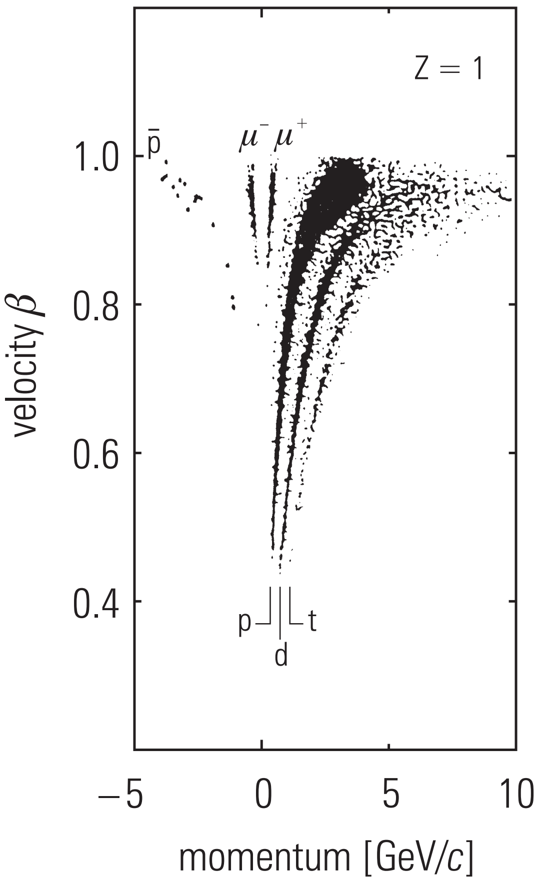

Figure 7.5: Identification of singly charged particles in cosmic rays at a flight altitude of balloons ($\hat{=}$ 5 g/cm^2 residual atmosphere) {21}

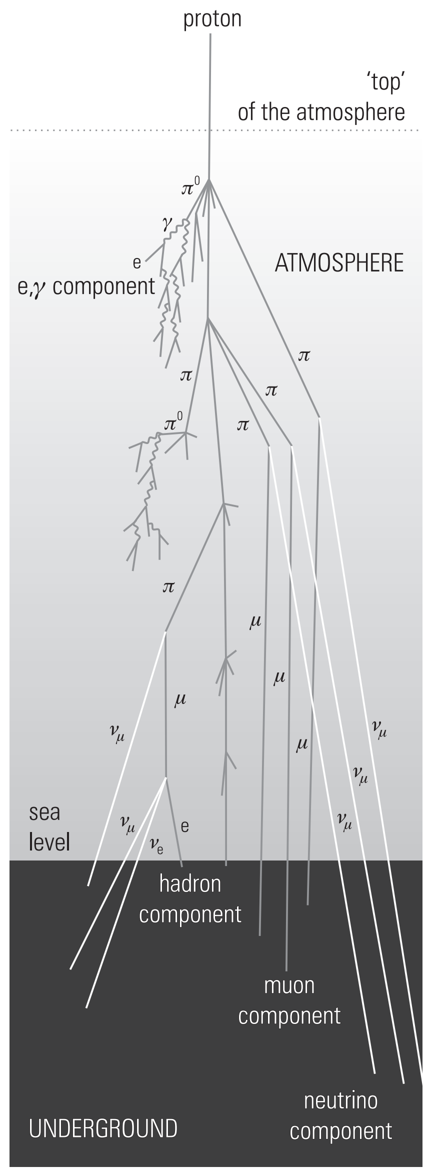

Figure 7.6: Transformation of primary cosmic rays in the atmosphere

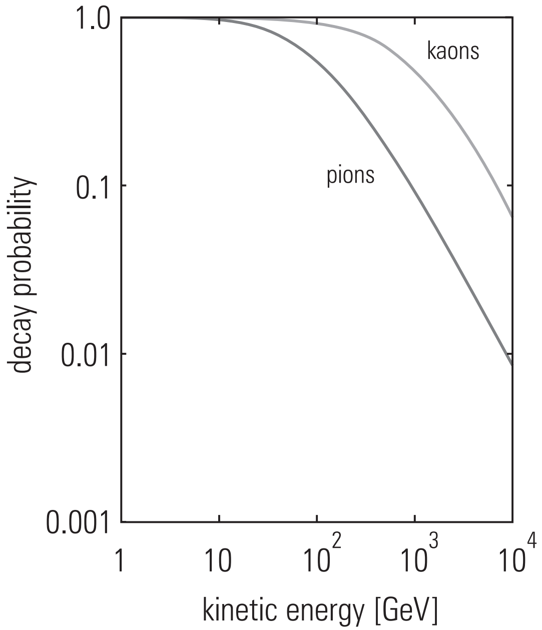

Figure 7.7: Decay probabilities for charged pions and kaons in the atmosphere as a function of their kinetic energy

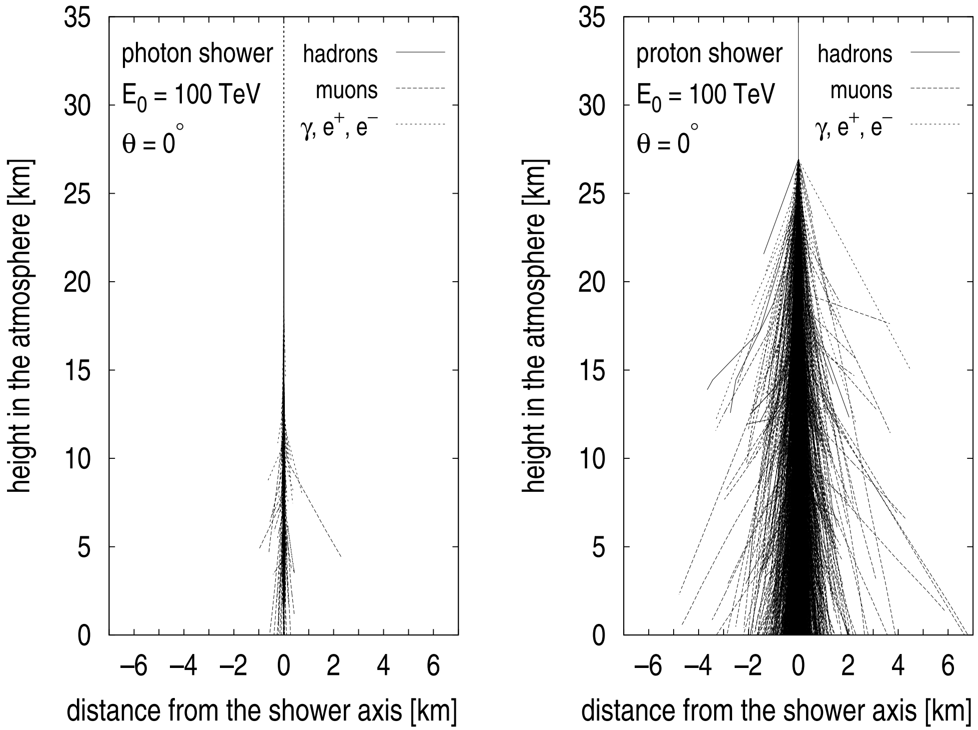

Figure 7.8: Comparison of the development of electromagnetic (100 TeV photon) and hadronic cascades (100 TeV proton) in the atmosphere. Only secondaries with $E \geq 1\,\mathrm{GeV}$ are shown {22}

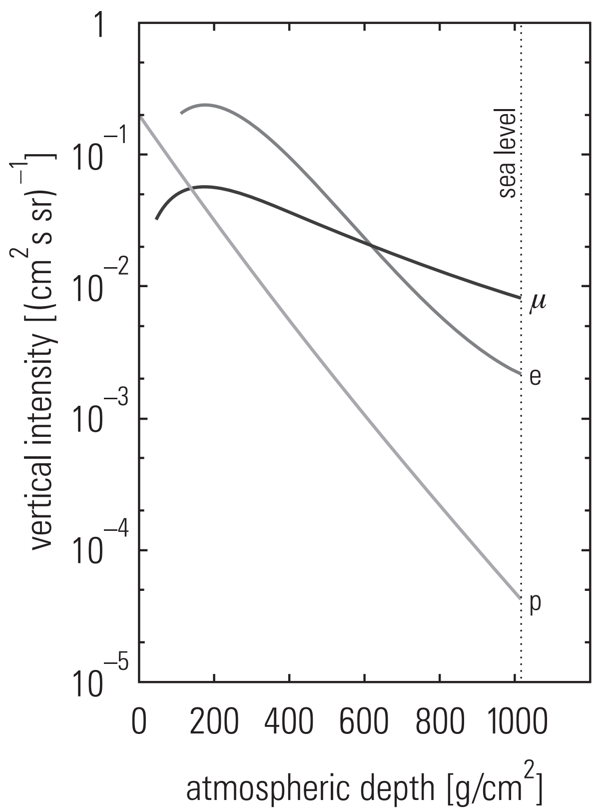

Figure 7.9: Particle composition in the atmosphere as a function of atmospheric depth

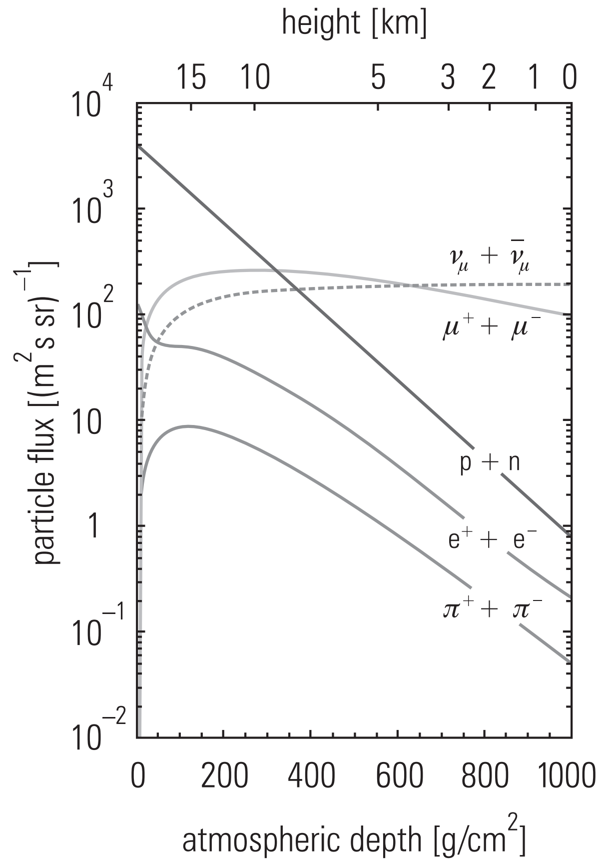

Figure 7.10: Intensities of cosmic-ray particles with energies $> 1\,\mathrm{GeV}$ in the atmosphere

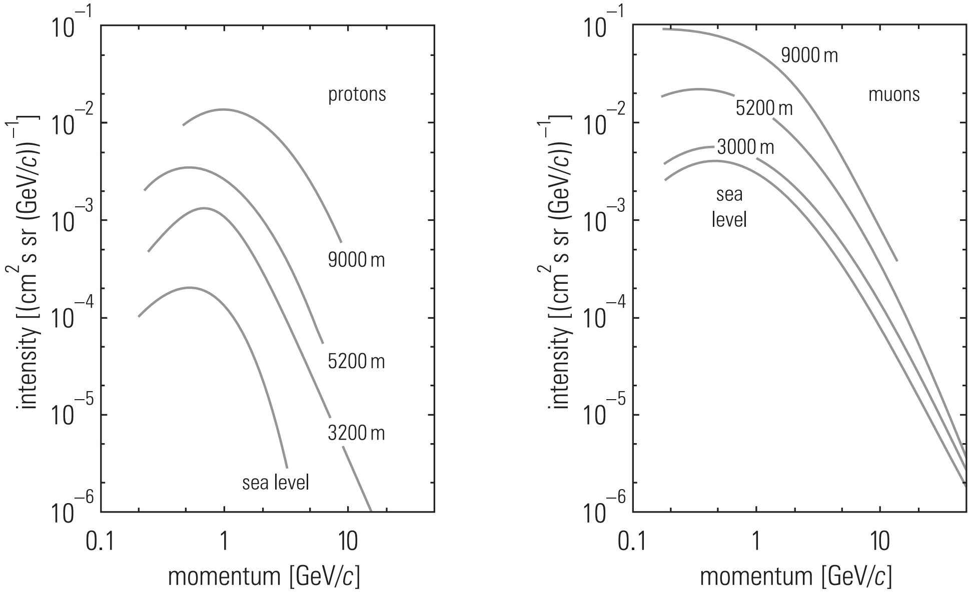

Figure 7.11: Momentum spectra of protons and muons at various altitudes in the atmosphere

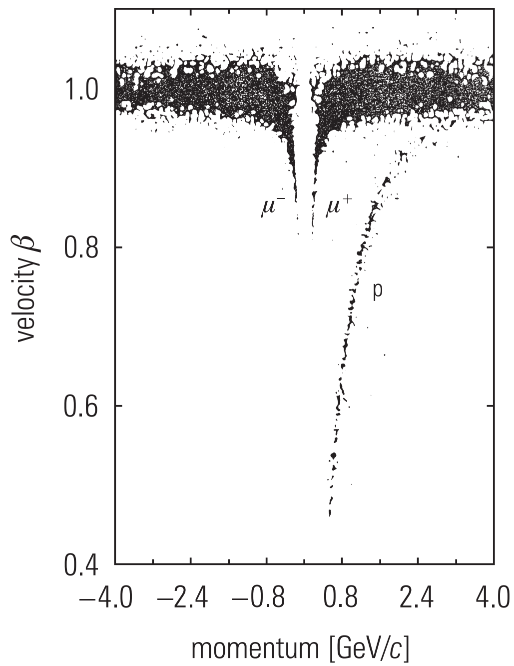

Figure 7.12: Measurement and identification of charged particles at sea level {21}

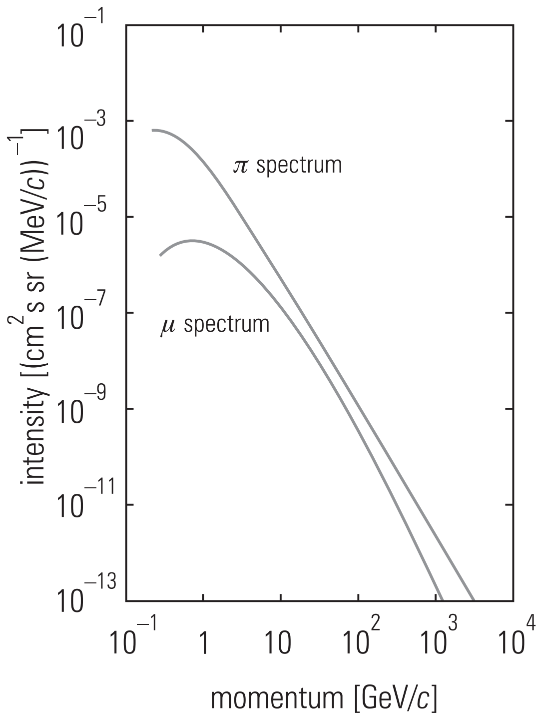

Figure 7.13: Sea-level muon spectrum in comparison to the pion parent source spectrum at production

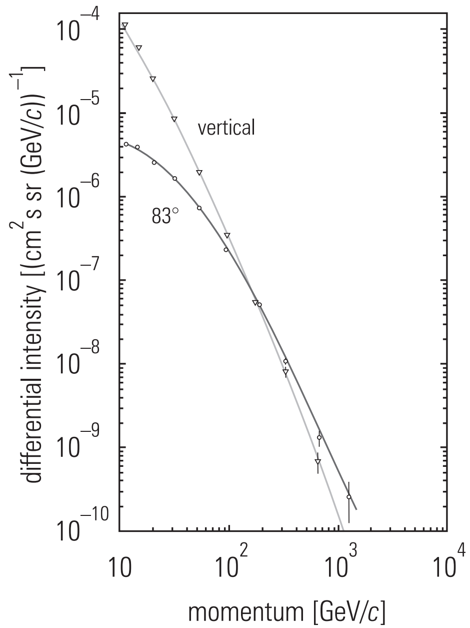

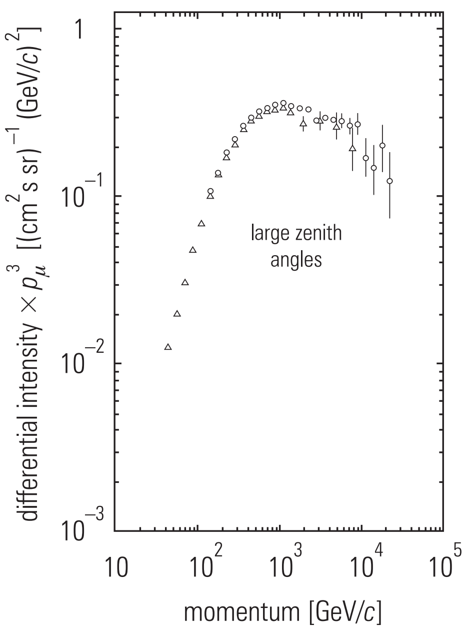

Figure 7.14: Sea-level muon momentum spectra for vertical and inclined directions

Figure 7.15: Momentum spectrum of muons at sea level for large zenith angles. In this figure the differential intensity is multiplied by p_μ^3

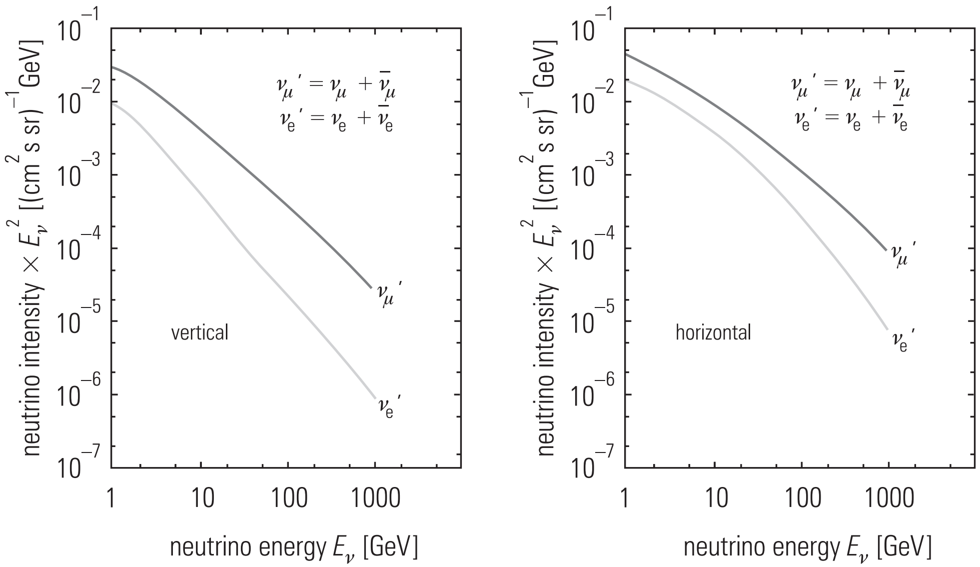

Figure 7.16: Energy spectra of muon and electron neutrinos for vertical and horizontal directions

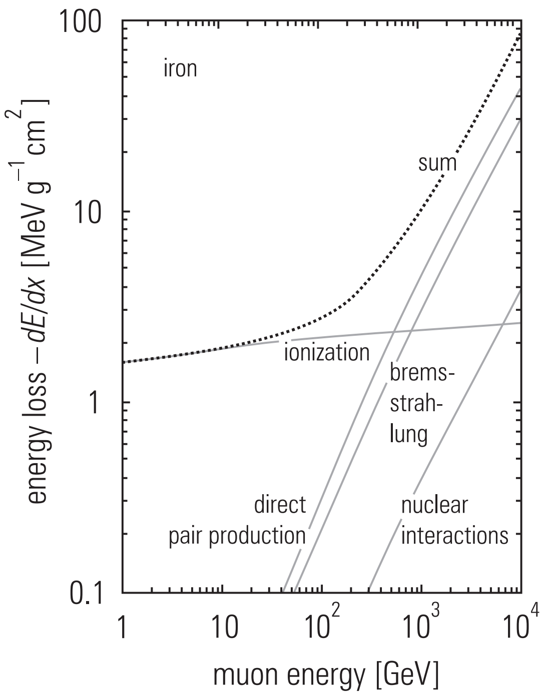

Figure 7.17: Contributions to the energy loss of muons in iron

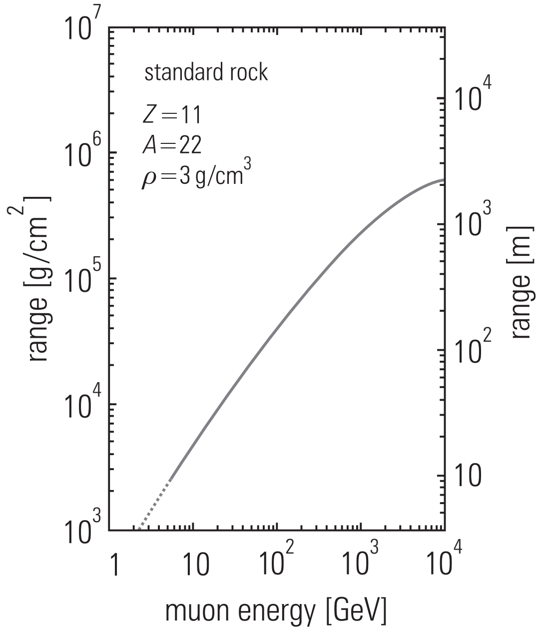

Figure 7.18: Range of muons in rock

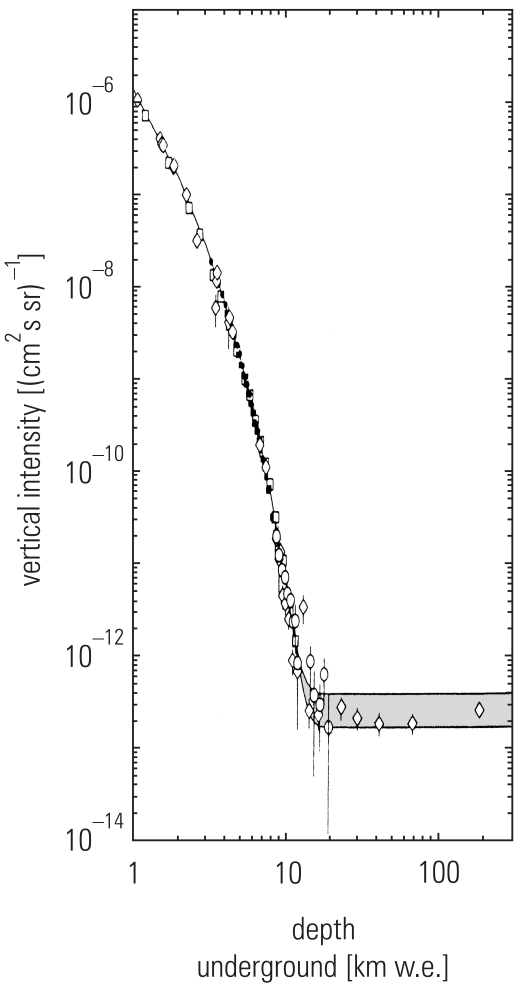

Figure 7.19: Depth–intensity relation for muons from vertical directions. The *grey-hatched band* at large depths represents the flux of neutrino-induced muons with energies above 2 GeV (*upper line:* horizontal, *lower line:* vertical upward neutrino-induced muons) [2]

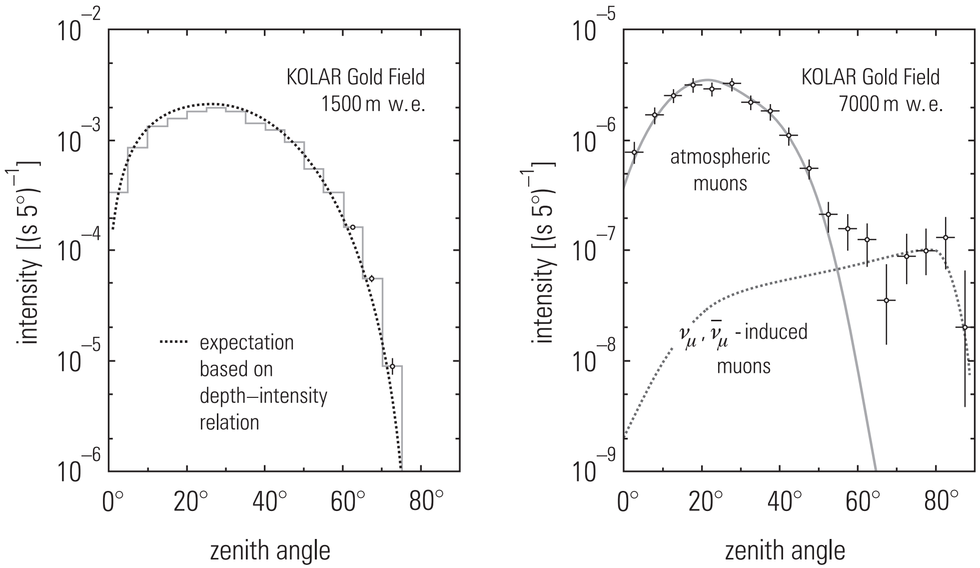

Figure 7.20: Zenith-angle distribution of atmospheric muons at depths of 1500 and 7000 m w.e.

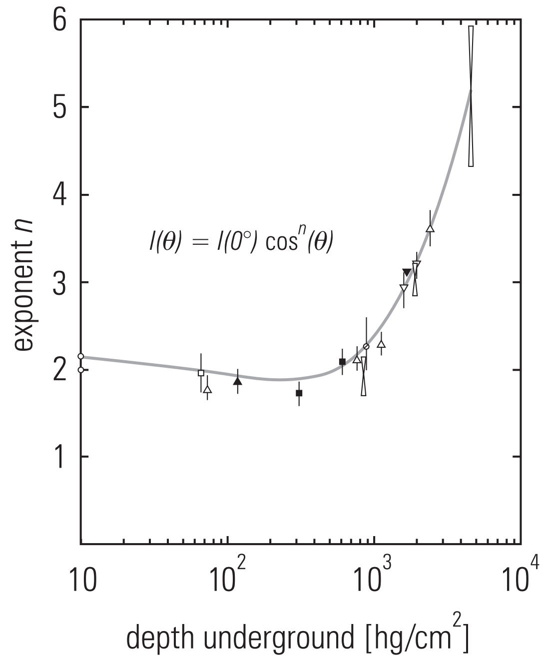

Figure 7.21: Variation of the exponent n of the zenith-angle distribution of muons with depth

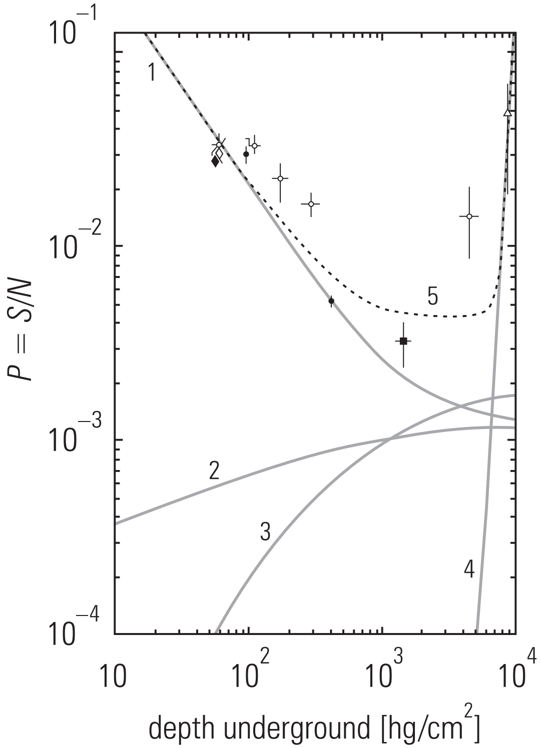

Figure 7.22: Ratio of stopping to penetrating muons as a function of depth in comparison to some experimental results. (*1*) Stopping atmospheric muons, (*2*) stopping muons from nuclear interactions, (*3*) stopping muons locally produced by photons, (*4*) neutrino-induced stopping muons, and (*5*) sum of all contributions

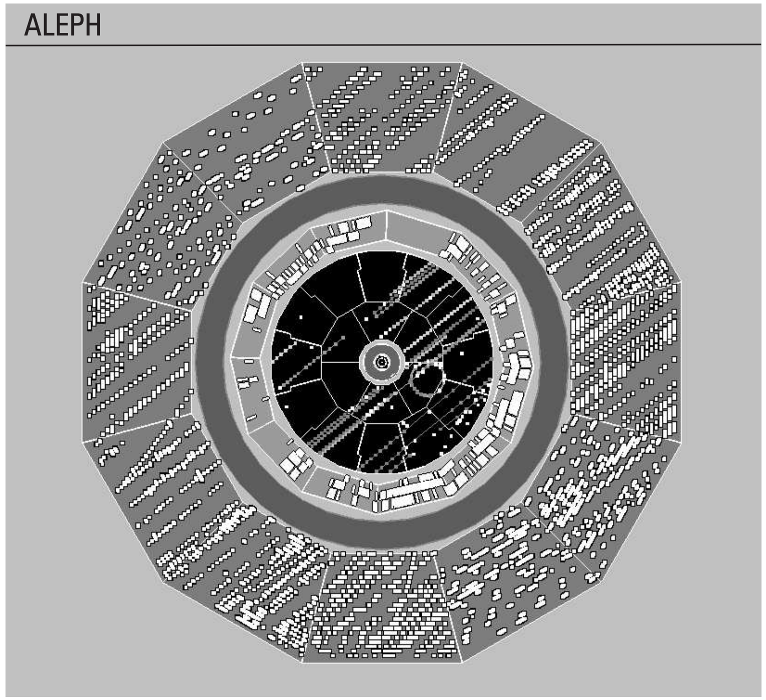

Figure 7.23: Muon shower in the ALEPH experiment. Muon tracks are seen in the central time-projection chamber and in the surrounding hadron calorimeter. Even though there is a strong 1.5 Tesla magnetic field perpendicular to the projection shown, the muon tracks are almost straight indicating their high momenta. Only a knock-on electron produced in the time-projection chamber by a muon is bent on a circle {23}

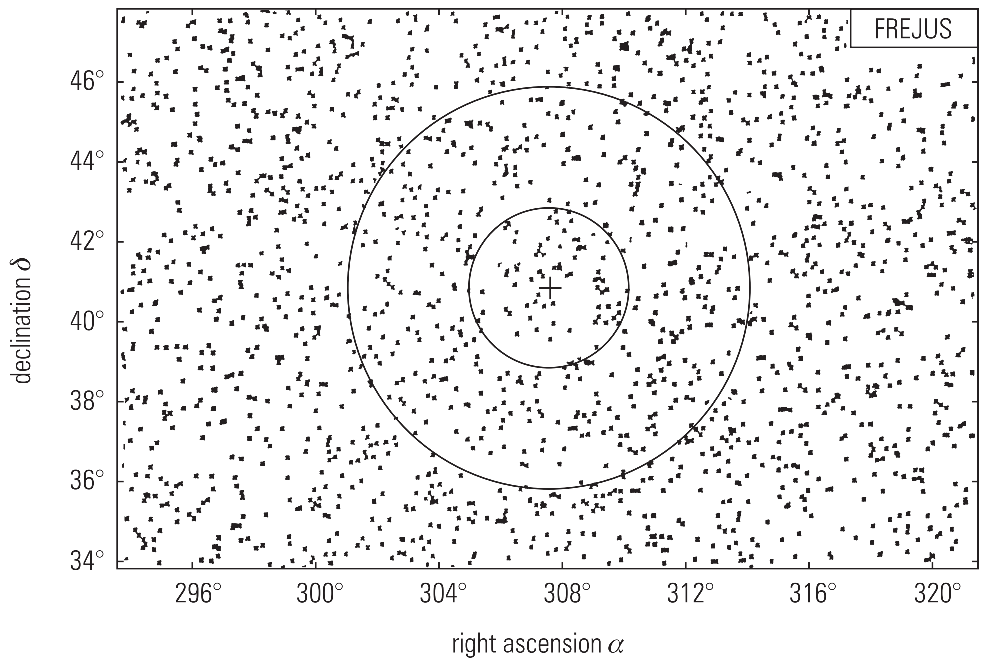

Figure 7.24: Sky map of muons and multi-muons from the direction of Cygnus X3. The cross indicates the optically known position of Cygnus X3. The circles around Cygnus X3 with angles of $\pm 2°$ and $\pm 5°$ correspond to a possible fuzziness, caused by multiple scattering of muons in rock {24}

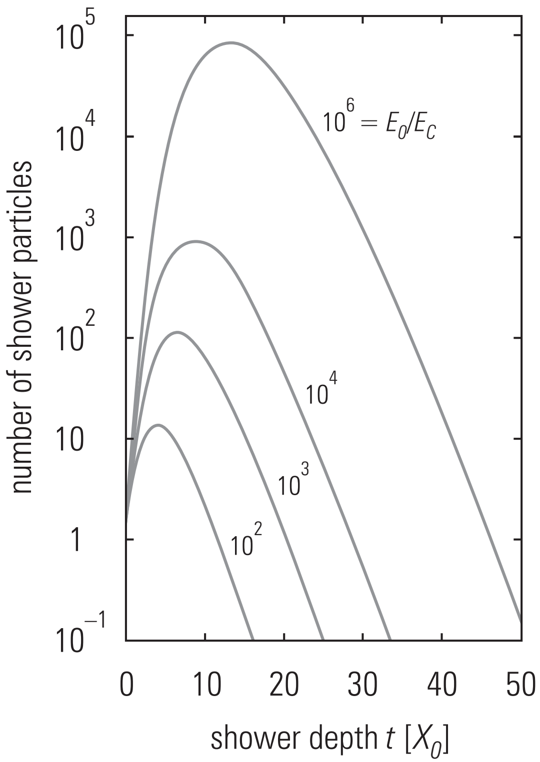

Figure 7.25: Longitudinal shower development of electromagnetic cascades. (The critical energy in air is $E_c = 84\,\mathrm{MeV}$)

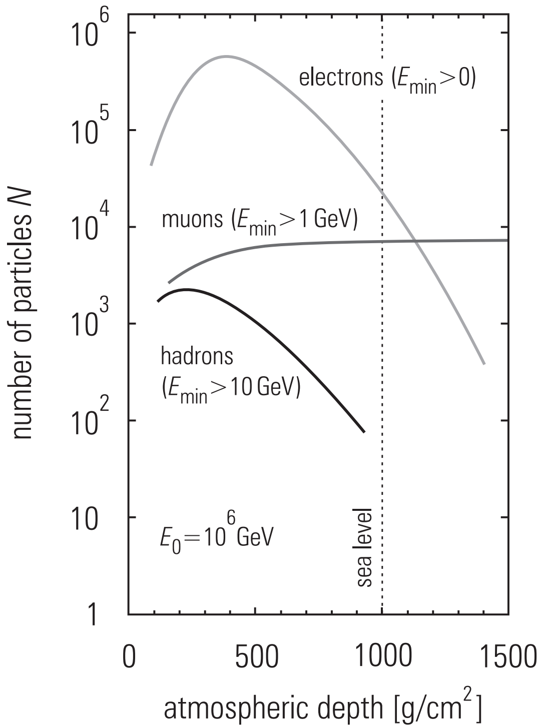

Figure 7.26: Average longitudinal development of the various components of an extensive air shower in the atmosphere

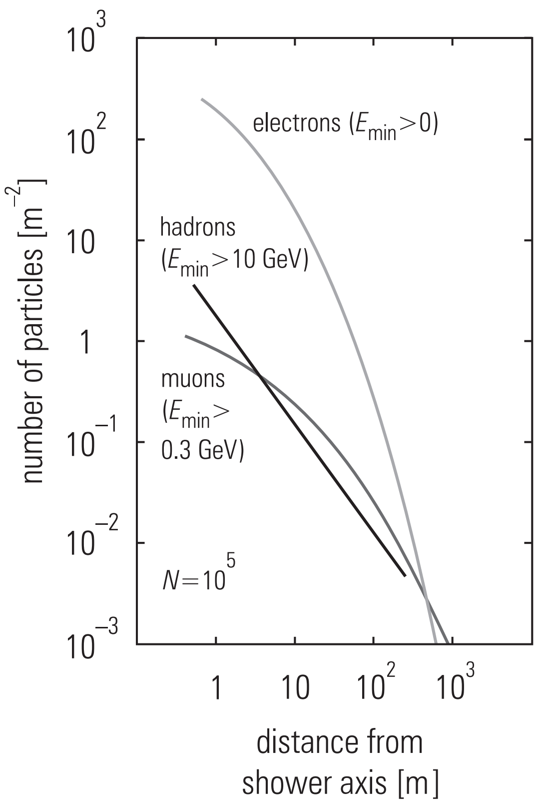

Figure 7.27: Average lateral distribution of the shower components for $N = 10^5$ corresponding to $E \approx 10^{15}$ eV

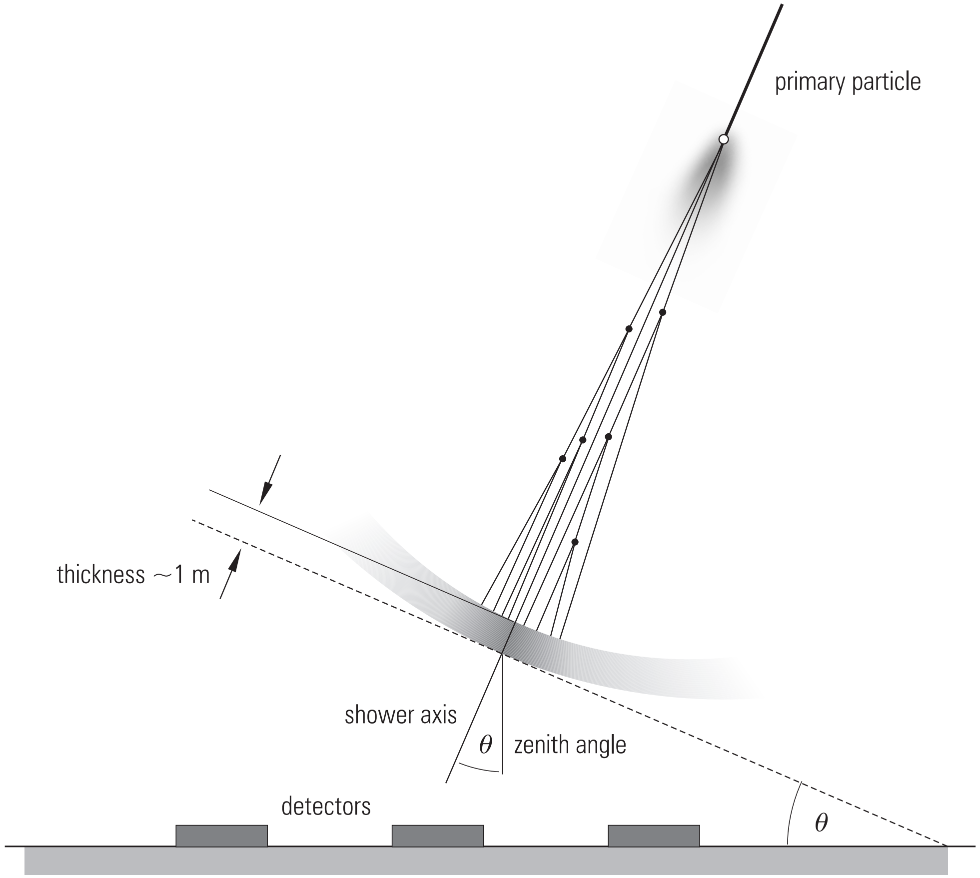

Figure 7.28: Air-shower measurement with sampling detectors

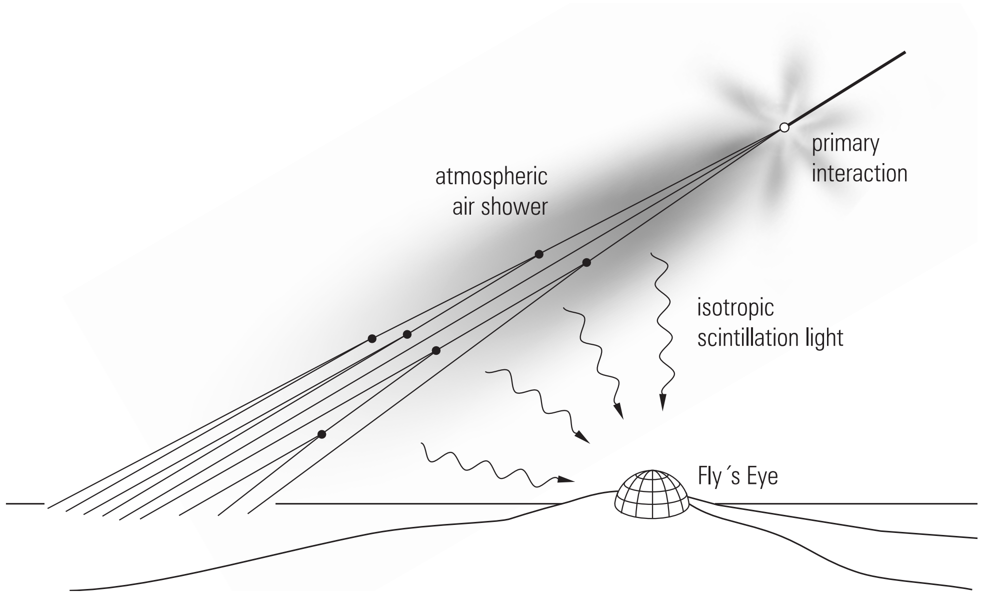

Figure 7.29: Principle of the measurement of the scintillation light of extensive air showers

Figure 7.30: Arrangement of mirrors and photomultipliers in the original Fly's Eye experiment of the Utah group {25}

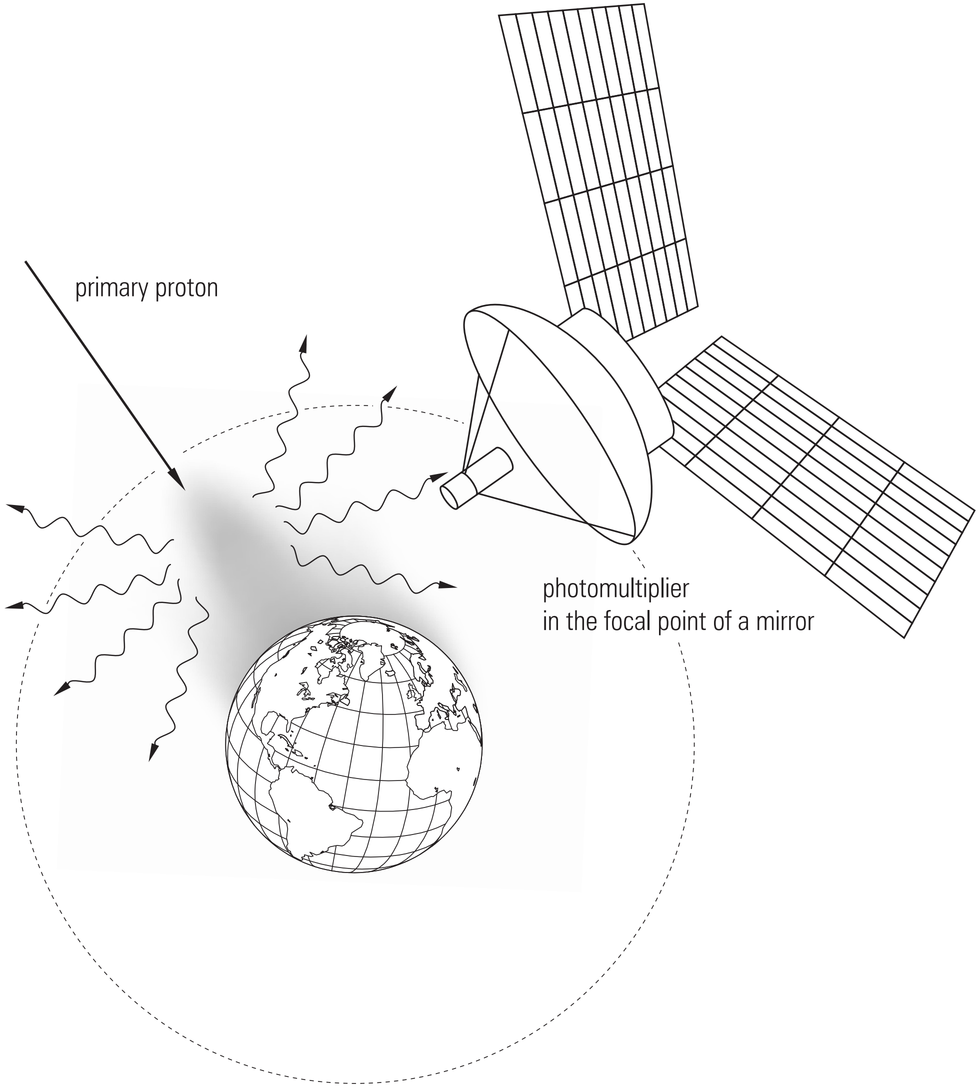

Figure 7.31: Measurement of the isotropic scintillation light of extensive air showers by Fly's Eye detectors on board of satellites ('Air Watch')

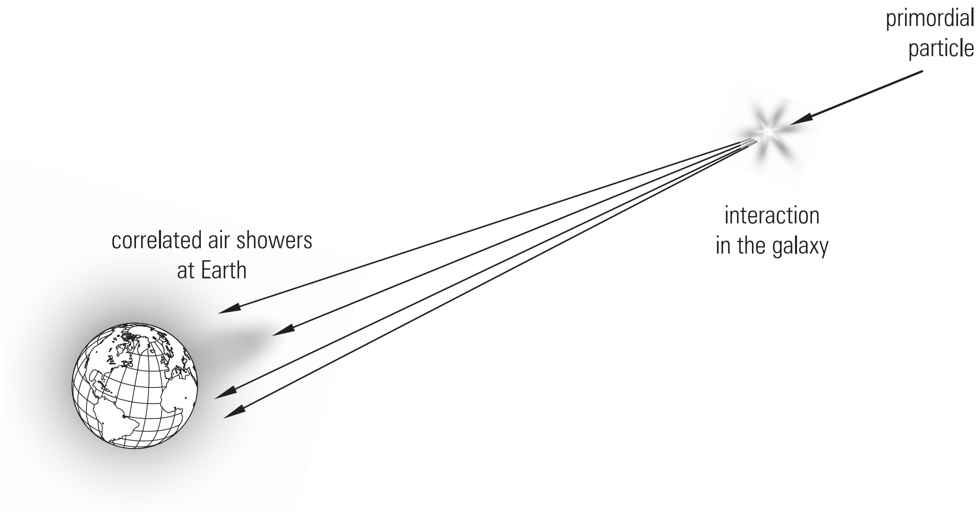

Figure 7.32: Possible explanation for correlations between distant extensive air showers

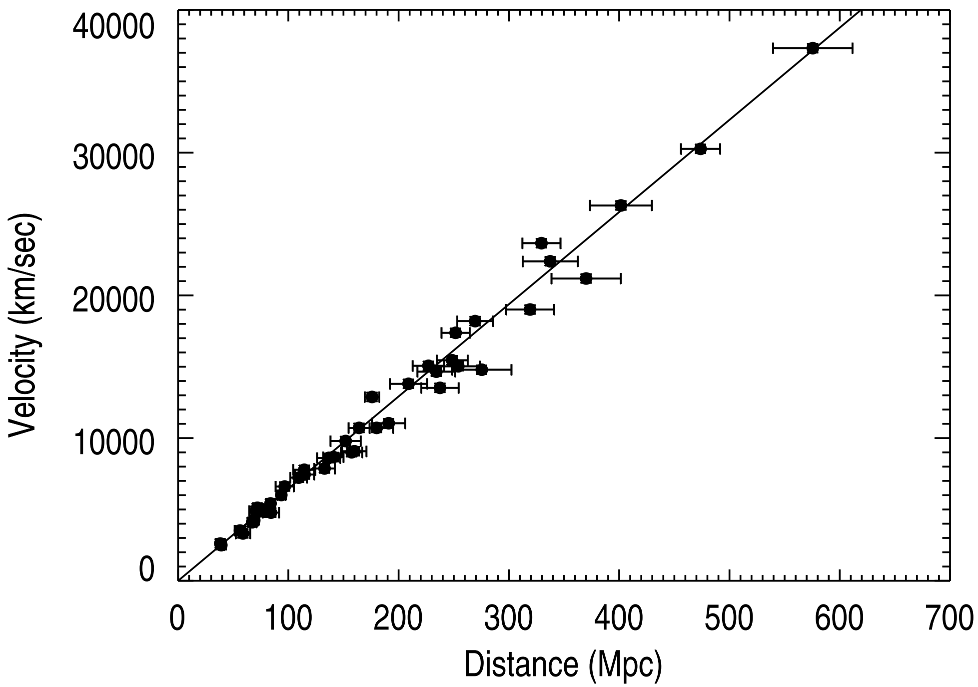

Figure 8.1: The speed versus distance for a sample of type-Ia supernovae (from [7])

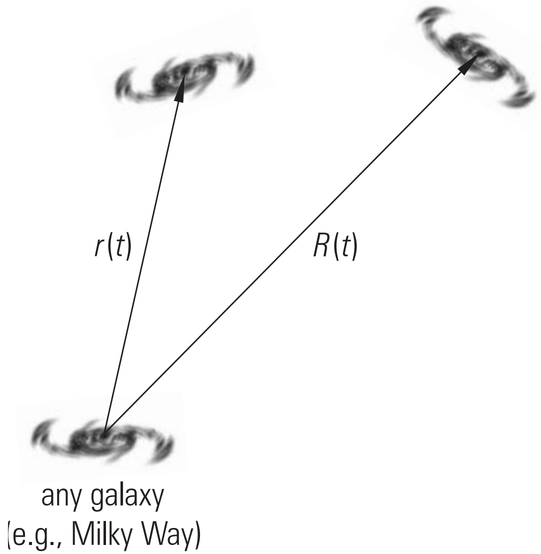

Figure 8.2: Two galaxies at distances $r(t)$ and $R(t)$ from our own

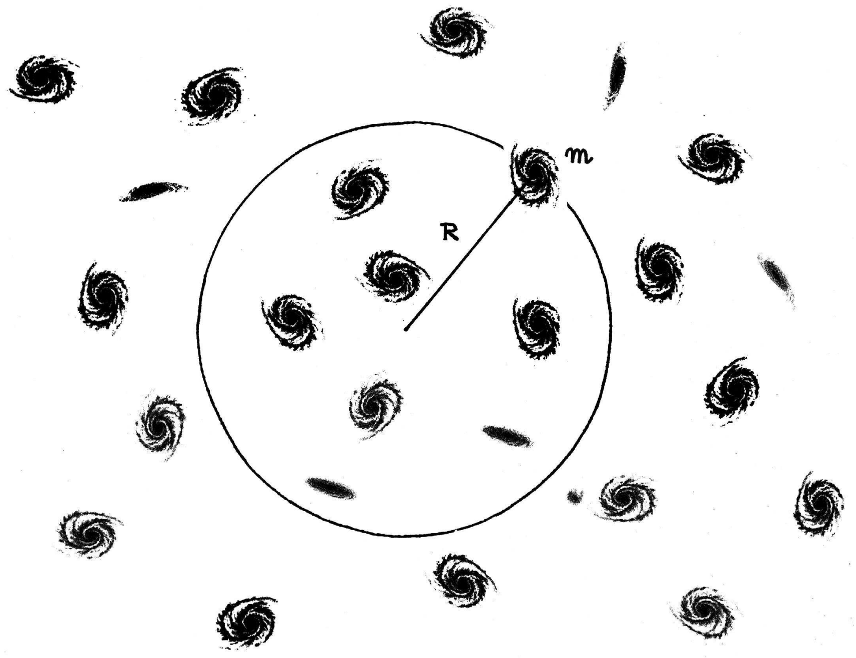

Figure 8.3: A sphere of radius R containing many galaxies, with a test galaxy of mass m at its edge

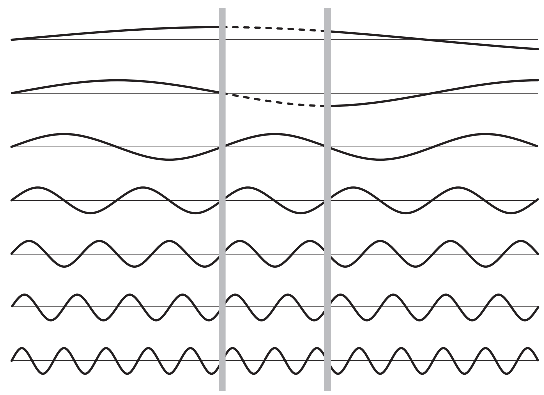

Figure 8.4: Illustration of the Casimir effect: Only certain wavelengths fit into the space between the plates. The outside of the plates does not limit the number of possible frequencies

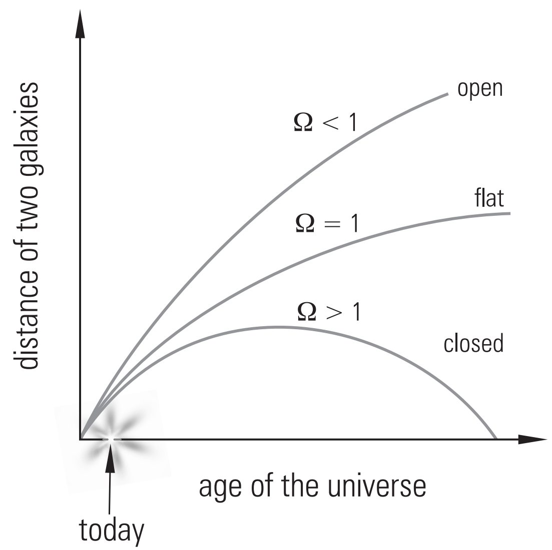

Figure 8.5: The scale factor R as a function of time for $\Omega < 1$, $\Omega > 1$, and $\Omega = 1$

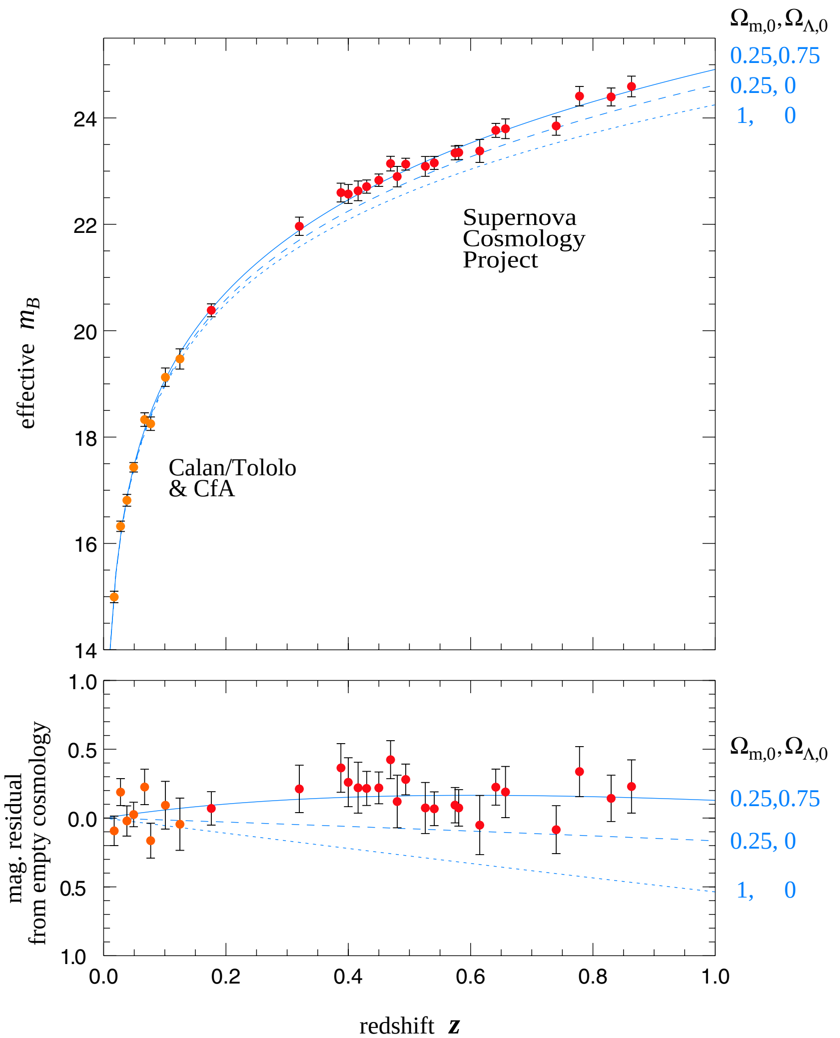

Figure 8.6: Magnitudes and residuals of supernovae of type Ia as a function of redshift of their host galaxies in comparison to the expectation of various models. The data are consistent with a flat universe with a fraction of about 75% of dark energy. Shown are data from the Supernova Cosmology Project, the Calan/Tololo group, and the Harvard–Smithsonian Center for Astrophysics (CfA) {26}

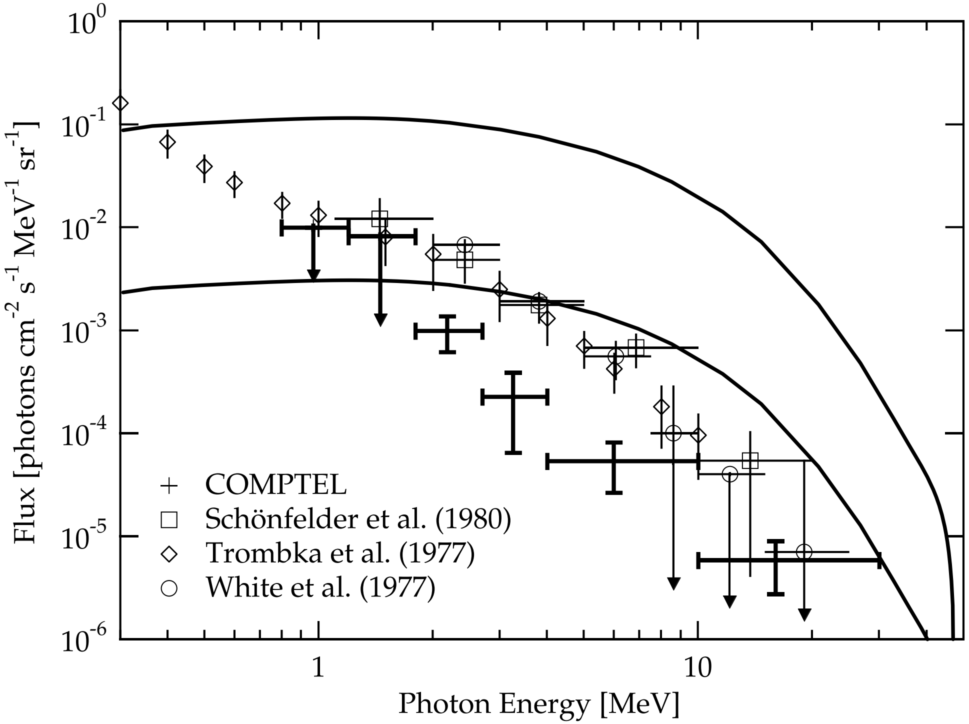

Figure 9.1: The measured gamma-ray flux (*data points*) along with the levels predicted to arise from interaction between domains of matter and antimatter. The *upper curve* corresponds to domain sizes of 20 Mpc, the *lower* for 1000 Mpc [14, 15]

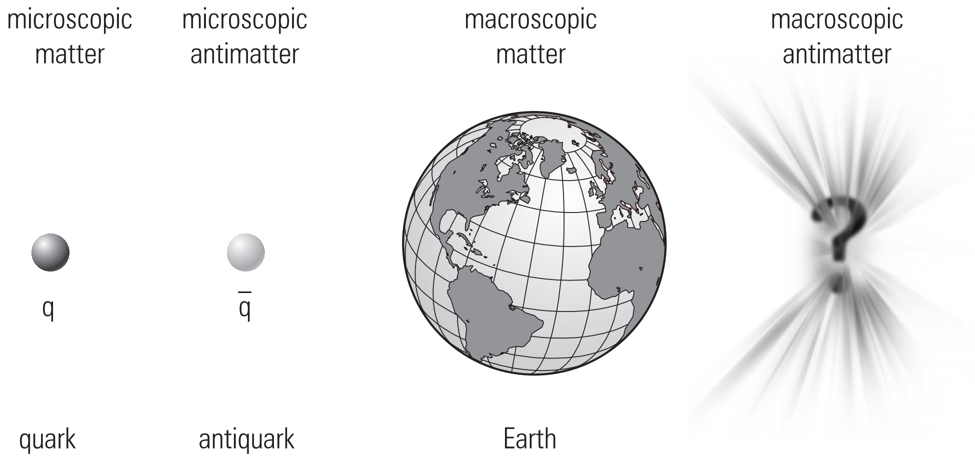

Figure 9.2: The matter–antimatter symmetry observed at microscopic scales appears to be broken at the macroscopic level

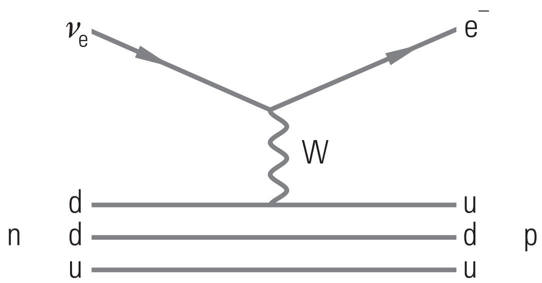

Figure 10.1: Feynman diagram for the reaction $n\nu_e \leftrightarrow pe^-$

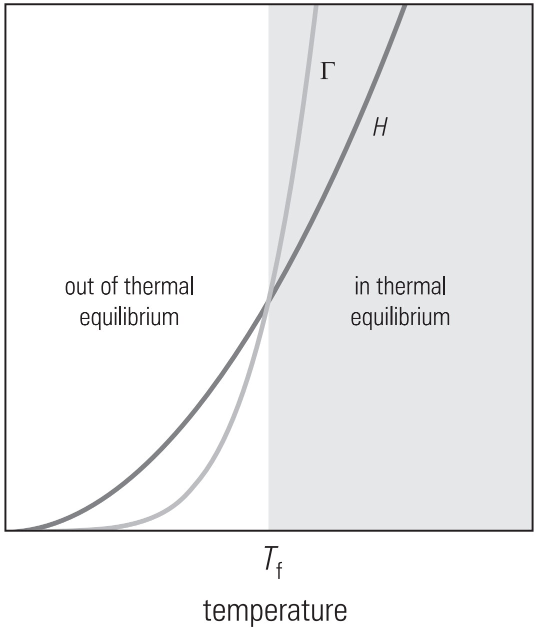

Figure 10.2: The reaction rate $\Gamma(\nu_e n \leftrightarrow e^- p)$ and the expansion rate H as a function of temperature

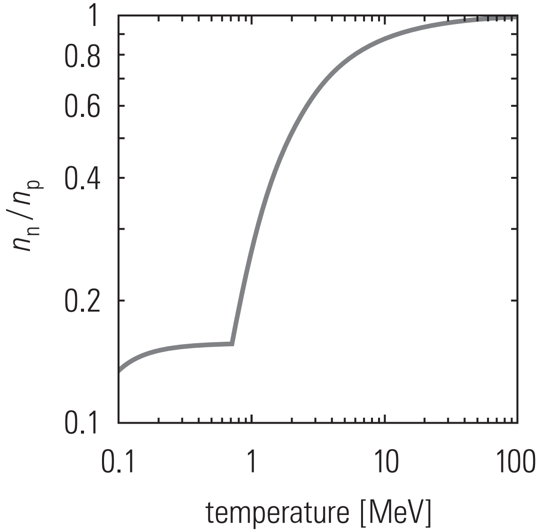

Figure 10.3: The ratio n_n/n_p as a function of the temperature

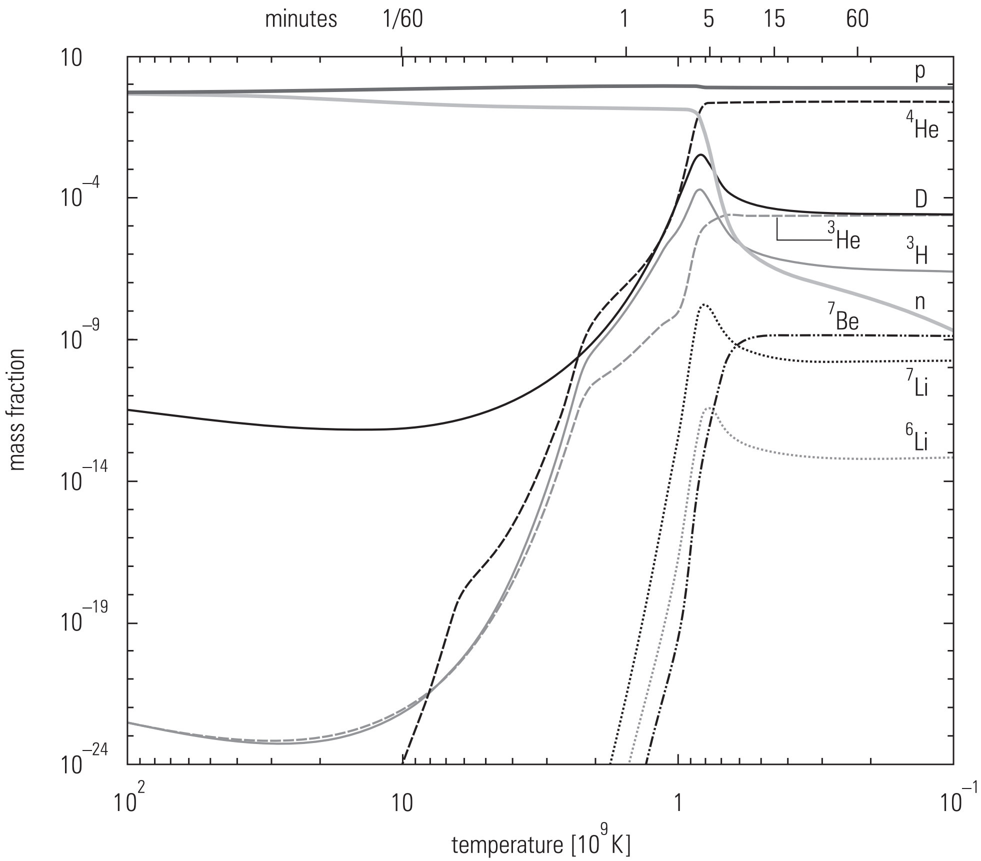

Figure 10.4: Evolution of the mass and number fractions of primordial elements. ^{4}He is given as a mass fraction while the other elements are presented as number fractions

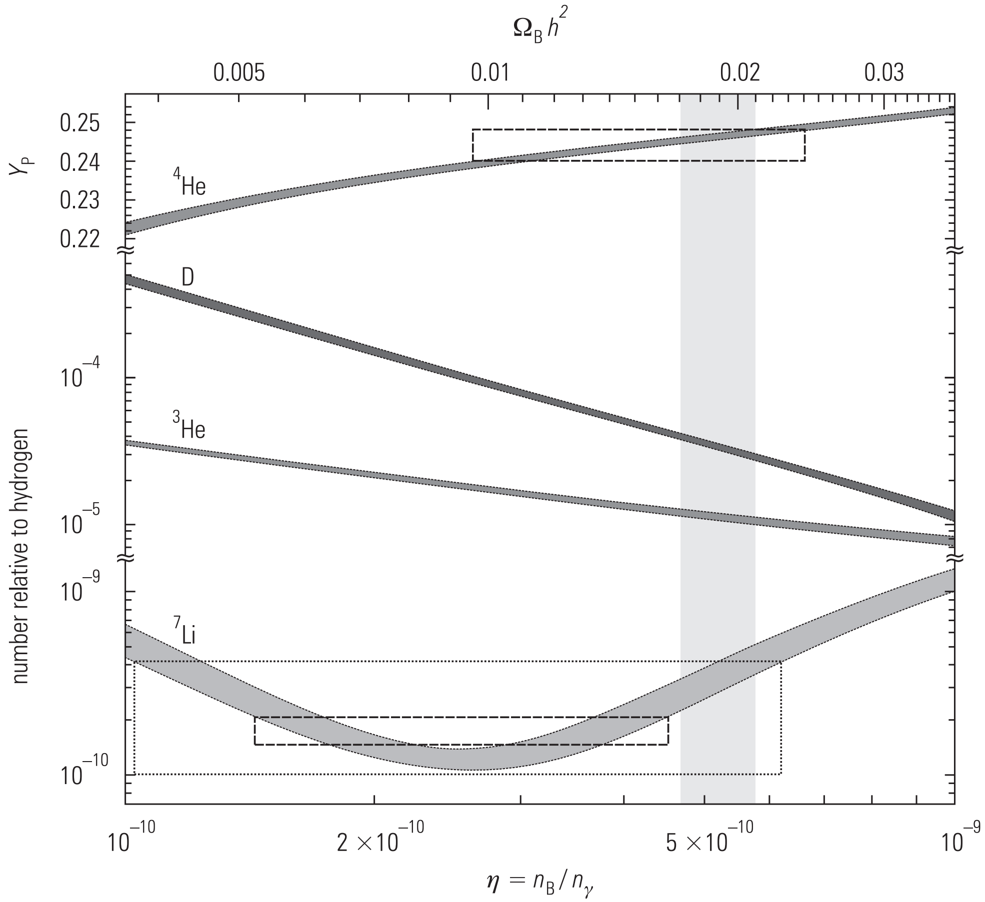

Figure 10.5: Predictions for the abundances of ^{4}He, D, and ^{7}Li as a function of the baryon-to-photon ratio η. Y_P is the primordial ^{4}He mass fraction. Traditionally, the ^{4}He content of the universe is given as mass fraction, while the other primordial elements are presented as number fraction (see also the *broken vertical scale*). The *larger box* for ^{7}Li/H includes the systematical error added in quadrature to the statistical error

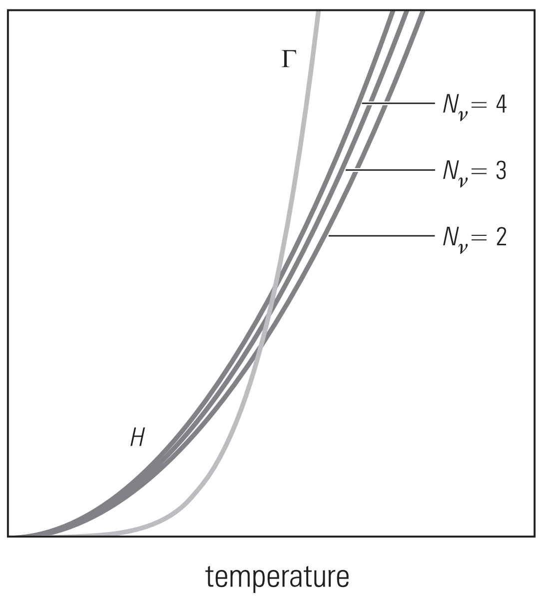

Figure 10.6: The reaction rate $\Gamma(\nu_e n \leftrightarrow e^- p)$ and the expansion rate H for $N_\nu = 2$, 3, and 4 as a function of temperature

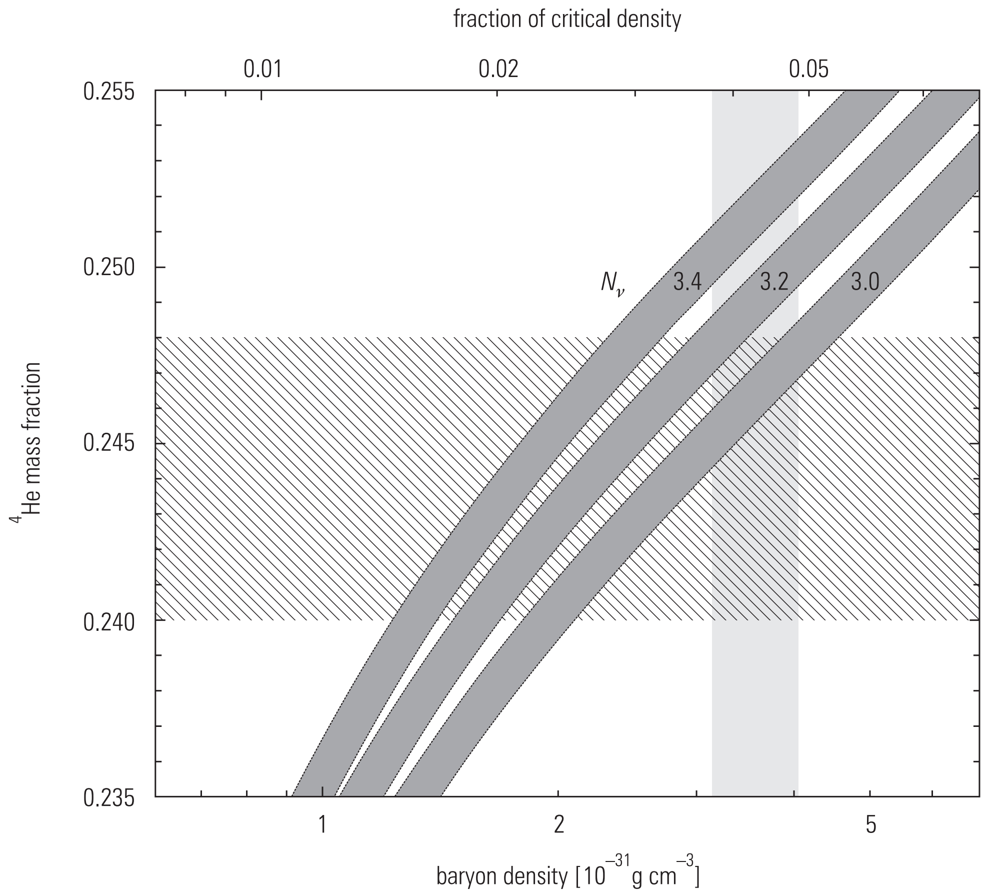

Figure 10.7: The predicted ^{4}He mass fraction as a function of η for different values of N_ν

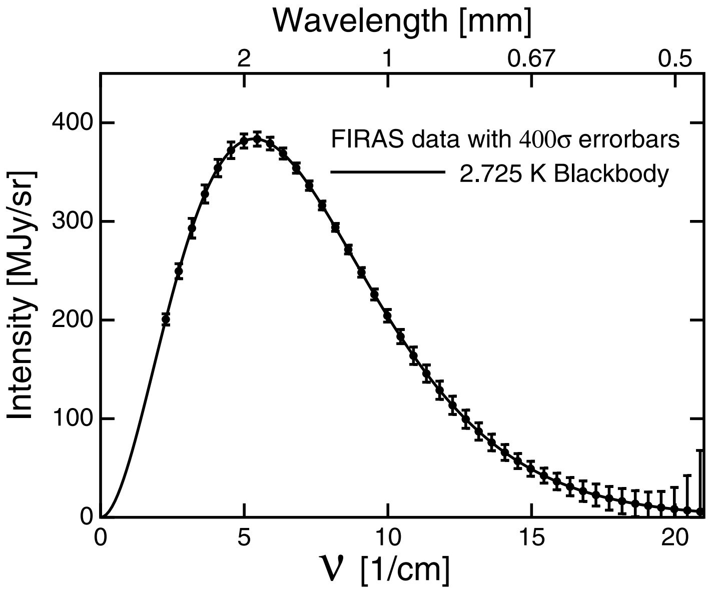

Figure 11.1: The spectrum of the CMB measured by the COBE satellite together with the blackbody curve for $T = 2.725\,\mathrm{K}$. The *error bars* have been enlarged by a factor of 400; any deviations from the Planck curve are less than 0.005% (from [26])

Figure 11.2: Map of the CMB temperature measured by the COBE satellite. The dipole pattern is due to the motion of the Earth through the CMB (from [27]) {27}

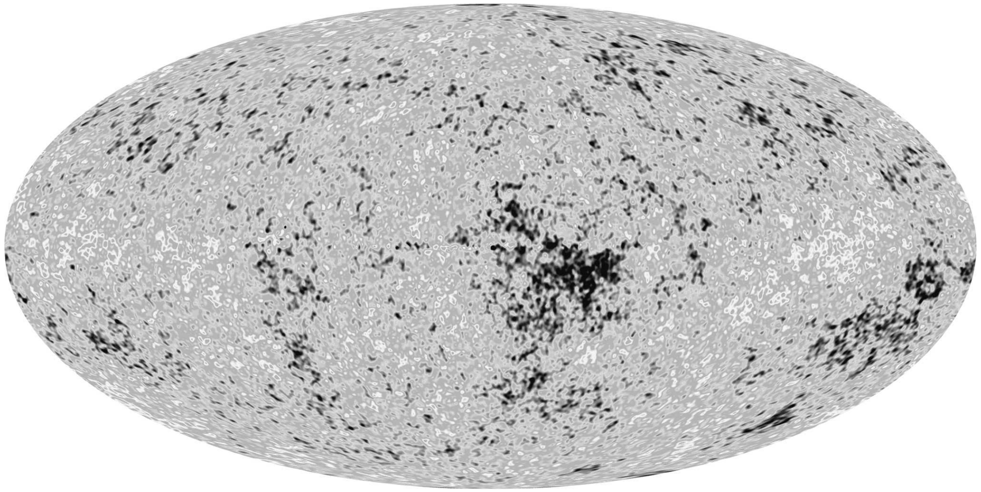

Figure 11.3: Cosmographic map of the CMB temperature measured by the WMAP satellite with the dipole component subtracted (from [28]) {28}

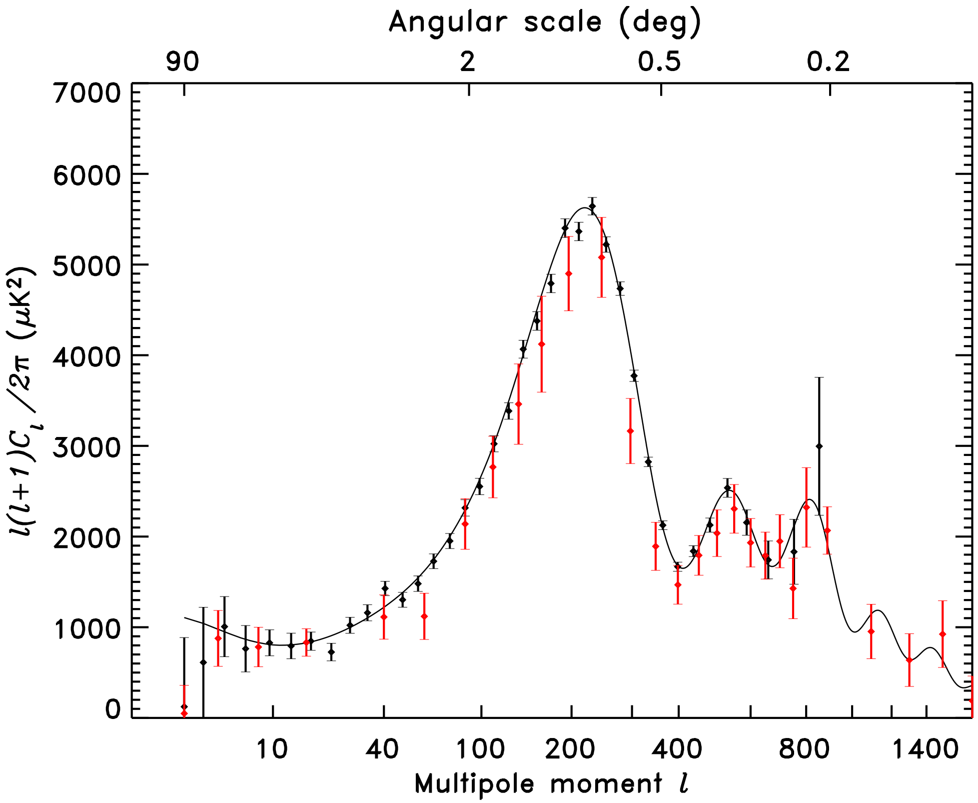

Figure 11.4: CMB power spectrum. The set of measurements with the smaller error bars is from WMAP; those with the larger errors represent an average of measurements prior to WMAP (from [29])

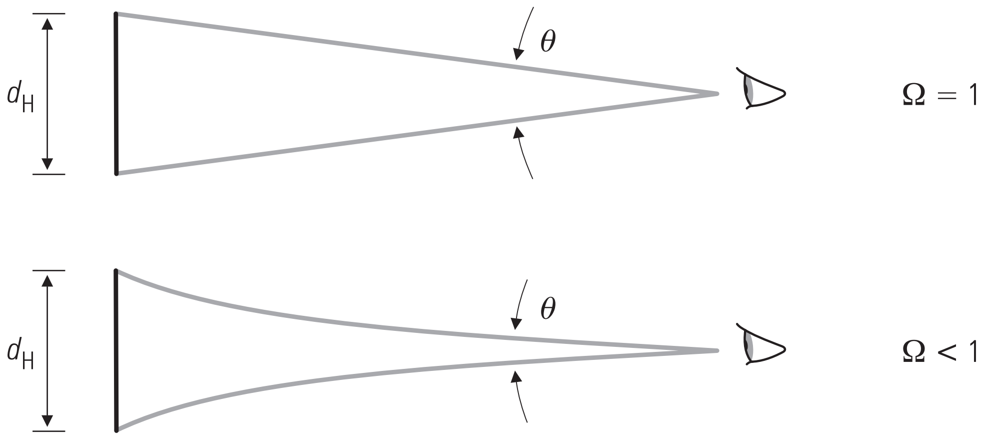

Figure 11.5: The horizon distance at the time of last scattering as viewed by us today in **(a)** a flat universe ($\Omega = 1$) and **(b)** an open universe ($\Omega < 1$)

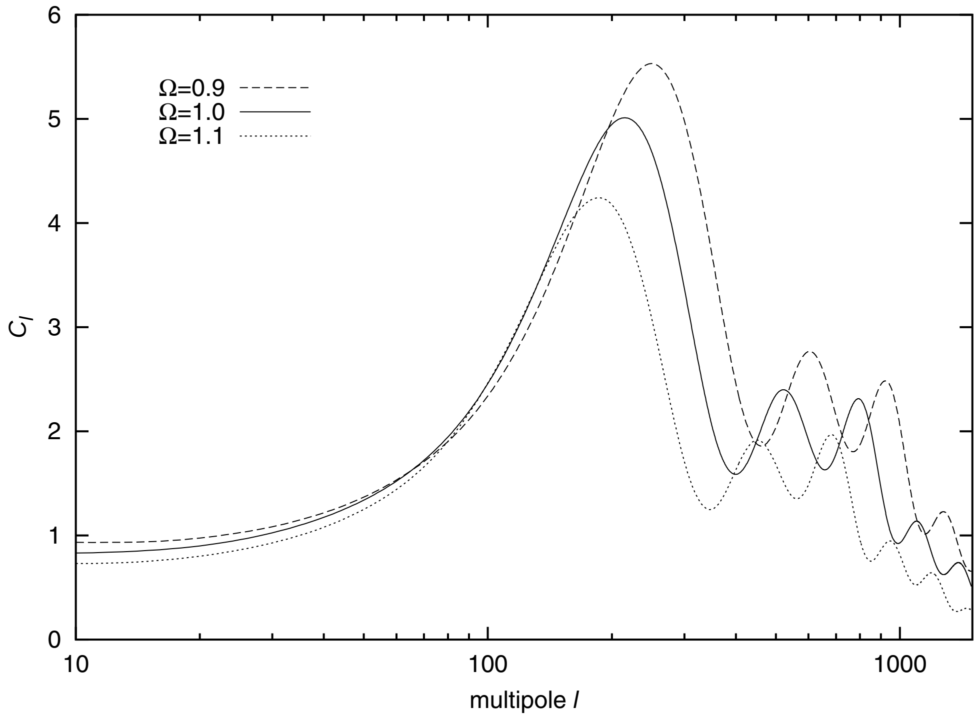

Figure 11.6: Predicted CMB power spectra for different values of the current total energy density (values computed with the program `CMBFAST` [32])

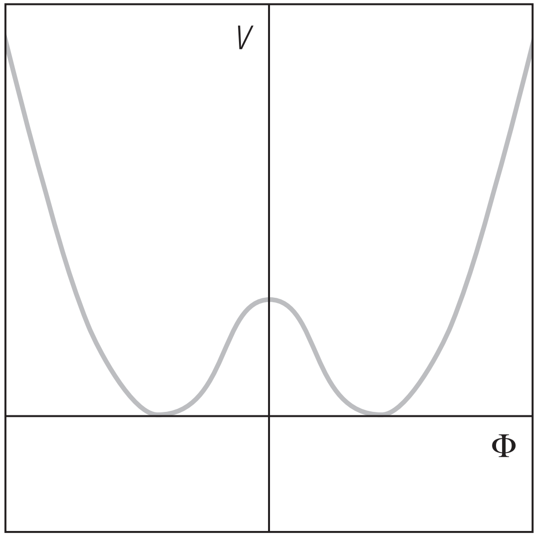

Figure 12.1: Schematic illustration of the potential $V(\phi)$ associated with the Higgs field ϕ in the Standard Model of particle physics

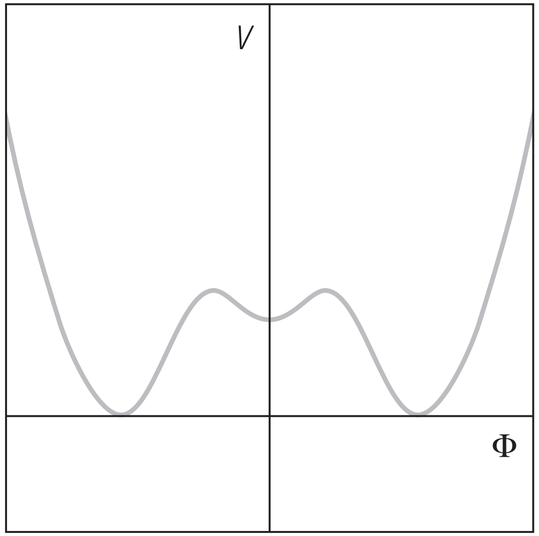

Figure 12.2: Schematic illustration of the potential $V(\phi)$ first proposed to provide inflation

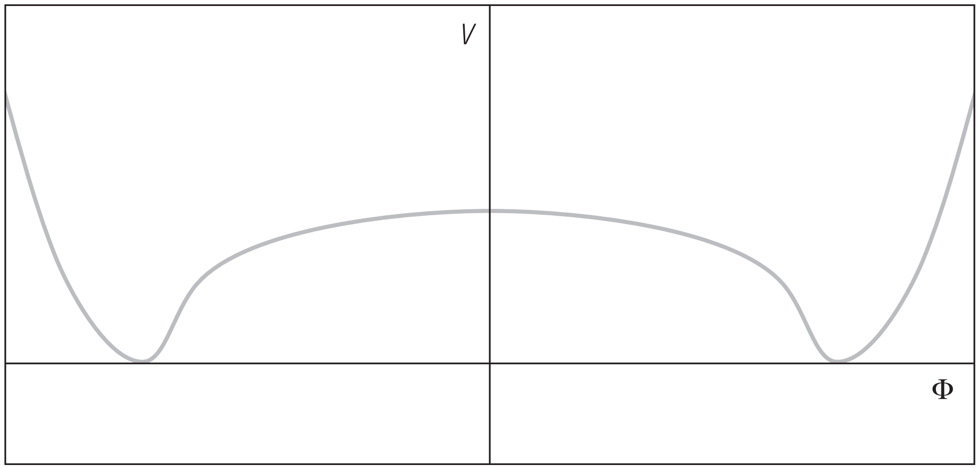

Figure 12.3: Schematic illustration of the potential $V(\phi)$ for 'new inflation'

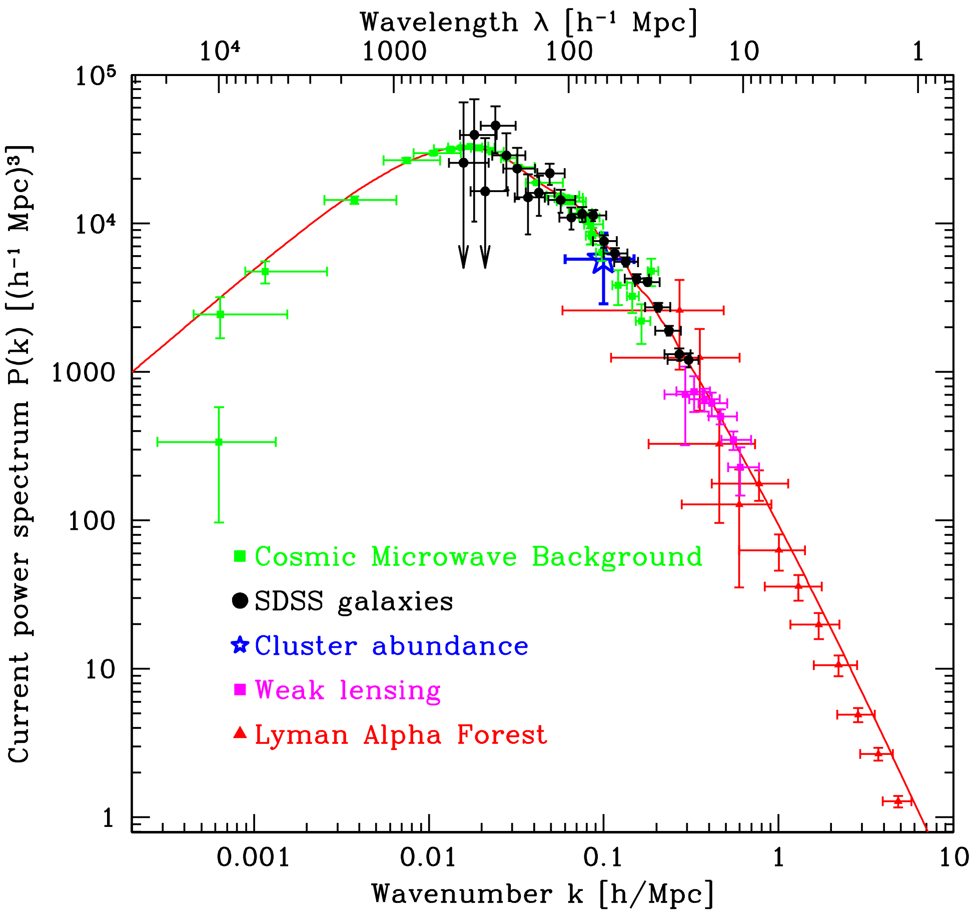

Figure 12.4: Measurements of the power spectrum $P(k)$ from several types of observations. The curve shows the prediction of a model with the spectral index n equal to unity. The parameter h is assumed to be 0.72 (from [42])

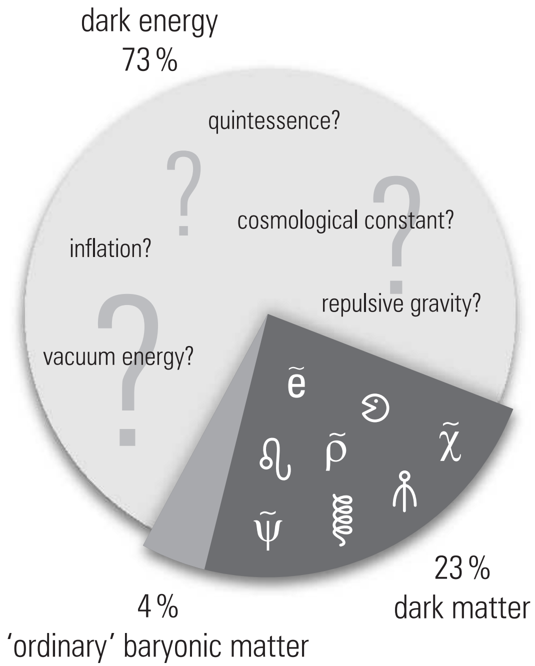

Figure 13.1: Illustration of the relative fractions of dark matter, dark energy, and baryonic matter

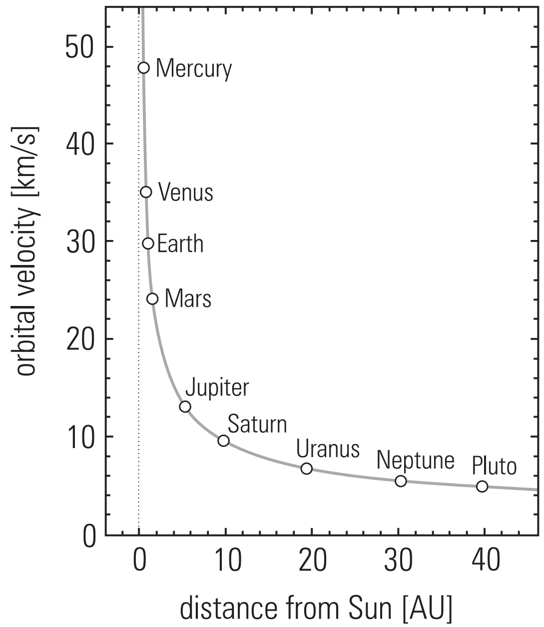

Figure 13.2: Rotational curves of planets in our solar system, 1 Astronomical Unit (AU) = distance Earth to Sun

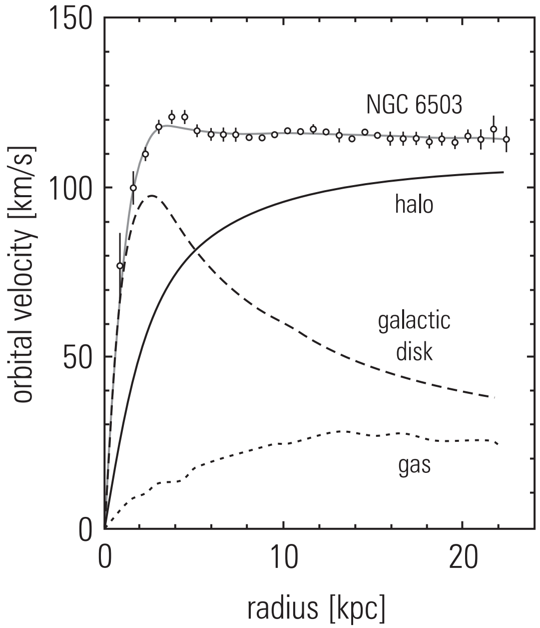

Figure 13.3: Rotational curves of the spiral galaxy NGC 6503. The contributions of the galactic disk, the gas, and the halo are separately shown

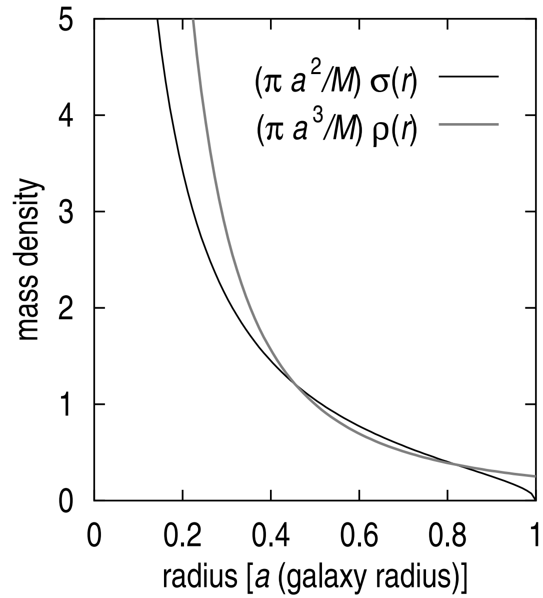

Figure 13.4: Mass density of a galaxy for a two- and three-dimensional model of the mass density

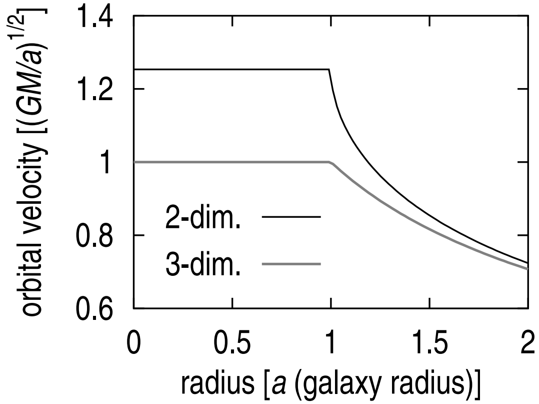

Figure 13.5: Flat rotational curves of stars in a galactic disk for two- and three-dimensional rotationally symmetric mass distributions

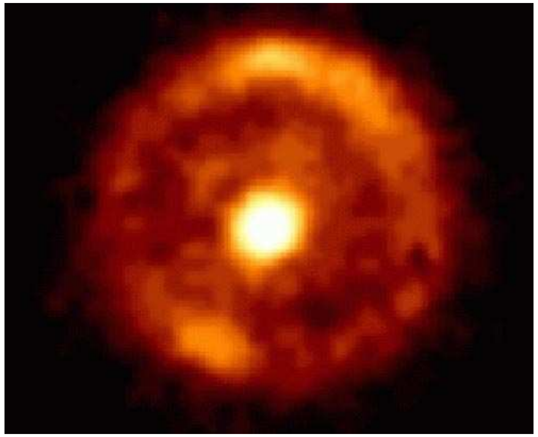

Figure 13.6: Image of a distant background galaxy as Einstein ring, where the foreground galaxy in the center of the figure acts as gravitational lens {29}

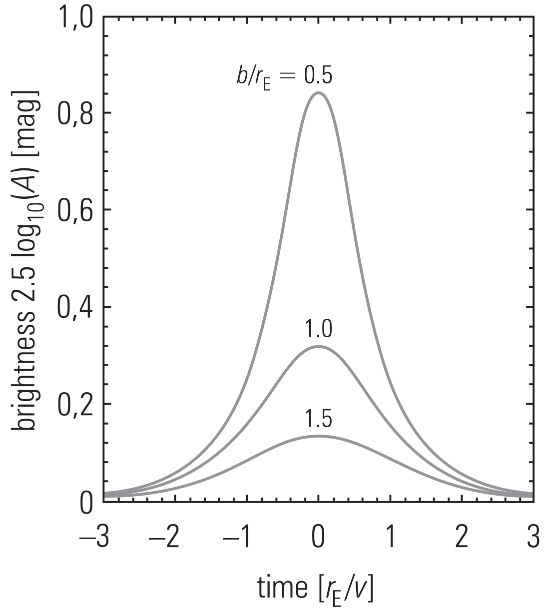

Figure 13.7: Apparent light curve of a bright star produced by microlensing, when a brown dwarf star passes the line of sight between source and observer. The brightness excursion is given in terms of magnitudes generally used in astronomy {30}

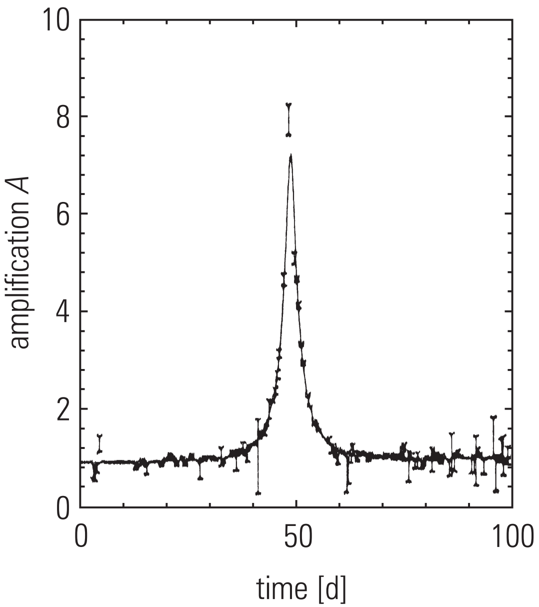

Figure 13.8: Light curve of a distant star caused by gravitational lensing. Shown is the first brown object found by the MACHO experiment in the galactic halo {30}

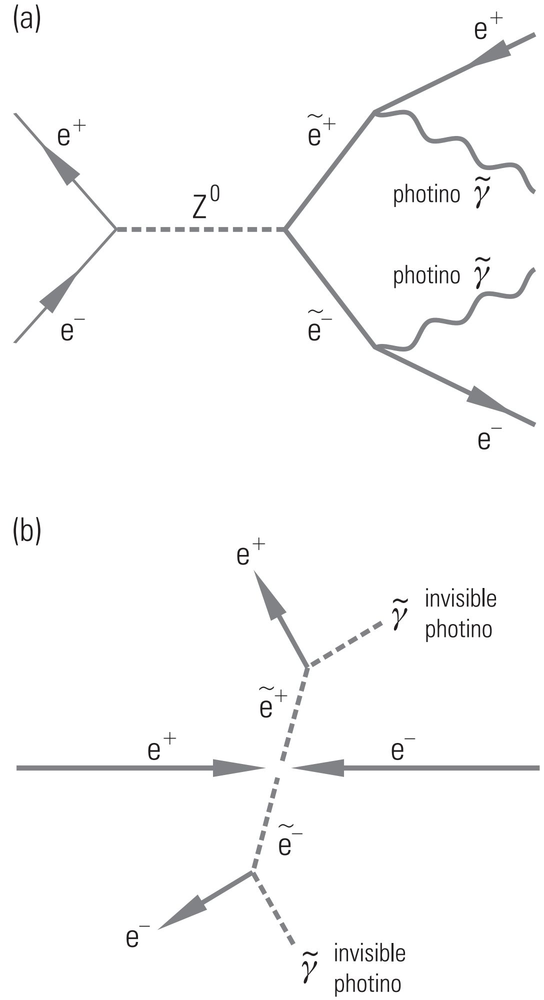

Figure 13.9: Production and decay of supersymmetric particles as Feynman diagram **(a)** and in the detector **(b)**

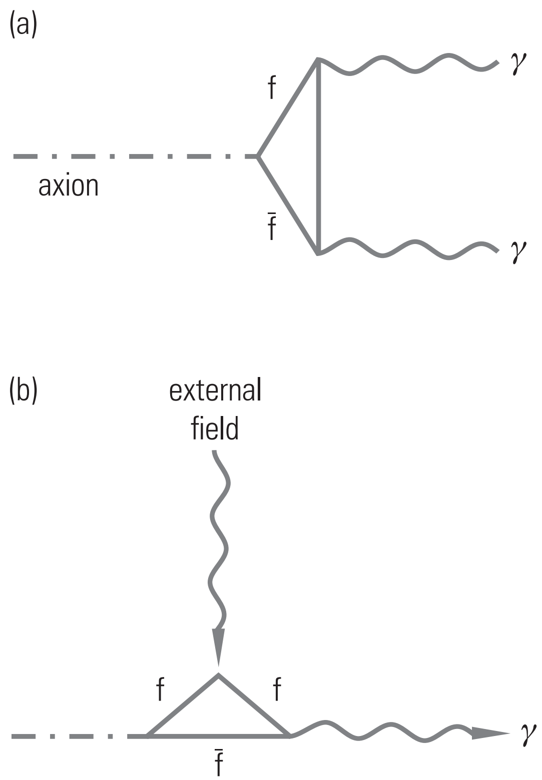

Figure 13.10: Coupling of an axion to two photons via a fermion loop **(a)**. Photons could also be provided by an electromagnetic field for axion conversion **(b)**

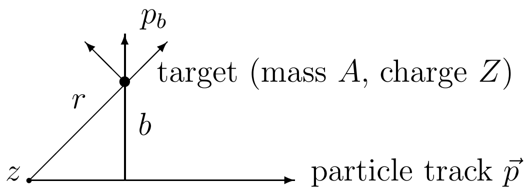
p_b
target (mass A, charge Z)
r
b
z
particle track $\vec{p}$

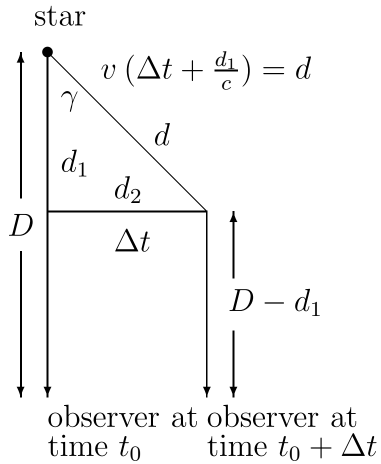
star
$v\,(\Delta t + \frac{d_1}{c}) = d$
γ
d
d_1
d_2
D
Δt
$D - d_1$
observer at time t_0
observer at time $t_0 + \Delta t$

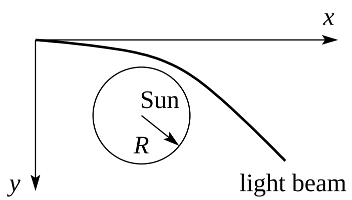
x
Sun
R
y
light beam

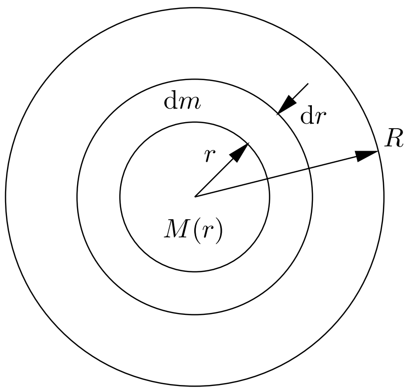
dm
dr
R
r
$M(r)$

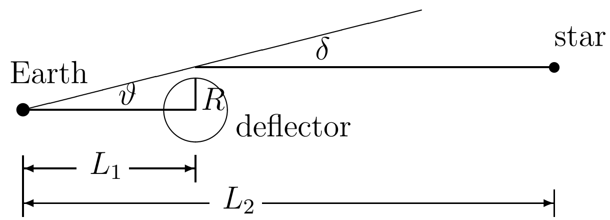
star
δ
Earth
ϑ
R
deflector
L_1
L_2

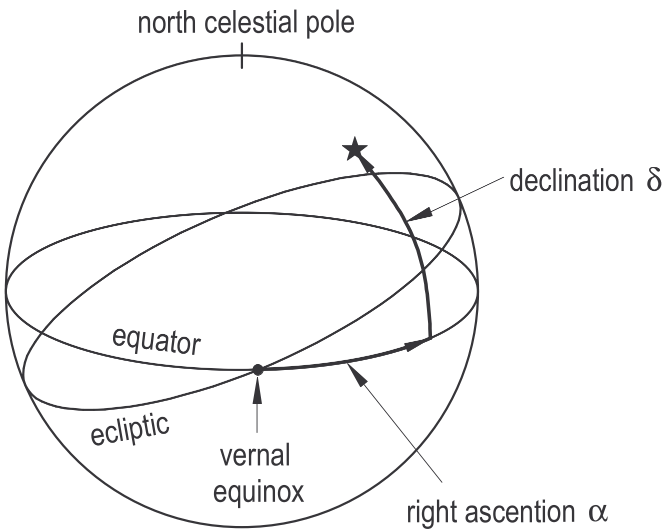

Figure C.1: Definition of the equatorial coordinates right ascension and declination

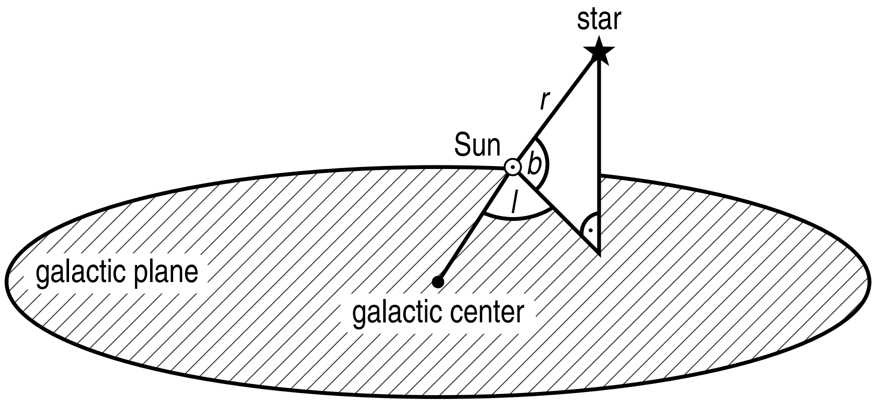

Figure C.2: Definition of the galactic coordinates latitude and longitude

References

[1] CERN Courier, May 2004, p. 13.

[2] Particle Data Group, S. Eidelman et al., Phys. Lett. **B592** (2004) 1.

[3] Claus Grupen, *Particle Detectors*, Cambridge University Press, Cambridge, 1996.

[4] M. Kleifges and H. Gemmeke, Auger Collaboration, IEEE Conference Rome, October 2004, to be published in the Proceedings.

[5] Y. Totsuka, IEEE conference, Portland, 2003.

[6] G. R. Farrar, T. Piran, Phys. Rev. Lett. **84** (April 2000) 3527.

[7] Michael S. Turner and J. Anthony Tyson, Rev. Mod. Phys. **71** (1999) 145.

[8] Andrew Liddle, *An Introduction to Modern Cosmology*, Wiley, Chichester, 1999.

[9] Torsten Flie"sbach, *Allgemeine Relativit"atstheorie*, Spektrum, Heidelberg, 1998.

[10] Bradley W. Carroll and Dale A. Ostlie, *An Introduction to Modern Astrophysics*, Addison-Wesley, Reading, Mass., 1996.

[11] S. Perlmutter et al., web site of the Supernova Cosmology Project,

`supernova.lbl.gov`.

[12] See the web site of the Relativistic Heavy Ion Collider, `www.bnl.gov/RHIC/`.

[13] See the web site of the Alpha Magnetic Spectrometer, `ams.cern.ch`.

[14] A. G. Cohen, *CP Violation and the Origins of Matter*, Proceedings of the 29th SLAC Summer Institute, 2001.

[15] A. G. Cohen, A. De Rujula and S. L. Glashow, Astrophys. J. **495** (1998) 539–549.

[16] A. D. Sakharov, JETP Letters, **5** (1967) 24.

[17] Edward W. Kolb and Michael S. Turner, *The Early Universe*, Addison-Wesley, Reading, Mass., 1990.

[18] BBN code can be downloaded from

`www-thphys.physics.ox.ac.uk/users/SubirSarkar/bbn.html`

[19] S. Burles and D. Tytler, Astrophys. J. **499** (1998) 699; **507** (1998) 732.

[20] The LEP and SLD experiments, *A Combination of Preliminary Electroweak Measurements and Constraints on the Standard Model*, CERN EP/2000-016 (2000).

[21] D. Denegri, B. Sadoulet and M. Spiro, Rev. Mod. Phys. **62** (1990) 1.

[22] G. Gamow, Phys. Rev. **74** (1948) 505.

[23] Ralph A. Alpher and Robert C. Herman, Phys. Rev. **75** (1949) 1089.

[24] A. A. Penzias and R. W. Wilson, Astrophys. J. **142** (1965) 419.

[25] R. H. Dicke, P. J. E. Peebles, P. G. Roll and D. T. Wilkinson, Astrophy. J. **142** (1965) 414.

[26] D. J. Fixsen et al., Astrophys. J. **473** (1996) 576;

`http://lambda.gsfc.nasa.gov/product/cobe/firas_overview.cfm`.

[27] C. L. Bennett et al., Astrophy. J. **464** (1996) L1–L4; web site of the COBE satellite,

`http://lambda.gsfc.nasa.gov/product/cobe/`.

[28] Web site of the Wilkinson Microwave Anisotropy Probe, `map.gsfc.nasa.gov`.

[29] G. Hinshaw et al., Astrophys. J. Suppl. **148** (2003) 135; `map.gsfc.nasa.gov`.

[30] Barbara Ryden, *Introduction to Cosmology*, Addison-Wesley, San Francisco, 2003.

[31] Wayne Hu, `background.uchicago.edu/~whu`; see also W. Hu and S. Dodelson, Ann. Rev. Astron. Astrophys. **40** (2002) 171, astro-ph/0110414.

[32] U. Seljak and M. Zaldarriaga, Astrophy. J. **469** (1996) 437–444; code for the program `CMBFAST` is available from `www.cmbfast.org`.

[33] CERN Courier July/August 2002; A. C. S. Readhead et al., astro-ph/0402359 (2004).

[34] Web site of the PLANCK experiment, `astro.estec.esa.nl/Planck`.

[35] Milton Abramowitz ans Irene Stegun, *Handbook of Mathematical Functions*, 9th printig, Dover Publ., New York, 1970.

[36] I. S. Gradstein and I. M. Ryshik, *Tables of Series, Products, and Integrals*, Harri Deutsch, Thun, 1981.

[37] B. Cabrera, Phys. Rev. Lett. **48** (1982) 1378.

[38] John A. Peacock, *Cosmological Physics*, Cambridge University Press, p. 329, Cambridge 2003.

[39] A. H. Guth, Phys. Rev. D **23** (1981) 347.

[40] A. D. Linde, Phys. Lett. **108B** (1982) 389.

[41] A. Albrecht and P. J. Steinhardt, Phys. Rev. Lett. **48** (1982) 1220.

[42] M. Tegmark et al., Astrophys. J. **606** (2004) 702–740.

[43] Alan H. Guth, *Inflation* in Carnegie Observatories Astrophysics Series, Vol. 2, *Measuring and Modeling the Universe*, ed. W. L. Freedman, Cambridge University Press, 2004; astro-ph/0404546.

[44] F. Zwicky, Astrophys. J. **86** (1937) 217.

[45] `www.hep.physik.uni-siegen.de/~grupen/astro/pot2drot.pdf`

[46] George B. Arfken and Hans-Jürgen Weber, *Mathematical Methods for Physicists*, 4th edition, Academic Press, New York (1995).

[47] Tony Guénault, *Statistical Physics*, 2nd edition, Kluwer Academic Publishers, Secaucus, NJ, 1995.

Further Reading

Claus Grupen, *Astroteilchenphysik: das Universum im Licht der kosmischen Strahlung*, Vieweg, Braunschweig, 2000.

Lars Bergström and Ariel Goobar, *Cosmology and Particle Astrophysics*, Wiley, Chichester, 1999.

H. V. Klapdor-Kleingrothaus and K. Zuber, *Particle Astrophysics*, IOP, 1997.

G. Börner, *The Early Universe: Facts and Fiction*, Springer, 1988.

S. Weinberg, *The First Three Minutes*, BasicBooks, New York, 1993.

Alan Guth, *The Inflationary Universe*, Vintage, Vancouver, USA, 1998.

G. Cowan, *Lecture Notes on Particle Physics*, RHUL Physics Dept. course notes for PH3520, 2002.

Web site of the European Organisation for Nuclear Research (CERN): `www.cern.ch`.

H. Georgi and S. L. Glashow, Phys. Rev. Lett. **32** (1974) 438.

Web site of the Super-Kamiokande experiment:

`www-sk.icrr.u-tokyo.ac.jp/doc/sk`.

M. Shiozawa et al., (Super-Kamiokande collaboration), Phys. Rev. Lett. **81** (1998) 3319.

G. Cowan, *Statistical Data Analysis*, Oxford University Press, 1998.

A. V. Filippenko and A. G. Riess, astro-ph/9807008 (1998).

T. D. Lee and C. N. Yang, Phys. Rev. **104** (1956) 254.

C. S. Wu et al., Phys. Rev. **105** (1957) 1413.

J. H. Christenson, J. W. Cronin, V. L. Fitch and R. Turlay, Phys. Rev. Lett. **13** (1964) 138.

Harold P. Furth, *Perils of Modern Living*, originally published in the New Yorker Magazine, 1956.

Ken Nollett, `www.phys.washington.edu/~nollett`.

David N. Schramm and Michael S. Turner, Rev. Mod. Phys. **70** (1998) 303.

Yuri I. Izotov and Trinh X. Thuan, *Heavy-element abundances in blue compact galaxies*, Astrophys. J. **511** (1999) 639–659.

Scott Burles, Kenneth M. Nollet, James N. Truran and Michael S. Turner, Phys. Rev. Lett. **82** (1999) 4176; astro-ph/9901157.

Web site of the ALEPH collaboration: `alephwww.cern.ch`, and the ALEPH public pages, `alephwww.cern.ch/Public.html`.

C. L. Bennett et al., Astrophys. J. Suppl. **148** (2003) 1; `map.gsfc.nasa.gov`.

Keith A. Olive, Primordial Big Bang Nucleosynthesis, astro-ph/9901231 (1999).

R. Hagedorn, *Relativistic Kinematics*, W. A. Benjamin Inc. Reading, Mass., 1963.

Otto C. Allkofer, Fortschr. d. Physik **15**, 113–196, 1967.

S. Hayakawa, *Cosmic Ray Physics*, Wiley-Interscience, New York, 1969.

Albrecht Uns"old, *Der Neue Kosmos*, Springer, Heidelberg, 1974.

Otto C. Allkofer, *Introduction to Cosmic Radiation*, Thiemig, M"unchen, 1975.

D. J. Adams, *Cosmic X-ray Astronomy*, Adam Hilger Ltd., Bristol, 1980.

Joseph Silk, *The Big Bang – The Creation and Evolution of the Universe*, Freeman, New York, 1980.

Frank H. Shu, *The Physical Universe: An Introduction to Astronomy*, Univ. Science Books, Mill Valley, California, 1982.

Rodney Hillier, *Gamma-Ray Astronomy*, Oxford Studies in Physics, Clarendon Press, Oxford 1984.

O. C. Allkofer, P. K. F. Grieder, *Cosmic Rays on Earth*, Fachinformationszentrum Karlsruhe, 1984.

Hans Sch"afer, *Elektromagnetische Strahlung – Informationen aus dem Weltall*, Vieweg, Wiesbaden, 1985.

W. D. Arnett et al., *Supernova 1987A*, Ann. Rev. Astron. Astrophysics **27** (1989) 629–700.

Thomas K. Gaisser, *Cosmic Rays and Particle Physics*, Cambridge University Press, Cambridge, 1990.

John Gribbin, *Auf der Suche nach dem Omega-Punkt*, Piper, M"unchen, 1990.

Martin Pohl, Reinhard Schlickeiser, *Exoten im Gamma-Licht*, Astronomie heute, Bild der Wissenschaft **3**, S. 92/93, 1993.

Neil Gehrels et al., *The Compton Gamma-Ray Observatory*, Scientific American, 38–45, Dec. 1993.

Charles D. Dermer, Reinhard Schlickeiser, Astrophys. J. **416** (1993) 458–484.

J.W. Rohlf, *Modern Physics from α to Z^0*, J. Wiley & Sons, New York, 1994.

T. Kifune, *The Prospects for Very High Energy Gamma-Ray Astronomy*, Inst. f. Cosmic Ray Research, Univ. Tokyo, ICRR-326-94-21, 1994.

H. V. Klapdor-Kleingrothaus, A. Staudt, *Teilchenphysik ohne Beschleuniger*, Teubner, Stuttgart, 1995.

Kitty Ferguson, *Das Universum des Stephen Hawking*, Econ, D"usseldorf, 1995.

Ulf Borgeest, Karl-Jochen Schramm, *Bilder von Gravitationslinsen*, Sterne und Weltraum, Nr. 1, 1995, S. 24–31.

Peter L. Biermann, *The Origin of Cosmic Rays*, MPI Radioastronomie Bonn, MPIfR 605, astro-ph/9501003, Phys. Rev. **D51** (1995) 3450.

Daniel Vignaud, *Solar and Supernovae Neutrinos*, 4th School on Non-Accelerator Particle Astrophysics, Trieste 1995, DAPNIA/SPP 95-26, Saclay.

Thomas K. Gaisser, Francis Halzen, Todor Stanev, Phys. Rep. **258**, No. 3, 1995.

Lexikon der Astronomie, Spektrum-Verlag, Heidelberg, 1995.

S. P. Plunkett et al., Astrophys. Space Sci. **231** (1995) 271; astro-ph/9508083, 1995.

Mordehai Milgrom, Vladimir Usov, Astrophys. J. **449** (1995) 37; astro-ph/9505009, 1995.

V. Berezinsky, *High Energy Neutrino Astronomy*, Gran Sasso Lab. INFN, LNGS-95/04, 1995.

John V. Jelley, Trevor C. Weekes, *Ground-Based Gamma-Ray Astronomy*, Sky & Telescope, Sept. 95, 20–24, 1995.

Volker Sch"onfelder, *Exotische Astronomie mit dem Compton"=Observatorium*, Physik in unserer Zeit **26**, 262–271, 1995.

A. C. Melissinos, *Lecture Notes on Particle Astrophysics*, Univ. of Rochester 1995, UR-1841, Sept. 1996.

Kitty Ferguson, *Gottes Freiheit und die Gesetze der Sch"opfung*, Econ, D"usseldorf, 1996.

Kitty Ferguson, *Prisons of Light – Black Holes*, Cambridge University Press, Cambridge, 1996.

Claus Grupen, *Particle Detectors*, Cambridge University Press, Cambridge, 1996.

Michel Spiro, Eric Aubourg, *Experimental Particle Astrophysics*, Int. Conf. on High Energy Physics, Varsovie (Pologne), 1996.

Karl Mannheim, Dieter Hartmann, Burkhardt Funk, Astrophys. J. **467** (1996) 532–536; astro-ph/9605108, 1996.

G. Battistoni, O. Palamara, *Physics and Astrophysics with Multiple Muons*, Gran Sasso Lab. INFN/AE 96/19, 1996.

John Ellis, Nucl. Phys. Proc. Suppl. **48** (1996) 522–544, CERN-TH/96-10, astro-ph/9602077, 1996.

H. V. Klapdor-Kleingrothaus, K. Zuber, *Teilchenastrophysik*, Teubner, Stuttgart, 1997, and *Particle Astrophysics*, Inst. of Physics Publ., 2000.

Georg G. Raffelt, *Astro-Particle Physics*, Europhysics Conference on High-Energy Physics, August 1997, Jerusalem, hep-ph/9712548, 1997.

Francis Halzen, *The Search for the Source of the Highest Energy Cosmic Rays*, Univ. of Madison Preprint MAD-PH 97-990, astro-ph/9704020, 1997.

G. Burdman, F. Halzen, R. Gandhi, Phys. Lett. **B417** (1998) 107-113, Univ. of Madison Preprint MAD-PH 97-1014, hep-ph/9709399, 1997.

Paolo Lipari, *Cosmology, Particle Physics and High Energy Astrophysics*, Conf. Proc. Frontier Objects in Astrophysics and Particle Physics, F. Giovannelli and G. Mannocchi (Eds.), Vol 57, p. 595, 1997.

Georg G. Raffelt, *Dark Matter: Motivation, Candidates and Searches*, Proc. 1997 European School of High Energy Physics, Menstrup, Denmark, hep-ph/9712538, 1997.

C. N. de Marzo, Nucl. Phys. Proc. Suppl. **70** (1999) 515–517, physics/9712039, 1997.

Hinrich Meyer, *Photons from the Universe: New Frontiers in Astronomy*, Univ. Wuppertal, Germany, hep-ph/9710362, 1997.

Particle Data Group (S. Eidelman et al.), *Review of Particle Physics*, Phys. Lett. **B592** (2004) 1–1109.

R. K. Bock, A. Vasilescu, *The Particle Detector Briefbook*, Springer, Berlin, Heidelberg, 1998.

Jonathan Allday, *Quarks, Leptons and the Big Bang*, Inst. of Physics Publ., Bristol, 1998.

Craig J. Hogan, *The Little Book of the Big Bang*, Copernicus, Springer, New York, 1998.

Lawrence M. Krauss, *A New Cosmological Paradigm: The Cosmological Constant and Dark Matter*, hep-ph/9807376, Case Western Reserve University, Cleveland, 1998.

Francis Halzen, *Ice Fishing for Neutrinos*, AMANDA Homepage,

`http://amanda.berkeley.edu/www/ice-fishing.html`.

Jochen Greiner, *Gamma-Ray Bursts: Old and New*, Astroph. Inst. Potsdam, astro-ph/9802222, 1998.

Volker Sch"onfelder, *Gammastrahlung aus dem Kosmos*, Phys. Bl. **54**, 325–330, 1998.

K. S. Capelle et al., Astropart. Phys. **8** (1998) 321–328, astro-ph/9801313, 1998.

Laura Whitlock, *Gamma-Ray Bursts*,

`http://imagine.gsfc.nasa.gov/docs/science/know_l1/burst.html`.

Glennys R. Farrar, *Can Ultra High Energy Cosmic Rays be Evidence for New Particle Physics?*, Rutgers Univ., USA, astro-ph/9801020, 1998.

Super-Kamiokande Collaboration, Phys. Lett. **B433** (1998) 9–18, hep-ex/9803006, 1998.

M. S. Turner, Publ. Astron. Soc. Pac. **111** (1999) 264–273, astro-ph/9811364, 1998.

J. P. Henry, U. G. Briel, H. B"ohringer, *Die Entwicklung von Galaxienhaufen*, Spektrum der Wissenschaft, 2/1999, S. 64–69.

Guido Drexlin, *Neutrino-Oszillationen*, Phys. Bl., Heft 2, S. 25–31, 1999.

G. Veneziano, *Challenging the Big Bang: A Longer History of Time*, CERN-Courier, March 1999, p. 18.

M. A. Bucher, D. N. Spergel, *Was vor dem Urknall geschah*, Spektrum der Wissenschaft, 3/1999, S. 55.

C. J. Hogan, R. P. Kirshner, N. B. Suntzeff, *Die Vermessung der Raumzeit mit Supernovae*, Spektrum der Wissenschaft, 3/1999, S. 40.

L. M. Krauss, *Neuer Auftrieb f"ur ein beschleunigtes Universum*, Spektrum der Wissenschaft, 3/1999, S. 47.

J. Tr"umper, *ROSAT und seine Nachfolger*, Phys. Bl. 55/9, S. 45, 1999.

Craig J. Hogan, Rev. Mod. Phys. **72** (2000) 1149–1161.

H. Bl"umer, *Die h"ochsten Energien im Universum*, Physik in unserer Zeit, S. 234–239, Nov. 1999.

Brian Greene, *"The Elegant Universe"*, Vintage 2000, London, 1999.

H. Völk, H. Blümer & K.-H. Kampert, H. Krawczynski et. al., Ch. Spiering, M. Simon, J. Jochum & F. von Feilitzsch: Phys. Bl., Schwerpunkt Astroteilchenphysik, März 2000, S. 35–68.

Paul J. Steinhardt, *"Quintessential Cosmology and Cosmic Acceleration"*, Selection of review papers under the heading *"Dark Energy and the Cosmological Constant"* `http://pancake.uchicago.edu/~carroll/reviewarticles.html`.

Peter K. F. Grieder, *Cosmic Rays at Earth*, Elsevier Science, 2001.

S. Hayakawa, *Cosmic Ray Physics*, Wiley Interscience, N.Y., 1969.

K. C. Cole, *The Hole in the Universe*, The Harvest Book/Harcourt Inc., San Diego, 2001.

Brian Greene, *The Fabric of the Cosmos: Space, Time and the Texture of Reality*, Alfred A. Knopf, N.Y., 2004.

John A. Bahcall, *Neutrino Astronomy*, Cambridge University Press, 1990.

Rodney Hillier, *Gamma Ray Astronomy*, Oxford Studies in Physics, 1984.

John A. Peacock, *Cosmological Physics*, Cambridge University Press, 2003.

Martin Rees, *Just Six Numbers: The Deep Forces That Shape the Universe*, Basic Books, New York, 2001.

Martin Rees, *New Perspectives in Astrophysical Cosmology*, Cambridge University Press, 2000.

S. M. Bilenky, *The History of Neutrino Oscillations*, hep-ph/0410090, 2004.

A. V. Filippenko and A. G. Riess, Phys. Rep. **307** (1999) 31.

Photo Credits

{1} T. Credner and S. Kohle, University of Bonn, Calar Alto Observatory

{2} Prof. Dr. D. Kuhn, University of Innsbruck, Austria

{3} Courtesy of The Archives, California Institute of Technology, Photo ID 1.22-5

{4} C. Butler and G. Rochester, Manchester University

{5} Prof. Dr. A. A. Penzias, Bell Labs, USA

{6} D. Malin, Anglo-Australian Observatory

{7} Particle Data Group, European Physical Journal C3, (1998), 144; `http://pdg.lbl.gov`

{8} Prof. Dr. Y. Totsuka, Institute for Cosmic Ray Research, Tokyo, Japan

{9} T. Kajita, Y. Totsuka, Rev. Mod. Phys. 73 (2001) p. 85

{10} Y. Fukuda et al., Phys. Rev. Lett. 81 (1998) 1562–1567

{11} Prof. Dr. R. Davis, Brookhaven National Laboratory, USA

{12} R. Svoboda and K. Gordan (Louisiana State University), `http://antwrp.gsfc.nasa.gov/apod/ap980605.html`. Equivalent figure in: A. B. McDonald et al., Rev. Sci. Instrum. 75 (2004) 293–316, astro-ph/0311343

{13} AMANDA Collaboration, Christian Spiering, private communication 2004

{14} Dr. D. Heck, Dr. J. Knapp, Forschungszentrum Karlsruhe, Germany

{15} Cangaroo Collaboration, Woomera, Australia

{16} CGRO Project Scientist Dr. Neil Gehrels, Goddard Space Flight Center, USA (1999)

{17} BATSE-Team, NASA, M. S. Briggs, (`http://www.batse.msfc.nasa.gov/batse/grb/skymap/`)

{18} Prof. Dr. J. Trümper, Max-Planck Institute for Extraterrestrial Physics, München, Garching

{19} ESA/XMM-Newton,

`http://xmm.vilspa.esa.es/external/xmm_science/gallery/public`

courtesy by L. Strüder

{20} ESA/XMM-Newton/Patrick Henry et al., courtesy by L. Strüder

{21} Prof. Dr. M. Simon, University of Siegen, Germany

{22} R. Tcaciuc, University of Siegen, 2004

{23} ALEPH Collaboration, CERN, courtesy by P. Dornan, Imperial College

{24} Frejus-Experiment, France/Italy, courtesy by Chr. Berger, RWTH Aachen

{25} Prof. Dr. P. Sokolsky, University of Utah, Salt Lake City, USA

{26} LBNL-53543, R. A. Knop et al., Astrophys. J. **598** (2003) 102–137; `http://supernova.lbl.gov/`, courtesy by Saul Perlmutter

{27} Courtesy of the COBE Science Working Group

{28} Courtesy of the WMAP Science Team

{29} Dr. L. J. King, University of Manchester, UK; NASA; King et al. 1998, MNRAS 295, L41

{30} Prof. Dr. G. G. Raffelt, Max-Planck Institute for Physics (Werner-Heisenberg Institute), München, Germany